Chapter IV. Towards designing alternate second coordination spheres for a *de novo* designed metalloprotein

Introduction

In general, it is well understood that secondary coordination sphere interactions are important for tuning metal binding, activity, substrate selectivity, and metal center acidity, among other properties. Biochemical studies on native proteins have been very successful in identifying which residues around the metal site may contribute to these interactions in many metalloenzymes and, in some cases, far away residues (beyond the second shell) have been shown to be important (Chapter 1). In carbonic anhydrase (CA)II, residues as far as 15 Å away from the Zn(II) center can alter the pK_a by as much as one unit and change the rate constant for proton transfer by up to four-fold.[1] Interestingly, a DFT study comparing the active sites of α- and β-CA's, which have very different first coordination spheres ($Zn(His)_3(H_2O)$ for α-CA's and $Zn(His)(Cys)_2(H_2O)$ for β-CA's), demonstrated that the second-shell interactions around each active site lead to the similar acidities of the coordinated water molecules and zinc-binding affinities.[2] While there is an increasing body of knowledge on *de novo* protein design and the incorporation of metal-binding sites, relatively little has been reported on tuning these binding sites, especially rationally. Successful examples for Zn(II) sites are on a case-by-case basis (usually lacking systematic studies, and often have not been accompanied by a crystal structure or kinetic analysis[3–5]), with no reliable rules for generating such interactions in any given structure. In order to apply protein design to the generation of efficient catalysts for industrial or other applications, it is important to understand how to use secondary interactions to tune a given metal-binding site.

In Chapter 2, I described the design of a dual metal-site 3SCC, containing a stabilizing HgS_3 site and a hydrolytic ZnN_3O site, similar to that found in CA.[6] The crystal structure of $[Hg(II)]_S[Zn(II)(OH_2/OH^-)]_N(\textbf{C}SL9PenL23H)_3{}^{n+}$ shows that the

ZnN$_3$O center makes an excellent minimal model for the first coordination sphere of CA and the hydrolytic activity is within ~100-fold of that for CA towards p-nitrophenyl acetate (pNPA).[6,7] The binding affinity for Zn(II), while strong ($K_d = 0.22 \pm 0.06$ μM at pH 9.0), is at least 100-fold or more weaker than CA.[8–10] Moving the designed ZnN$_3$O site to different positions in the three-stranded coiled coil (3SCC) results in altered substrate, solvent, and inhibitor access, small variations in binding affinity and rate, and, for one example, an increase in the pK_a.[7] However, in all cases the maximal catalytic efficiency displayed little variation. In CA, significant variations in pK_a, catalytic efficiency, and binding affinities are observed upon interruption of second-shell interactions. It can be hypothesized that building such interactions into this designed system may allow for improvement of the zinc site's properties (stronger metal binding, lower pK_a, and higher catalytic activity).

The sequences for the peptides used in this chapter (Table 4-1) contain potential hydrogen-bonding residues around the ZnHis$_3$ site. Both **TRI** and **Grand** (for extra stability to support engineering of polar residues into the hydrophobic core) are used. The hydrogen-bonding Thr199 residue in CA is used as inspiration for engineering secondary interactions in the designed coiled coil. As described in Chapter 1, T199 forms a hydrogen bond with Zn(II)-bound solvent for both orientation of the nucleophile for

Table 4-1. TRI and Grand peptide family sequences used in these studies.

Peptide	a b c d e f g					
TRIL2W	Ac-G **W**KALEEK	LKALEEK	LKALEEK	LKALEEK		G-NH$_2$
TRIL23H	Ac-G LKALEEK	LKALEEK	LKALEEK	**H**KALEEK		G-NH$_2$
TRIL2WL23H	Ac-G **W**KALEEK	LKALEEK	LKALEEK	**H**KALEEK		G-NH$_2$
TRIL9CL23H	Ac-G LKALEEK	**C**KALEEK	LKALEEK	**H**KALEEK		G-NH$_2$
TRIL9CL19T L23H	Ac-G LKALEEK	**C**KALEEK	LKA**T**EEK	**H**KALEEK		G-NH$_2$
GRL2WL16C L30H	Ac-G **W**KALEEK	LKALEEK	**C**KALEEK	LKALEEK	**H**KALEEK	G-NH$_2$
GRL16CL26T L30H	Ac-G LKALEEK	LKALEEK	**C**KALEEK	LKA**T**EEK	**H**KALEEK	G-NH$_2$
GRL16CL26D L30H	Ac-G LKALEEK	LKALEEK	**C**KALEEK	LKA**D**EEK	**H**KALEEK	G-NH$_2$

N- and C-termini are capped by Ac and NH$_2$ groups (acetylated and amidated), respectively.

reaction and tuning the acidity of the metal center.[11,12] Mutation of this residue results in decreased Zn(II)-binding affinity, a 1.5 unit increase in the pK_a, and a loss of catalytic efficiency of ~100-fold for both CO_2 hydration and pNPA hydrolysis. While it is acknowledged that a network of hydrogen bonds will ultimately be needed to finely tune the designed metal center, the bottom-up approach is to begin by engineering the first hydrogen bond and analyzing the resulting design before building up further complexity. This chapter will describe the incorporation of polar residues to mimic the T199 hydrogen bond to Zn(II)-bound solvent found in CA. Further, the use of spectroscopic probe metals, Cd(II) and Co(II), both for which metal-substituted data on CA is available, will be explored towards developing a deeper understanding about the designed sites and as useful comparators within the design family.

Materials and Methods

The nomenclature used to describe the metal complexes prepared in these studies is as described in Chapter 2.

Peptide Synthesis and Purification. Peptides were synthesized on an Applied Biosystems 433A peptide synthesizer using standard protocols[13] and purified as described previously[14] (by reverse-phase HPLC on a C18 column at a flow rate of 10 mL/min using a linear gradient varying from 0.1% TFA in water to 0.1% TFA in 9:1 $CH_3CN:H_2O$ over 25-35 minutes). Pure peptides were characterized by electrospray mass spectrometry. Peptide stock solutions were prepared in doubly distilled water that had been purged with argon to minimize oxidation of thiol-containing peptides. The concentrations for **TRI** peptides containing Cys sites were determined by calculating the thiol concentration using a published assay with 5,5'-dithiobis-(2-nitrobenzoic acid) (Ellman's reagent).[15,16] The concentrations for **Grand** peptides (one heptad repeat longer) containing Cys sites were similarly determined using a published assay with 4,4'-dipyridyl disulphide[17] or were based on the tryptophan absorbance at 280 nm using $\varepsilon = 5500$ M^{-1} cm^{-1}. Concentrations of **TRI**L2WL23H solutions were based on the tryptophan absorbance at 280 nm using $\varepsilon = 5500$ M^{-1} cm^{-1}. Concentrations of **TRI**L23H solutions were based on

amino acid analysis performed by the Protein Structure Facility at the University of Michigan.

Circular Dichroism (CD) and Ultraviolet-Visible (UV-Vis) Spectroscopy. CD and UV-Vis spectra were recorded in quartz cuvettes at 25 °C on an AVIV 62DS spectrometer and Cary 100 Bio UV/Vis spectrometer, respectively. Guanidine hydrochloride (GuHCl) CD titrations were performed at pH 8.5 as described previously.[18] All solutions were purged with argon prior to use in order to minimize oxidation of peptides and formation of disulfide bonds.

Competitive Zn(II)-Binding Titrations. The apparent binding constants were determined by competition assay with the colorimetric Zn(II) chelator, Zincon (2-carboxy-2'-hydroxy-5'-(sulfoformazyl)benzene).[19,20] Zn(II) forms a 1:1 complex with Zincon (Zi) with a distinct absorption band at 620 nm ($\varepsilon \sim 16000 \text{ M}^{-1}\text{cm}^{-1}$) at pH 7.5 and apparent dissociation constant ($K_{d,app}$) of 2.80 x 10^{-6} M (consistent with the range of reported values).[19,21–25] These parameters were evaluated for each pH and each buffer used in my experiments (pH 7.5 in 50 mM HEPES, 0.1 M Na_2SO_4 and pH 9.0 in 50 mM CHES, 0.1 M Na_2SO_4) by titrating Zn(II) (stock solutions were standardized using inductively coupled plasma-optical emission spectroscopy) into a solution of 10 μM Zi. For pH 9.0, $\varepsilon_{620} \sim 27500 \text{ M}^{-1}\text{cm}^{-1}$ and $K_{d,app} = 5$ x 10^{-8} M (a 5 cm pathlength cell was used for the calibration titration at this pH). For experiments involving peptide, an excess of Zi over $ZnSO_4$ (30 μM Zi and 15 μM Zn(II) to ensure most Zn(II) is bound to ligand) was used as the starting point of the titration (except at pH 9.0 for [Hg(II)]$_S$(**GR**L16CL26TL30H)$_3^{n-}$, 25 μM Zi and 12.5 μM Zn(II) was used). Analogously, Zn(II) was bound to an excess of peptide (4 μM pep_3 and 2 μM Zn(II)) for the reverse titration at pH 9.0. At pH 7.5, Zincon could not compete with either peptide, even with very small amounts of peptide at the start of the titration. Both approaches should give similar apparent binding constants for $Znpep_3$, indicating equilibrium had been reached. The binding equilibrium for this competition experiment can be expressed by eq 1.

$$Znpep_3 + Zi \rightleftharpoons pep_3 + ZnZi$$

(1)

152
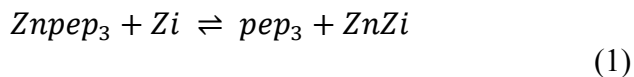
The apparent dissociation constant of Znpep$_3$ can be calculated using eq 2.

$$\frac{K_{d,Znpep3}}{K_{d,ZnZi}} = \frac{([ZnZi][pep_3])}{([Znpep_3][Zi])}$$

(2)

For the forward titration, where a solution of Zi is titrated into Znpep$_3$, the absorption band at 620 nm is due to the ZnZi complex, and increases as Zi is added to Znpep$_3$, reflecting transfer of Zn(II) from pep$_3$ to Zi and therefore yielding [ZnZi] and [Znpep$_3$] for eq 2. [Znpep$_3$] can be defined as the total amount of Zn(II) present ([Zn]$_T$) minus the Zn(II)-bound fraction ([ZnZi]), under the conditions of this experiment. The amount of unbound peptide can then be defined as the total peptide minus the Zn(II)-bound fraction, [pep$_3$] = [pep$_3$]$_T$ − [Znpep$_3$] = [pep$_3$]$_T$ − ([Zn]$_T$ − [ZnZi]). The amount of free Zi is then related to the total amount of Zi minus the Zn(II)-bound fraction, [Zi] = [Zi]$_T$ − [ZnZi]. Substituting all of the above into eq 2 yields a quadratic expression, eq 3, which can be solved for [ZnZi]. Since this quantity is directly related to the absorbance at 620 nm by the Beer-Lambert law, the real solution to eq 3 can be inserted into eq 4 to give an equation which can be fitted in Prism 5 (GraphPad Software)[26] to yield the dissociation constant for Znpep$_3$.

$$\left(\frac{K_{d,Znpep3}}{K_{d,ZnZi}} - 1\right)[ZnZi]^2$$
$$+ \left(-\frac{K_{d,Znpep3}}{K_{d,ZnZi}}x - \frac{K_{d,Znpep3}}{K_{d,ZnZi}}[Zn]_T - [pep_3]_T + [Zn]_T\right)[ZnZi] + \frac{K_{d,Znpep3}}{K_{d,ZnZi}}[Zn]_T x$$
$$= 0$$

(3)

$$A_{620} = y = \varepsilon * b * [ZnZi]$$

(4)

An analogous approach was used for the reverse titration, in which pep$_3$ is added to ZnZi.

[113]Cd(II) NMR. All spectra were collected at 25 °C on a Varian VNMRS 700 spectrometer (115.25 MHz for [113]Cd) equipped with a 5 mm broadband probe and externally referenced to a 0.1 M Cd(ClO$_4$)$_2$ solution in D$_2$O. A spectral width of 1073 ppm (123712 Hz) was sampled using a 5.0 μs 90° pulse and a 0.05 second acquisition time with no delay between scans. Samples were prepared under a flow of argon by

dissolving 70-75 mg of the lyophilized and degassed peptides (**TRI**L23H) in 400-550 μL 15% D_2O/H_2O solution. The peptide concentrations were (based on previous amino acid analysis) 10-14.4 mM trimer. The final samples were prepared by the addition of the appropriate amount (to result in 0.9 equivalents per trimer) of 250 mM $^{113}Cd(NO_3)_2$ solution (prepared from 95% isotopically enriched ^{113}CdO obtained from Oak Ridge National Laboratory) and adjustment of the pH with KOH or HNO_3 solutions. The pH value was measured both before and after the experiment. For the bicarbonate experiments, a solution of 0.6 M $KHCO_3$ was added to the necessary amount. An argon atmosphere was maintained when possible but the samples came into brief contact with air during addition of $^{113}Cd(NO_3)_2$, pH adjustment, and acquisition. The data were analyzed using the software MestRe-C.[27] The free induction decays were zero-filled and treated with an exponential function with a line-broadening value of 100 Hz before Fourier transformation.

Co(II)-Binding Titrations.

a) Direct Co(II) binding. Co(II) into peptide titrations were performed at room temperature and monitored by UV-Vis spectroscopy in a 1 cm quartz cuvette. Aliquots of a $CoSO_4$ stock solution (0.0944 M, standardized using inductively coupled plasma-optical emission spectroscopy) were added to a 2.5 mL solution of 0.44-0.57 mM peptide trimer and 50 mM HEPES with 0.1 M Na_2SO_4 at pH 7.5. The pH was measured at the end of each titration to determine the actual pH without altering the concentration of peptide in solution. The absorbance spectra were recorded from 400-750 nm. For all titrations, the difference spectra were obtained by subtracting the background spectrum of the peptide under identical conditions but in the absence of metal (each time metal was added to the sample, an equivalent addition of ddH_2O was added to the reference cuvette). In this way, changes in the difference spectra may be attributed to metal-peptide interactions. After the addition of each aliquot, the solutions were left to equilibrate, with stirring for five minutes, before recording each absorbance spectrum. The first and last spectra at a given point were compared to ensure equilibrium had been reached.

The titrations were analyzed using non-linear least square fits (in Prism 5 (GraphPad Software)[26]) of the absorbance (at the appropriate λ_{max} for each peptide) as a function of the concentration of titrant (CoSO$_4$) added. The binding equilibrium for this experiment is described using eq 5.

$$Co + pep_3 \rightleftharpoons Copep_3$$

(5)
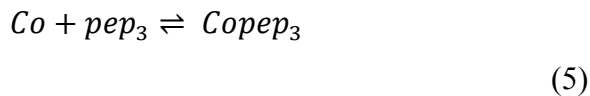
The apparent dissociation constant can be calculated using eq 6.

$$K_d = \frac{[pep_3][Co]}{[Copep_3]}$$

(6)

Two equations may be written for the total concentration of Co(II) and total concentration of $[pep_3]$. Rearranging the K_d equation in terms of $[Copep_3]$ (eq 7) and substituting it into the equation for the total concentration of Co(II) (could alternatively use the equation for $[pep_3]_T$) generates eq 8.

$$[Copep_3] = \frac{[pep_3][Co]}{K_d}$$

(7)

$$[Co]_T = [Co] + \frac{[pep_3][Co]}{K_d} = [Co] * \left(1 + \frac{[pep_3]}{K_d}\right)$$

(8)

Rearranging eq 8 in terms of $[Co]$ and substituting it into eq 7 results in eq 9.

$$[Copep_3] = \frac{[Co]_T[pep_3]K_d}{\left(1 + \frac{[pep_3]}{K_d}\right)}$$

(9)

Which can be substituted into the equation for $[pep_3]_T$ to generate eq 10.

$$[pep_3]_T = [pep_3] + \frac{[Co]_T[pep_3]K_d}{\left(1 + \frac{[pep_3]}{K_d}\right)}$$

(10)

Eq 10 can be expanded and simplified to generate a quadratic equation (eq 11) with $[pep_3]$ as the variable,

$$-\frac{1}{K_d}[pep_3]^2 + \left(\frac{[pep_3]_T}{K_d} - 1 - [Co]_T K_d\right)[pep_3] + [pep_3]_T = 0$$

(11)

for which the real solution is eq 12.

$$
\begin{aligned}
[pep_3] \\
= -\left(\left(\frac{[pep_3]_T}{K_d} - 1 - [Co]_T K_d\right)\right. \\
\left. - \sqrt{\left(\frac{[pep_3]_T}{K_d} - 1 - [Co]_T K_d\right)^2 - 4*\left(-\frac{1}{K_d}\right)*[pep_3]_T}\right) \div \left(2*\left(-\frac{1}{K_d}\right)\right)
\end{aligned}
$$

(12)

Then, the Beer-Lambert law can be used to convert these equations into a measurable quantity, that is the absorbance for Co(II) binding (which is peptide-dependent). There are two potential species contributing to this absorbance, $Copep_3$ and apo-pep_3, therefore by using eq 13 and substituting eq 7 and eq 12, the final equation which can be fitted in Prism 5 (GraphPad Software)[26] is obtained. $[Co]_T$ may be treated as the variable.

$$A = y = \varepsilon * b * [pep_3] + \varepsilon * b * [Copep_3]$$

(13)

b) Co(II)-Binding pH Titration. The increase in pH of a solution containing 0.47 mM (**TRI**L2WL23H)$_3$ and 0.23 mM CoSO$_4$ (to ensure complete Co(II) binding to the peptide) at room temperature was monitored by UV-Vis spectroscopy in a 1 cm quartz cuvette. In order to avoid altering the concentration of peptide in the sample, an identical sample was prepared and used to monitor the pH continuously. The pH of the sample was measured at the end of the titration to ensure it was the same as the pH of the reference sample. The titration was initiated at pH 3 and small increments of concentrated KOH were added up to pH 11.75. At least five minutes equilibration time was allowed between additions and the first and last spectra for several points were compared to ensure that equilibrium had been reached.

c) Co(II)-Peptide and Chloride Titration. Chloride binding to the Co(II)-peptide complex was monitored at pH 7.5 in 50 mM HEPES with 0.1 M Na_2SO_4 using UV-Vis spectroscopy in a 1 cm quartz cuvette. The titration was initiated with a solution of 0.65 mM (**TRI**L2WL23H)$_3$, to which up to 0.8 equivalent of $CoSO_4$ was added (0.52 mM $[Co(II)(OH_2/OH^-)_x]_N$(**TRI**L2WL23H)$_3{}^{n+}$). An equivalent reference sample lacking Co(II) was prepared as described in section a) for direct Co(II) binding. After the 0.8:1 Co(II):(**TRI**L2WL23H)$_3$ complex was formed, increments of KCl were added up to 0.3 M (~800 equivalents). A clear isosbestic point for chloride binding is observed in the spectra. Plotting the λ_{max} for the final spectrum (590 nm) vs the concentration of chloride generates a binding curve which may be fitted to obtain an estimate for the dissociation constant for chloride binding to $[Co(II)(OH_2/OH^-)_x]_N$(**TRI**L2WL23H)$_3{}^{n+}$. The fitting equation is similar to that used for direct Co(II) binding using the following equilibrium (eq 14).

$$Cl^- + Copep_3 \rightleftharpoons CoClpep_3$$

(14)
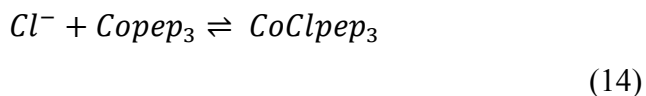
Esterase Activity Assays. The esterase activities of Zn(II)-bound peptides were determined spectrophotometrically with pNPA substrate (200-1400 mM) at 25 °C. Measurements were made at 348 nm, the isosbestic point for p-nitrophenol and p-nitrophenolate anion (ε = 5000 M^{-1} cm^{-1}).[28] The procedure is similar to that which was previously described[6] in Chapter 2, with some modifications. The substrate solution was prepared by quickly diluting a 0.1 M pNPA acetone solution into doubly-distilled water (ddH$_2$O) to a concentration of 3 mM. The procedure for measuring esterase activity is as follows: in a 1 mm pathlength quartz cuvette, buffer (50 mM, HEPES if pH 7.5 or 8.0, CHES for pH 8.5-9.65, both buffers with 0.1 M Na_2SO_4), ddH$_2$O, and metal-peptide solution were mixed. pNPA was added, mixed, and the absorbance increase recorded every 25 seconds for 7-20 minutes. Metal-peptide solutions contained either excess peptide or excess $ZnSO_4$ in order to ensure all Zn(II) was bound to the peptide. Controls then contained either apo-peptide or $ZnSO_4$, respectively, and their initial rates were subtracted from those of Zn(II)-bound peptide samples. The controls containing $ZnSO_4$ do not exhibit any activity over blank controls, but there is some activity from the free

peptide, due to unbound His residues.[6] Initial rates determined from linear fits of the first 2-10% of the reaction were plotted as a function of pNPA concentration and fitted to the Michaelis-Menten equation in Prism 5 (GraphPad Software).[26] The concentration of enzyme is 20 μM and is accounted for in all reported values.

The esterase activity of $[Cd(II)(OH_2/OH^-)_x]_N(\textbf{TRI}L23H)_3{}^{n+}$ was determined spectrophotometrically with pNPA (275-1400 mM) at pH 8.5 and 9.5 (50 mM CHES, 0.1 M Na$_2$SO$_4$), following a procedure similar to that described above Zn(II)-bound peptides, with one exception. Unlike for Zn(II), the control containing just CdCl$_2$ (standardized stock solutions were purchased from SPEX CertiPrep) in the absence of any peptide displayed altered activity compared to the blank containing only buffer (CdCl$_2$ appeared to slow the activity). Therefore, all activity for the Cd(II)-bound peptide was measured using an excess of peptide to ensure complete binding of Cd(II) (4x excess peptide). The control contained apo-peptide and the initial rates were subtracted from those for the Cd(II)-bound peptide.

The esterase activity of $[Co(II)(OH_2/OH^-)_x]_N(\textbf{TRI}L2WL23H)_3{}^{n+}$ was determined spectrophotometrically with pNPA (275-1400 mM) at pH 9.5 (50 mM CHES, 0.1 M Na$_2$SO$_4$), following a procedure similar to that for the Zn(II)-bound peptides, with one exception. While no reactivity is observed for the control containing just CoSO$_4$, a larger excess of Co(II) relative to peptide was initially used to achieve complete binding (24x). As a result, and using **TRI**L2W (no binding site), it was discovered that there was a non-specific contribution to the activity, likely due to Co(II) on the surface of the 3SCC. This was not tested using smaller amounts of excess Co(II), and therefore the best estimate of the activity was obtained by using an excess of peptide (4x excess) and subtracting out the initial rates of the apo-peptide as determined in parallel from the control.

Results

Characterization of Structural and Catalytic Sites.

a) Circular Dichroism (CD) of Apo- and Metal-Bound Peptides. To measure the folding and whether the presence of the HgS$_3$ center confers thermodynamic stability
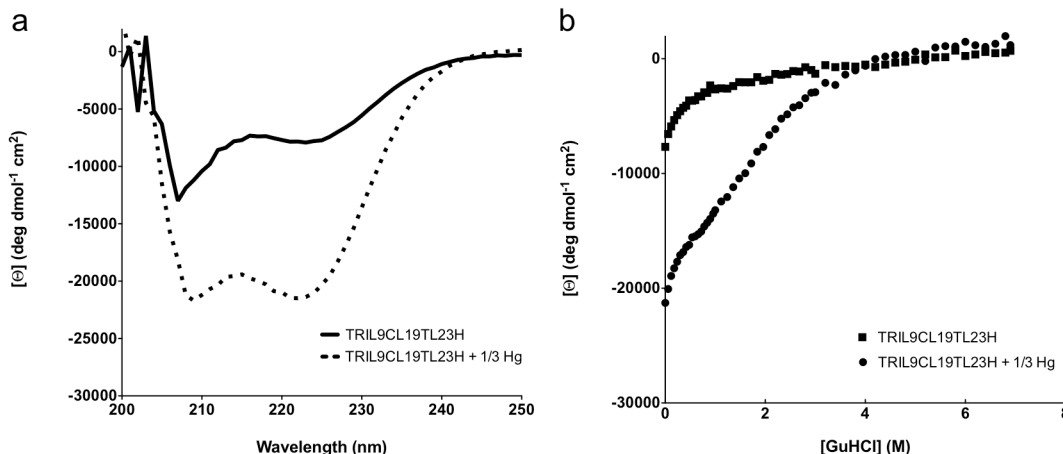
Figure 4-1. Folding of TRIL9CL19TL23H (apo and + 1/3 Hg(II)) as monitored by CD. a) CD spectra of TRIL9CL19TL23H and TRIL9CL19TL23H + 1/3 Hg(II) at pH 8.5 and 25 °C. The molar ellipticities [Θ] at 222 nm are ~ -7700 and ~ -21300 deg dmol^{-1} cm^2, respectively. b) GuHCl denaturation titrations represented by the [Θ] at 222 nm vs denaturant concentration for TRIL9CL19TL23H and TRIL9CL19TL23H + 1/3 Hg(II).

on the structures formed by the sequences **TRI**L9CL19TL23H, **GR**L16CL26TL30H, and **GR**L16CL26DL30H, GuHCl denaturation titrations were monitored using CD spectroscopy (Figures 4-1-4-2). The folding of each sequence in the presence and absence of one equivalent of Hg(II) per trimer at pH 8.5 was examined. The CD spectra for α-helical coiled coils yield characteristic peaks with negative minima at 208 and 222 nm. The spectrum for apo-(**TRI**L9CL19TL23H)$_3^{n-}$ indicates that this sequence does not fold well (Figure 4-1). Generally, for well-folded α-helical coiled coils, the peak at 222 nm is larger than that at 208 nm. In this case, the peak at 222 nm is smaller and the molar ellipticity [Θ] (~ -7700 deg dmol^{-1} cm^2) is only ~20% of what would be expected for an ideal, fully folded structure. The folding is better in the presence of Hg(II) (~ -21300 deg dmol^{-1} cm^2), and the CD spectrum is characteristic of an α-helical coiled coil, but it is still 10% less α-helical than the original model. The midpoint for chemical denaturation is shifted to a higher concentration of GuHCl in the presence of the HgCys$_3$ site, similar to the observation for the **TRI** peptides described in Chapters 2-3 (Figure 4-1). The CD spectra for apo- and Hg(II)-bound (**GR**L16CL26TL30H)$_3^{n-}$ indicate a well-folded α-helical coiled coil structure with [Θ] values at 222 nm of ~ -31700 deg dmol^{-1} cm^2 and ~ -32100 deg dmol^{-1} cm^2, respectively (~90% α-helical content) (Figure 4-2). Similarly, the

159

CD spectra for apo- and Hg(II)-bound $(\mathbf{GR}L16CL26DL30H)_3{}^{n-}$ also indicate well-folded α-helical coiled coil structures with molar ellipticity values at 222 nm of ~ -25200 deg dmol^{-1} cm^2 and ~ -26300 deg dmol^{-1} cm^2, respectively. As evidenced by GuHCl denaturation titrations, the addition of Hg(II) to the Cys$_3$ site further stabilizes both $(\mathbf{GR}L16CL26TL30H)_3{}^{n-}$ and $(\mathbf{GR}L16CL26DL30H)_3{}^{n-}$, as for $(\mathbf{TRI}L9CL23H)_3{}^{n-}$ (Figure 4-3).
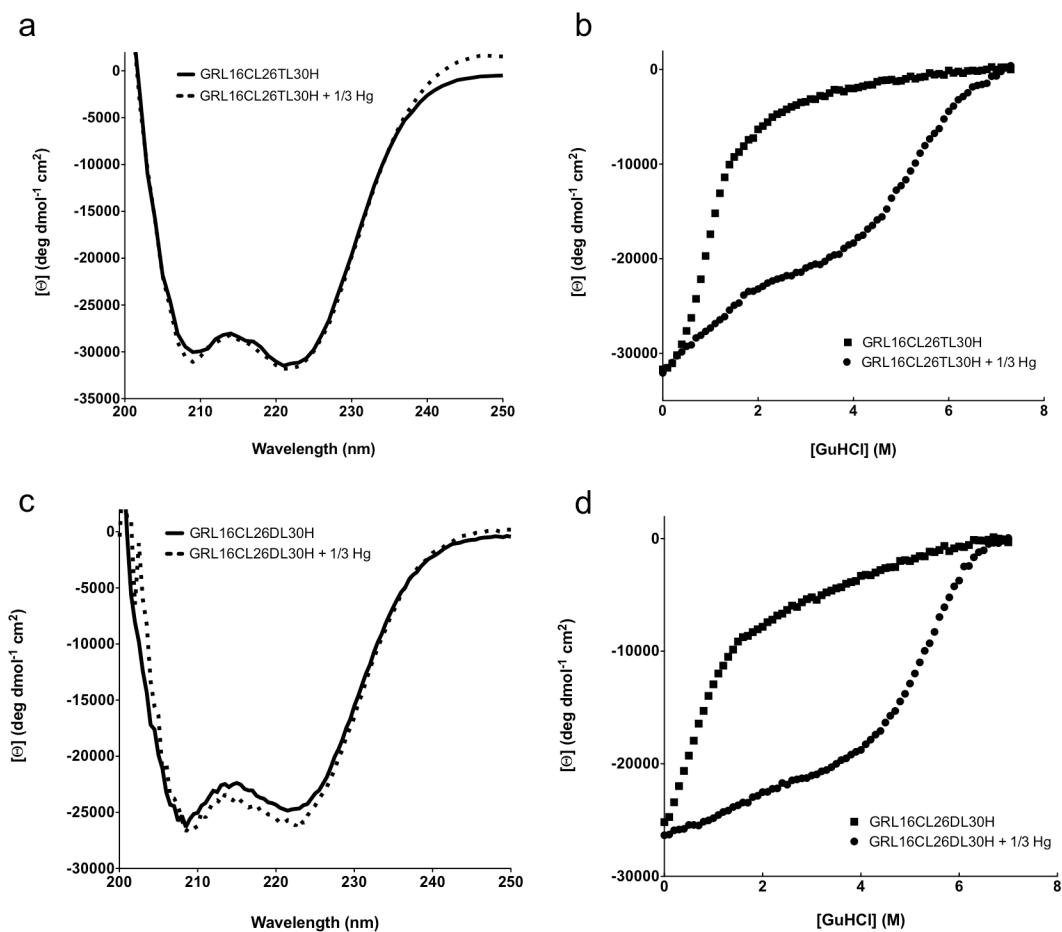
Figure 4-2. Folding of GRL16CL26TL30H (apo and + 1/3 Hg(II)) and GRL16CL26DL30H (apo and + 1/3 Hg(II)) as monitored by CD. a) CD spectra of GRL16CL26TL30H and GRL16CL26TL30H + 1/3 Hg(II) at pH 8.5 and 25 °C. The [Θ] values at 222 nm are ~ -31700 and ~ -32100 deg dmol^{-1} cm^2, respectively. b) GuHCl denaturation titrations represented by [Θ] at 222 nm vs denaturant concentration for GRL16CL26TL30H and GRL16CL26TL30H + 1/3 Hg(II). c) CD spectra of GRL16CL26DL30H and GRL16CL26DL30H + 1/3 Hg(II) at pH 8.5 and 25 °C. The [Θ] values at 222 nm are ~ -25200 and ~ -26300 deg dmol^{-1} cm^2, respectively. d) GuHCl denaturation titrations represented by [Θ] at 222 nm vs denaturant concentration for GRL16CL26DL30H and GRL16CL26DL30H + 1/3 Hg(II).
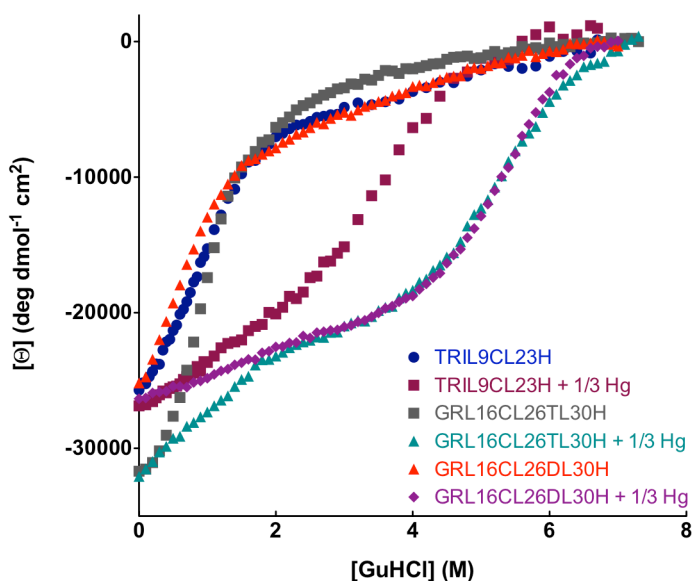
Figure 4-3. Comparison of the unfolding of TRIL9CL23H (apo and + 1/3 Hg(II)) to GRL16CL26TL30H (apo and + 1/3 Hg(II)) and GRL16CL26DL30H (apo and + 1/3 Hg(II))[6]**. GuHCl denaturation titrations at pH 8.5 represented by the molar ellipticity values [Θ] at 222 nm vs denaturant concentration for TRIL9CL23H, GRL16CL26TL30H, and GRL16CL26DL30H. For each of the Cys-containing peptides, when comparing the apo versions and the Hg(II)-bound peptides, the midpoint is shifted to a higher denaturant concentration, demonstrating that the structural site confers stability on each of the constructs.**

b) Zn(II) Binding to His$_3$ Sites. The colorimetric chelator Zincon was used in competitive binding titrations to measure the apparent binding affinities of Zn(II) to $[\text{Hg(II)}]_S(\textbf{GR}\text{L16CL26TL30H})_3{}^{n-}$ and $[\text{Hg(II)}_S](\textbf{GR}\text{L16CL26DL30H})_3{}^{n-}$, both of which represent potential His$_3$ binding sites. The binding affinities were measured at pH 7.5 and 9.0 and apparent dissociation constants resulting from fits of the data (as described in Materials and Methods) are reported in Table 4-2, along with comparisons to data from Chapters 2 and 3. Representative plots of fitted data are shown for each peptide, $[\text{Hg(II)}]_S(\textbf{GR}\text{L16CL26TL30H})_3{}^{n-}$ and $[\text{Hg(II)}_S](\textbf{GR}\text{L16CL26DL30H})_3{}^{n-}$, at pH 7.5 and 9.0 (Figures 4-4-4-5). For both complexes, Zn(II) binding was weaker at pH 7.5 but with strong dissociation constants in the low nM range (~6 nM for $[\text{Hg(II)}]_S(\textbf{GR}\text{L16CL26TL30H})_3{}^{n-}$ and ~4 nM for $[\text{Hg(II)}_S](\textbf{GR}\text{L16CL26DL30H})_3{}^{n-}$). Notably, at pH 7.5, Zincon could not compete with Zn(II)-bound peptide and so the competitive binding experiment was only successful in the reverse direction (where

161

Table 4-2. Apparent dissociation constants for Zn(II) binding to His$_3$ sites in the TRI and Grand peptides.[a]

Peptide complex	$K_{d,app}$ (µM) at pH 7.5	$K_{d,app}$ (µM) at pH 9.0
$[Zn(II)(OH_2/OH^-)]_N$ (**TRI**L2WL23H)$_3{}^{n+}$	0.6 ± 0.1	0.24 ± 0.02
$[Hg(II)]_S[Zn(II)(OH_2/OH^-)]_N$ (**TRI**L9CL23H)$_3{}^{n+}$	0.8 ± 0.1	0.22 ± 0.06
$[Zn(II)(OH_2/OH^-)]_N[Hg(II)]_S$ (**TRI**L9HL23C)$_3{}^{n+}$	~8	0.8 ± 0.3
$[Hg(II)]_S[Zn(II)(OH_2/OH^-)]_N$ (**TRI**L9CL19H)$_3{}^{n+}$	3.7 ± 1.3	0.4 ± 0.2
$[Hg(II)]_S[Zn(II)(OH_2/OH^-)]_N$ (**GR**L2WL16CL30H)$_3{}^{n+}$	0.4 ± 0.1	0.11 ± 0.05
$[Hg(II)]_S[Zn(II)(OH_2/OH^-)]_N$ (**GR**L16CL26TL30H)$_3{}^{n+}$	~0.006[b]	0.0031 ± 0.0005
$[Hg(II)]_S[Zn(II)(OH_2/OH^-)]_N$ (**GR**L16CL26DL30H)$_3{}^{n+}$	~0.004[b]	0.0023 ± 0.0014

a. pH 7.5 measured in 50 mM HEPES buffer, 0.1 M Na$_2$SO$_4$; pH 9.0 measured in 50 mM CHES buffer, 0.1 M Na$_2$SO$_4$.

b. The estimated apparent dissociation constant is based solely on the reverse titration (ZnZi + pep$_3$) because Zincon could not sufficiently compete with the peptide for zinc to obtain a complete titration in the forward direction.
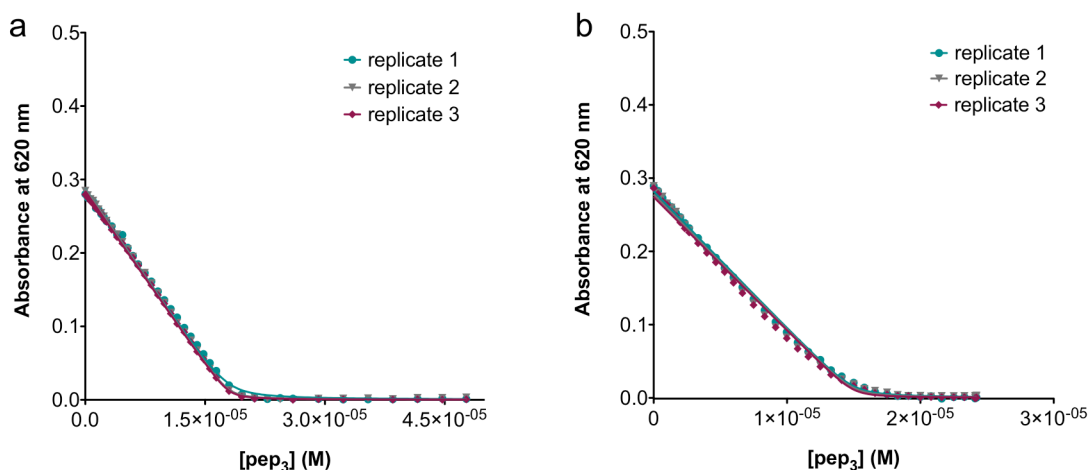

Figure 4-4. Competitive Zn(II)-binding titrations against Zincon at pH 7.5 for [Hg(II)]$_S$(GRL16CL26TL30H)$_3{}^{n-}$ and [Hg(II)]$_S$(GRL16CL26DL30H)$_3{}^{n-}$. Plots of absorbance at 620 nm vs [pep$_3$] for the reverse titrations of a) [Hg(II)]$_S$(GRL16CL26TL30H)$_3{}^{n-}$ (15 µM Zn(II)Zi) and b) [Hg(II)]$_S$(GRL16CL26DL30H)$_3{}^{n-}$ (15 µM Zn(II)Zi).

increments of Hgpep$_3$ are added to ZnZi). At pH 9.0, where the binding affinity of Zn(II) to Zincon is stronger, the competition was successful in both directions. Dissociation constants of 3.1 ± 0.5 nM and 2.3 ± 1.4 nM were obtained for Zn(II) binding to

[Hg(II)]$_S$(**GR**L16CL26TL30H)$_3^{n-}$ and [Hg(II)$_S$](**GR**L16CL26DL30H)$_3^{n-}$, respectively, and may be slightly stronger than those estimated at pH 7.5. These are significantly (~70-100-fold) stronger than those for the L23H sites in **TRI** peptides and ~40-fold stronger than the 30H site in **GR**L2WL16CL30H).
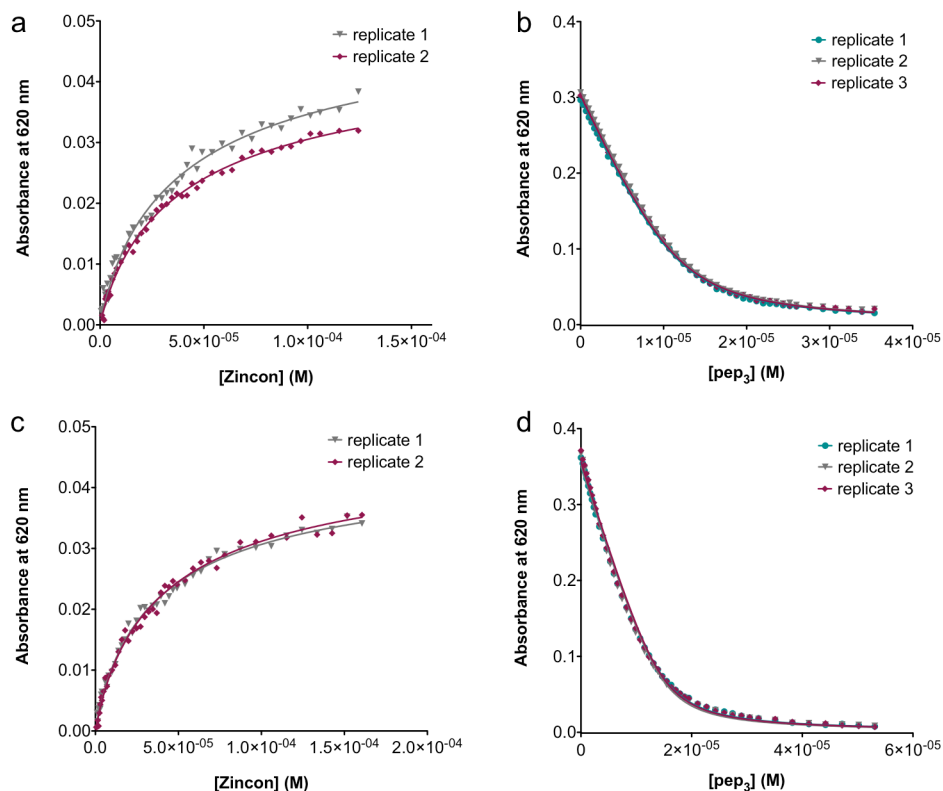

Figure 4-5. Competitive Zn(II)-binding titrations against Zincon at pH 9.0 for [Hg(II)]$_S$(GRL16CL26TL30H)$_3^{n-}$ and [Hg(II)]$_S$(GRL16CL26DL30H)$_3^{n-}$. Plots of absorbance at 620 nm vs [Zincon] for the forward titrations of a) 2 µM [Zn(II)(OH$_2$/OH$^-$)]$_N$[Hg(II)]$_S$(GRL16CL26TL30H)$_3^{n+}$, b) 2 µM [Zn(II)(OH$_2$/OH$^-$)]$_N$[Hg(II)]$_S$(GRL16CL26DL30H)$_3^{n+}$ and vs [pep$_3$] for the reverse titrations of c) [Hg(II)]$_S$(GRL16CL26TL30H)$_3^{n-}$ (12.5 µM Zn(II)Zi), and d) [Hg(II)]$_S$(GRL16CL26DL30H)$_3^{n-}$ (15 µM Zn(II)Zi).

c) [113]Cd **NMR Spectroscopy for Cd(II) Binding to His$_3$ Sites.** The [113]Cd NMR spectrum of **TRI**L23H was recorded in the presence of 0.9 equivalents of [113]Cd(NO$_3$)$_2$ beginning at pH 5.6 and titrating up to pH 9.8 (Figure 4-6). A low intensity chemical shift at 146 ppm was observed at pH 5.6. The signal did not shift with an increase in pH but the intensity did increase noticeably from pH 5.6 to 7.5. A single chemical shift was observed all the way to pH 9.0. At pH 9.25 and 9.5, a second chemical shift appeared at
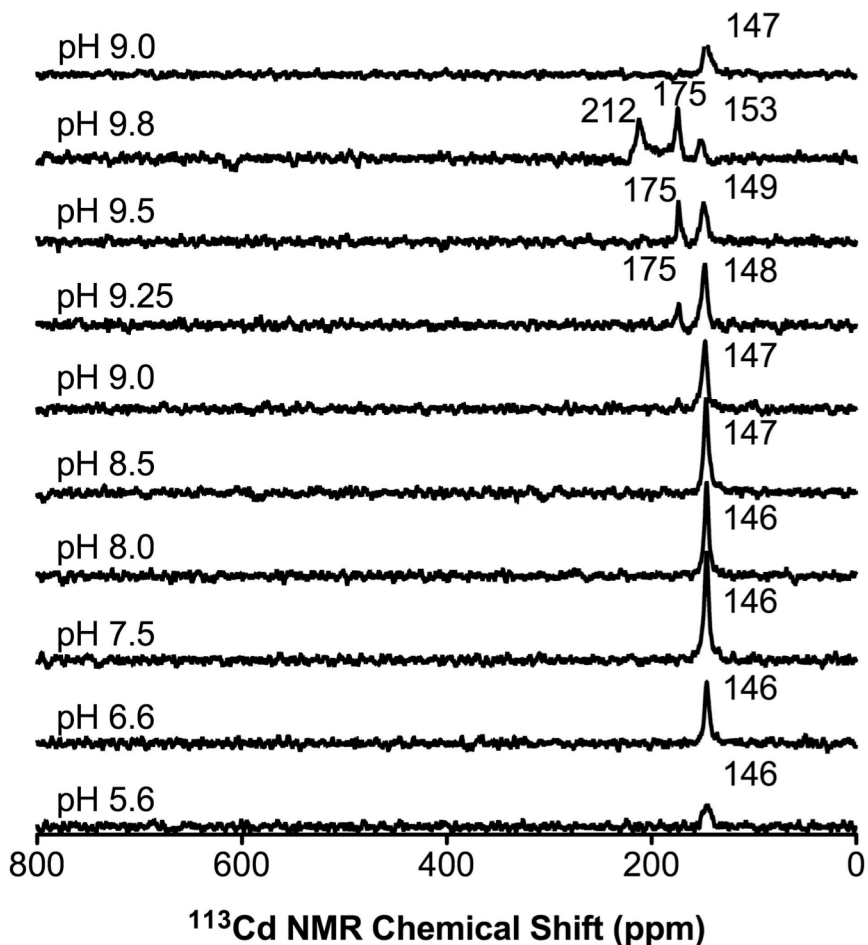
163

Figure 4-6. [113]Cd NMR spectra of a solution of 10 mM (TRIL23H)$_3$ and 0.9 equiv. [113]Cd(NO$_3$)$_2$ at different pH values from 5.6 to 9.8. The titration was initiated at low pH and the pH increased using a concentrated potassium hydroxide solution. At the end of the titration, the pH was decreased back to pH 9.0 using a concentrated nitric acid solution.

175 ppm and increased in intensity with increasing pH. At pH 9.5, the two chemical shifts are roughly equal in height, but may differ in their peak widths. Above pH 9.5, the original peak around 150 ppm decreases further in intensity and a third peak appears at 212 ppm. It is important to keep in mind that the 3SCC structure may begin unfolding under high pH conditions such as these. Titration back down to pH 9.0 (with nitric acid) leads to a regeneration of the single chemical shift at 147 ppm, demonstrating that pH-dependent changes to the Cd(II) coordination environment are reversible. There has been some discussion in the CA literature regarding the substitution of [113]Cd and the resulting chemical shifts and their discrepancies.[29–31] While this will be described in more detail in
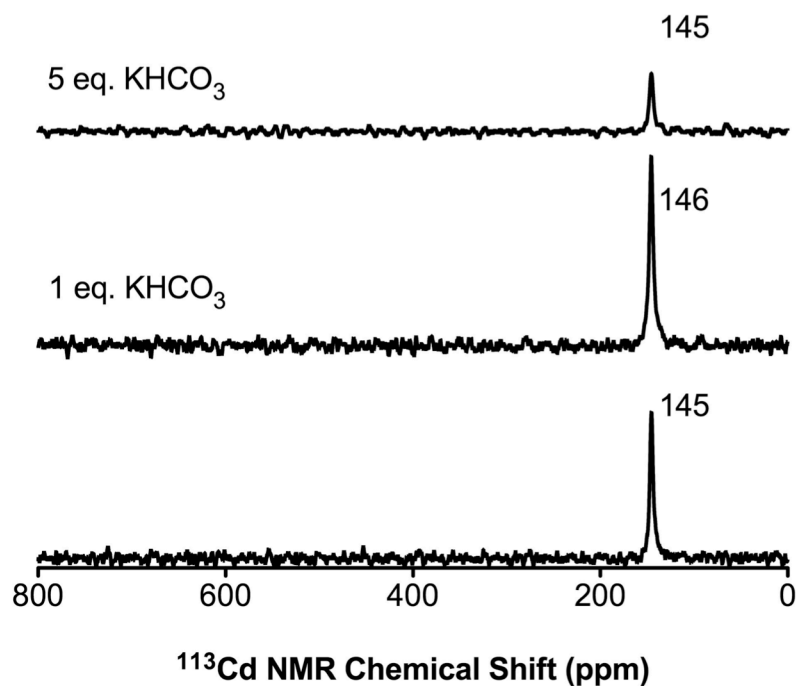
Figure 4-7. ^{113}**Cd NMR spectra of a solution of 14.4 mM (TRIL23H)₃ and 0.9 equiv.** ^{113}**Cd(NO₃)₂ in the absence and presence of one (diluting the peptide trimer concentration to 12.9 mM) and five (diluting the peptide trimer concentration to < 6.5 mM) equivalents of potassium bicarbonate at pH 8.3.**

the Discussion section, it was proposed that binding of bicarbonate to the Cd(II) center at pH 8.3 (from reacting with CO_2 in solution) could result in an upfield chemical shift.[31] Therefore, care was taken throughout this titration and in a freshly prepared sample to thoroughly de-gas with argon and minimize air exposure to the solution. Potassium bicarbonate was then titrated into a fresh sample (after ensuring the initial signal was the same as observed in the pH titration experiment) to determine if a shift in the signal could be observed at pH 8.3. There was no shift up to five equivalents (~30 mM accounting for dilution) (Figure 4-7). Further, CO_2 hydration experiments that will be described in Chapter 5 indicate that the CO_2 present from air in the solution is less than 2.5 mM, so the K_M (assuming it roughly represents the dissociation constant of CO_2 to the Cdpep₃ complex) for the CO_2 reaction would need to be very low (it is not, it is ~9 mM, which is relatively high and reflects the lack of a designed substrate-binding pocket).

d) Co(II) Binding. UV-Vis spectroscopy was used to measure the binding of CoSO₄ to **TRI**L2W**L23H**, **GR**L16C**L26T**L30H, **GR**L16C**L26D**L30H, and **TRI**L2W as a
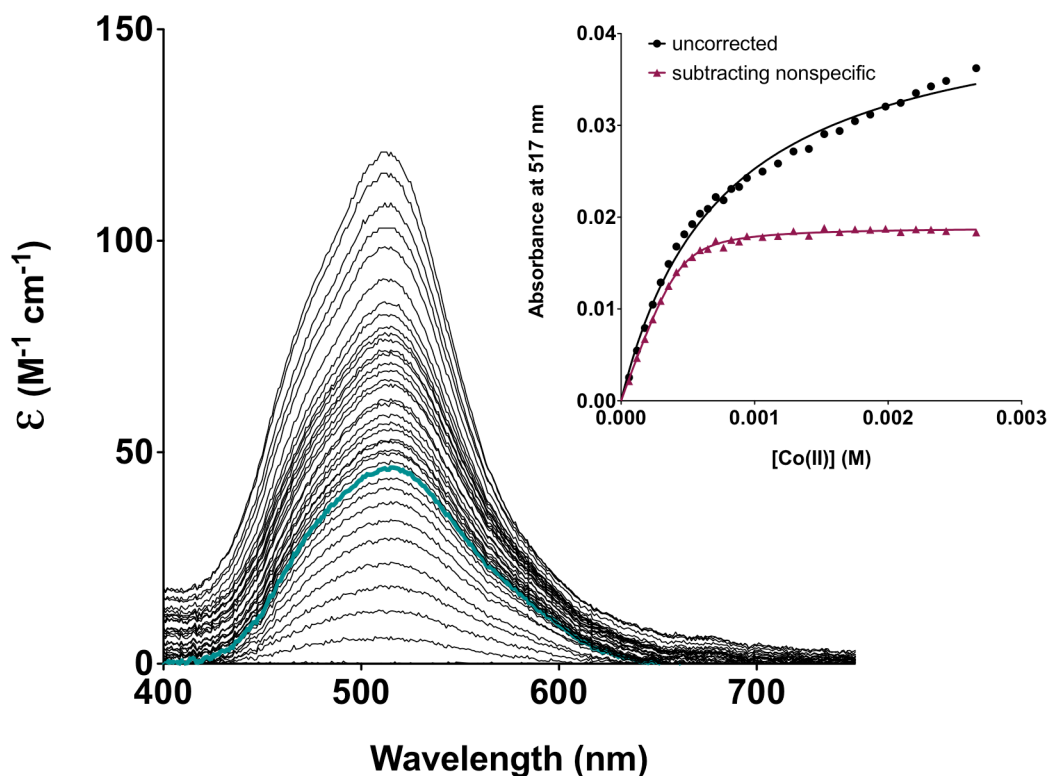
Figure 4-8. UV-Vis titration of $CoSO_4$ into a solution of 0.44 mM $(TRIL2WL23H)_3$ at pH 7.6 in 50 mM HEPES buffer, 0.1 M Na_2SO_4. The data are plotted as molar extinction coefficient (ε, determined using the peptide trimer concentration) vs wavelength. Additions are made in 0.1 equivalent increments up to 1.6 equivalents and then in larger increments (0.2 up to 4.2 equivalents, 0.4 up to 5 equivalents, 0.8 up to 9 equivalents, and then another equivalent up to 10). The spectrum at 1:1 is shown in teal. The inset to the figure displays the titration curve plotted as absorbance at 517 nm (λ_{max}) vs $[CoSO_4]$. The black circles represent the raw absorbance data and the magenta triangles represent the absorbance corrected for non-specific binding, as described in the Results section. The concentration of $CoSO_4$ is corrected for dilution. The data is fitted as described in Materials and Methods.

control. For Co(II) binding to **TRI**L2WL23H, aliquots of $CoSO_4$ were added to a solution of 0.44 mM pep_3 in 50 mM HEPES buffer with 0.1 M Na_2SO_4 at pH 7.6 and the absorbance spectra were measured from 400-750 nm. With increasing [Co(II)], the absorbance spectrum grows with λ_{max} at 517 nm (Figure 4-8). As a control, aliquots of $CoSO_4$ were added to a solution of 0.45 mM $(\mathbf{TRI}L2W)_3$ in 50 mM HEPES buffer with 0.1 M Na_2SO_4 at pH 7.8 and the absorbance spectrum measured from 400-750 nm. As for **TRI**L2WL23H, the absorbance spectrum grows with increasing [Co(II)], but the λ_{max} is
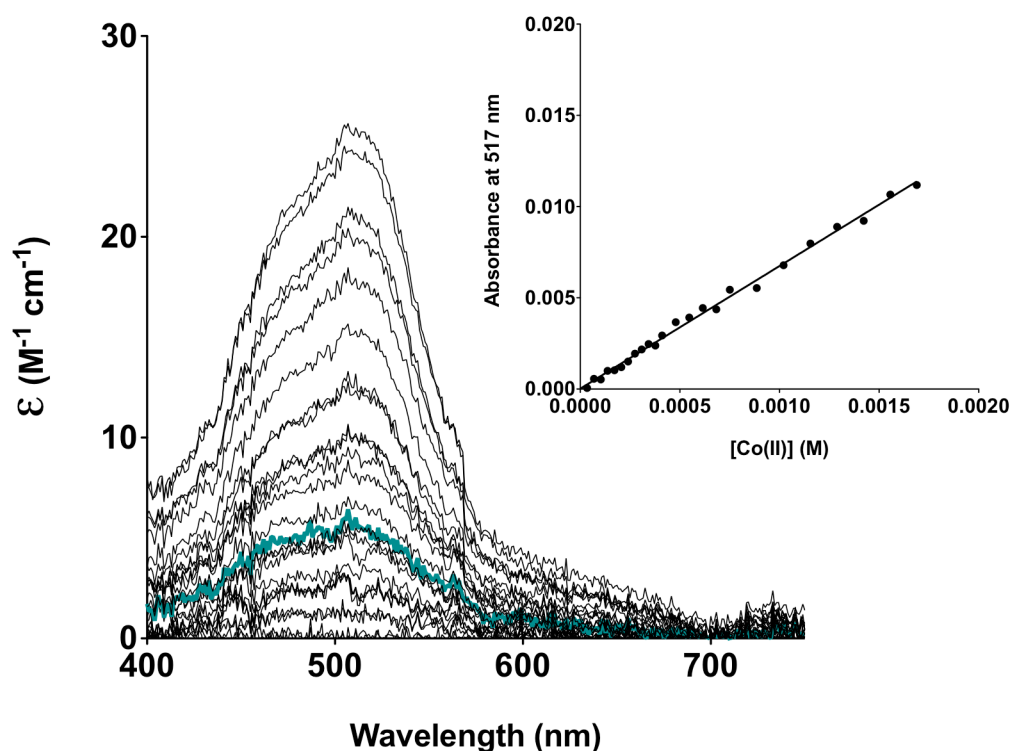
Figure 4-9. UV-Vis titration of CoSO$_4$ into a solution of 0.45 mM (TRIL2W)$_3$ at pH 7.8 in 50 mM HEPES buffer, 0.1 M Na$_2$SO$_4$. The data are plotted as molar extinction coefficient (ε, determined using the peptide trimer concentration) vs wavelength. Additions are made in 0.1 equivalent increments up to 1.2 equivalents and then in larger increments (0.2 up to 2.2 equivalents and 0.4 up to 5 equivalents). The spectrum at 1:1 is shown in teal. The inset to the figure displays the titration curve plotted as absorbance at 517 nm vs [CoSO$_4$]. The black circles represent the raw absorbance data and the concentration of CoSO$_4$ is corrected for dilution. The data is fitted as described in the Results section.

shifted to 510 nm with a shoulder at 470 nm (Figure 4-9). This absorbance spectrums matches very well with that reported for $[Co(OH_2)_6]^{2+}$.[32] The absorbance at λ_{max} for each peptide is plotted vs the concentration of CoSO$_4$. For **TRIL2WL23H**, the plot looks like a binding curve and, while the slope changes at ~1 equivalent, it does not level off as expected for 1:1 binding. For **TRIL2W**, the plot increases linearly, indicating that there is no single binding site. The observed absorbance may be due to aqueous Co(II) in solution or to some non-specific binding to carboxylate groups on the surface of the 3SCC. However, the absorbance spectrum for **TRIL2W** indicates that there is a significant contribution to the absorbance at 517 nm even in the absence of the His$_3$-binding site. Therefore, reasoning that this non-specific contribution to the absorbance may be

affecting the spectra for **TRI**L2WL23H, it was manually subtracted. This was done by first plotting the absorbance at 517 nm vs [CoSO$_4$] for **TRI**L2W to get the extinction coefficient from the slope of a linear fit (ε = 6.72 M^{-1} cm^{-1}). This may then be used to estimate the contribution to the absorbance by using the Beer-Lambert law and the concentration of Co(II) at each absorbance. The estimated absorbance contribution was then subtracted from the total absorbance at each concentration of Co(II). The resulting plot now clearly demonstrates 1:1 Co(II) to (**TRI**L2WL23H)$_3$ binding. Fitting the binding curve directly (as described in Materials and Methods) resulted in K_d = 35 ± 4 µM and ε = 43 ± 1 M^{-1} cm^{-1} (Table 4-3). The low extinction coefficient is representative of a six-coordinate Co(II)-binding site, likely CoHis$_3$(H$_2$O)$_3$.[33,34]

Table 4-3. Apparent dissociation constants and extinction coefficients for Co(II) binding to His$_3$ sites in the TRI and Grand peptides.

Peptide complex	$K_{d,app}$ (µM)	λ_{max} (M^{-1} cm^{-1})
[Zn(II)(OH$_2$/OH$^-$)]$_N$(**TRI**L2WL23H)$_3$$^{n+(a)}$	35 ± 4	43 ± 1
[Zn(II)(OH$_2$/OH$^-$)]$_N$(**TRI**L2WL23H)$_3$$^{n+(b)}$	NA	~30
[Zn(II)(OH$_2$/OH$^-$)]$_N$(**TRI**L2WL23H)$_3$$^{n+}$ + chloride$^{(c)}$	NA	~200
[Hg(II)]$_S$[Zn(II)(OH$_2$/OH$^-$)]$_N$(**GR**L16CL26TL30H)$_3$$^{n+(d)}$	3.2 ± 1.0	296 ± 4
[Hg(II)]$_S$[Zn(II)(OH$_2$/OH$^-$)]$_N$(**GR**L16CL26DL30H)$_3$$^{n+(e)}$	25 ± 4	101 ± 3

a. pH 7.6 measured in 50 mM HEPES buffer, 0.1 M Na$_2$SO$_4$. λ_{max} at 517 nm.
b. pH 10.65, unbuffered and estimated from pH titration. λ_{max} at 580 nm.
c. pH 7.5, 50 mM HEPES buffer, 0.1 M Na$_2$SO$_4$. λ_{max} at 590 nm. Extinction coefficient determined using final spectrum.
d. pH 7.6, 50 mM HEPES buffer, 0.1 M Na$_2$SO$_4$. λ_{max} at 557 nm.
e. pH 7.3, 50 mM HEPES buffer, 0.1 M Na$_2$SO$_4$. λ_{max} at 543 nm.

Next, I wanted to determine whether the Co(II)-binding site would change with pH. For Co(II)-substituted CA, a pH-dependent spectroscopic change in the UV-Vis spectrum is observed and correlates well with the kinetic pK_a for Zn(II)-catalyzed hydrolysis, representing a transition from metal-bound water to active metal-bound hydroxide species.[35–37] Assuming that the pK_a is not shifted between Zn(II) and Co(II) in **TRI**L2WL23H, a similar pH dependence in the Co(II) spectra may be observed. Aliquots of KOH were added to a solution of 0.47 mM (**TRI**L2WL23H)$_3$ and 0.23 mM CoSO$_4$ and the absorbance spectra measured from 400-750 nm. The pH titration from pH ~3-11.75 indicates Co(II) binding from pH 5.5 up. Relatively small changes are observed up to pH 9.75 (Figure 4-10a). Above pH 9.75, the peak at 517 nm levels off and
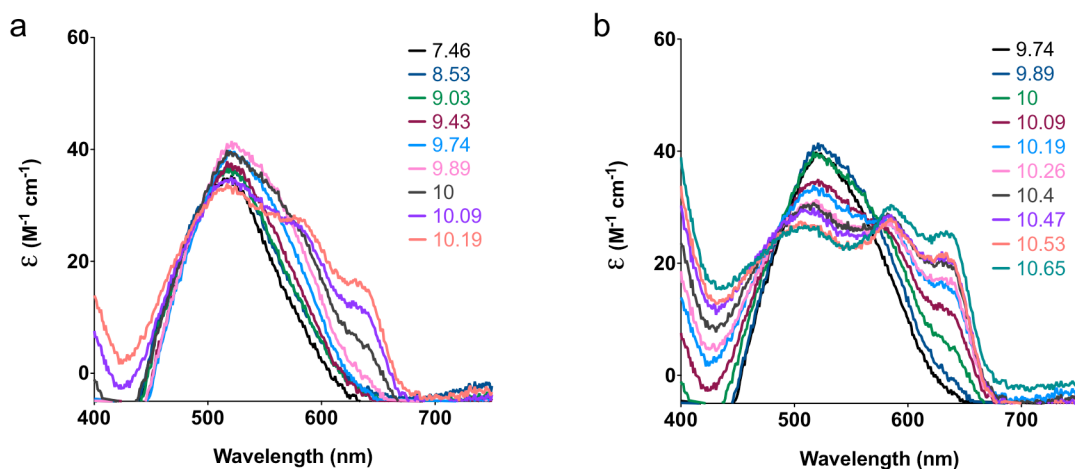
Figure 4-10. UV-Vis spectra representing the pH titration of 0.47 mM (TRIL2WL23H)$_3$ + 0.23 mM CoSO$_4$. The data are plotted as molar extinction coefficient (ε, determined using the peptide trimer concentration) vs wavelength. pH values are color-coded. The pH titration was initiated at low pH and increased using concentrated potassium hydroxide solutions. Selected spectra are shown and split into two separate plots for clarity. a) Spectra from pH 7.46 to 10.19. b). Spectra from pH 9.74 to 10.65.

begins to decrease, and a shoulder at ~580 nm and peak at ~630 nm begin to grow in. As the pH is increased further, the peak at 517 nm shifts to higher energy (up to 507 nm) and those at 580 and 630 nm continue to grow up to pH 10.65 (Figure 4-10b). All absorbance values decrease at even higher pH, probably due to unfolding of the peptide complex (which is also likely to occur beginning above pH 9.5, but in this case it appears that the presence of Co(II) prevents complete unfolding until pH > 10.65).

Anion binding to the Co(II) center in proteins can also be investigated. To determine the effects on the $[Co(II)(OH_2/OH^-)_x]_N(\mathbf{TRI}L2WL23H)_3{}^{n+}$ complex, aliquots of KCl were added to a solution containing 0.52 mM $[Co(II)(OH_2/OH^-)_x]_N$ $(\mathbf{TRI}L2WL23H)_3{}^{n+}$ in 50 mM HEPES buffer with 0.1 M Na$_2$SO$_4$ at pH 7.5. With a total addition of ~800 equivalents of KCl (0.3 M final concentration of chloride), the UV-Vis spectrum changes significantly (Figure 4-11). The absorbance at λ_{max} (517 nm) decreases and a spectrum with three new peaks grows in (λ_{max} at 590 nm with shoulders at 555 nm and 609 nm). Based on the final spectrum, the extinction coefficient at 590 nm is ~200 M^{-1} cm^{-1}. The increased extinction coefficient supports a decrease in the coordination number on the Co(II) center to either four- or five-coordinate. The
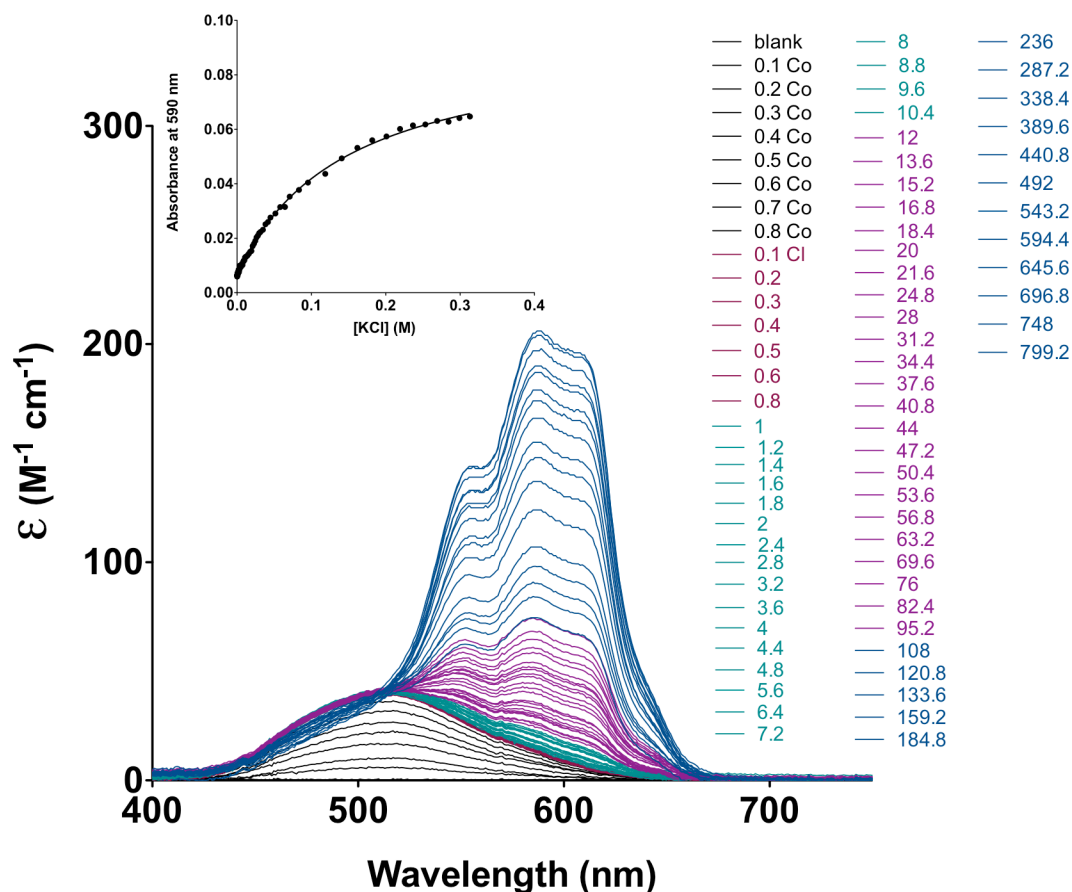
Figure 4-11. UV-Vis spectra for the chloride-binding titration of 0.52 mM [Co(II)(OH$_2$/OH$^-$)$_x$]$_N$(TRIL2WL23H)$_3^{n+}$ at pH 7.5 in 50 mM HEPES buffer, 0.1 M Na$_2$SO$_4$. The data are plotted as molar extinction coefficient (ε, determined using the peptide trimer concentration) vs wavelength. Additions are made in 0.1 equivalent increments up to 1.0 equivalents for Co(II). Chloride addition increments are gradually increased from 0.1 equivalents to ~50 equivalents at the end of the titration (total of ~800 equivalents) in order to observe the changes associated with chloride binding. Batches of data are color-coded as indicated in the figure legend. The inset to the figure displays the titration curve plotted as absorbance at 590 nm (λ$_{max}$ in the presence of chloride) vs [Cl$^-$]. The black circles represent the raw absorbance data. The concentrations of CoSO$_4$ and Cl$^-$ are corrected for dilution. The data is fitted as described in Materials and Methods.

absorbance at 590 nm for each addition of KCl is plotted vs the concentration of KCl and fitted to estimate a dissociation constant for the chloride anion, 0.145 ± 0.004 M. While fairly weak, this is stronger than the dissociation constant for chloride binding to a Co(II)-Cys$_2$His site in a zinc finger mutant peptide (K_d = 0.8 M).[38] Also notable is that the kinetic inhibition constant for chloride-induced inhibition of CA (which binds directly
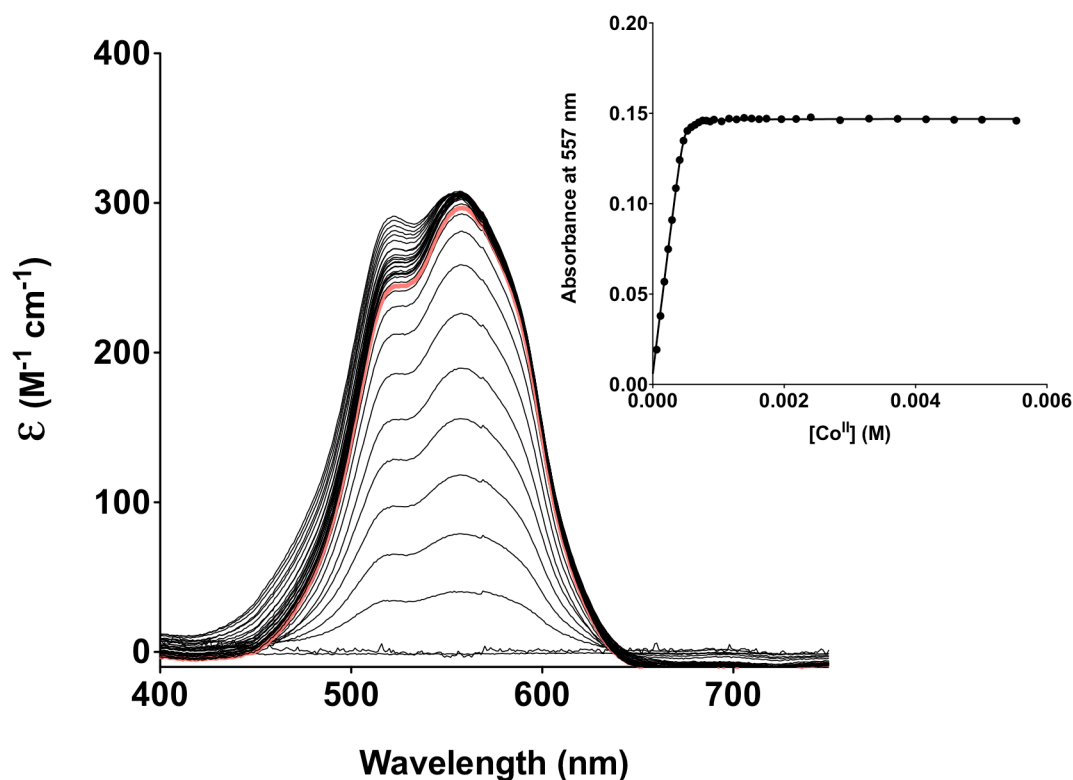
Figure 4-12. UV-Vis titration of CoSO$_4$ into a solution of 0.48 mM [Hg(II)]$_S$(GRL16CL26TL30H)$_3{}^{n-}$ at pH 7.6 in 50 mM HEPES buffer, 0.1 M Na$_2$SO$_4$. The data are plotted as molar extinction coefficient (ε, determined using the peptide trimer concentration) vs wavelength. Additions are made in 0.1 equivalent increments up to 1.6 equivalents and then in larger increments (0.2 up to 3 equivalents, 0.4 up to 4.2 equivalents, 0.8 up to 9 equivalents and then another equivalent up to 10). The spectrum at 1:1 is shown in pink. The inset to the figure displays the titration curve plotted as absorbance at 557 nm (λ_{max}) vs [CoSO$_4$]. The black circles represent the raw absorbance data (which did not have to be corrected for non-specific binding in this case) and the concentration of CoSO$_4$ is corrected for dilution. The data is fitted as described in Materials and Methods.

to Zn(II)) is 0.19 M at pH 7.55.[39–41] Finally, the estimated chloride-binding affinity to [Co(II)(OH$_2$/OH$^-$)$_x$]$_N$(**TRI**L2WL23H)$_3{}^{n+}$ is also ~two-fold stronger than the inhibition constant determined for acetate-induced inhibition of *p*NPA hydrolysis by [Zn(II)(OH$_2$/OH$^-$)]$_N$(**TRI**L2WL23H)$_3{}^{n+}$ (0.34 ± 0.01 M), as reported previously[7] and described in Chapter 2.

For Co(II) binding to [Hg(II)]$_S$(**GR**L16CL26TL30H)$_3{}^{n-}$, aliquots of CoSO$_4$ were added to a solution of 0.48 mM pep$_3$ in 50 mM HEPES buffer with 0.1 M Na$_2$SO$_4$ at pH 7.6 and the absorbance spectra measured from 400-750 nm. With increasing [Co(II)], the
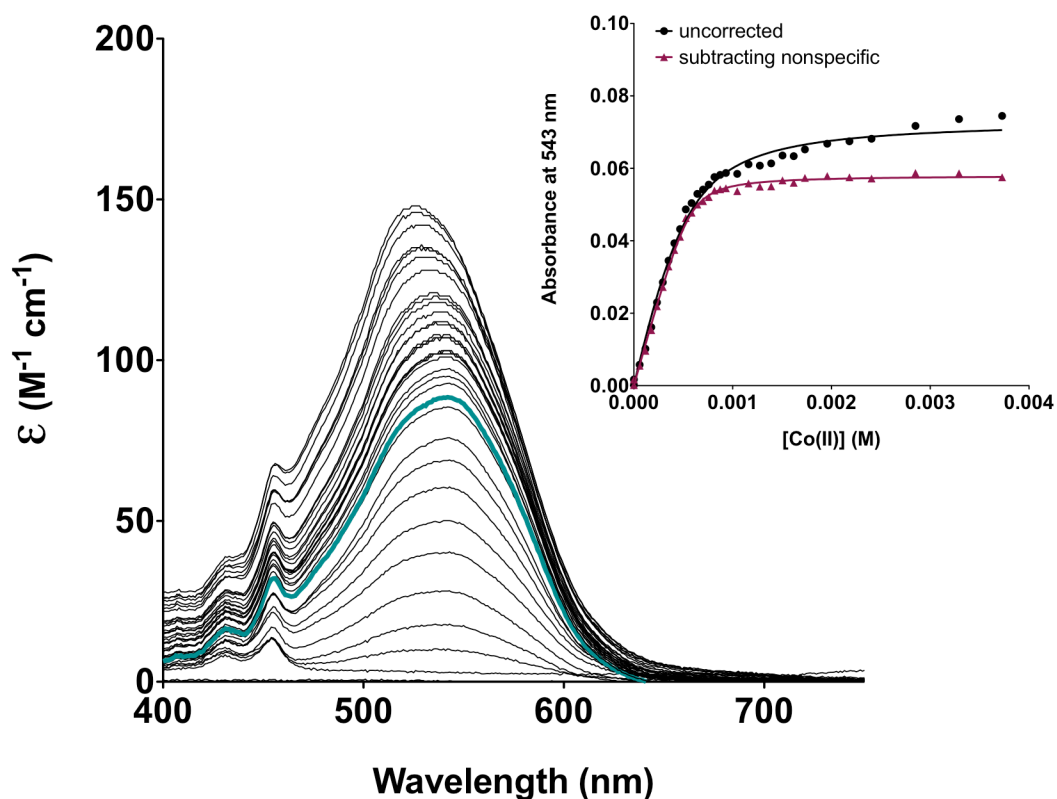
171

Figure 4-13. UV-Vis titration of CoSO$_4$ into a solution of 0.57 mM [Hg(II)]$_S$(GRL16CL26DL30H)$_3^{n-}$ at pH 7.3 in 50 mM HEPES buffer, 0.1 M Na$_2$SO$_4$. The data are plotted as molar extinction coefficient (ε, determined using the peptide trimer concentration) vs wavelength. Additions are made in 0.1 equivalent increments up to 1.6 equivalents and then in larger increments (0.2 up to 4.2 equivalents, 0.4 up to 5 equivalents, 0.8 up to 9 equivalents, and then another equivalent up to 10). The spectrum at 1:1 is shown in teal. The inset to the figure displays the titration curve plotted as absorbance at 543 nm (λ_{max}) vs [CoSO$_4$]. The black circles represent the raw absorbance data and the magenta triangles represent the absorbance corrected for non-specific binding, as described in the Results section. The concentration of CoSO$_4$ is corrected for dilution. The data is fitted as described in Materials and Methods.

absorbance spectrum grows with λ_{max} at 557 nm and a shoulder at 522 nm (Figure 4-12). The absorbance at 557 nm is plotted vs the concentration of CoSO$_4$ to give a binding curve. In this case, the absorbance levels off at one equivalent, indicating a single binding site. The absorbance around 522 nm continues to increase, as expected from the observed non-specific binding for **TRI**L2W and **TRI**L2WL23H. The dissociation constant for Co(II) binding obtained from the fitting is 3.2 ± 1.0 μM and ε_{557} is 296 ± 4 M^{-1} cm^{-1} (Table 4-3). This affinity for Co(II) binding to [Hg(II)]$_S$(**GR**L16CL26TL30H)$_3^{n-}$ is ~10-

172

Table 4-4. pH-dependent kinetic parameters for hydrolysis of pNPA by Zn(II)-bound TRI and Grand peptides.[a]

Peptide complex[b]	pH[c]	k_{cat}/K_M [M^{-1} s^{-1}]	k_{cat} [s^{-1}]	K_M [mM]
[Zn(II)(OH$_2$/OH$^-$)]$_N$ (**TRI**L2WL23H)$_3^{n+}$	7.5	0.41 ± 0.03	0.0011 ± 0.0002	2.7 ± 0.8
	8.0	1.07 ± 0.06	0.0029 ± 0.0005	2.7 ± 0.6
	8.5	3.3 ± 0.2	0.0060 ± 0.0007	1.8 ± 0.3
	9.0	8.9 ± 0.4	0.016 ± 0.001	1.8 ± 0.2
	9.25	12.9 ± 0.4	0.022 ± 0.001	1.7 ± 0.2
	9.5	15.5 ± 0.4	0.033 ± 0.002	2.1 ± 0.2
[Hg(II)]$_S$[Zn(II)(OH$_2$/OH$^-$)]$_N$ (**TRI**L9CL23H)$_3^{n+(d)}$	7.5	1.38 ± 0.04	0.0022 ± 0.0005	1.6 ± 0.4
	8.0	3.1 ± 0.1	0.0054 ± 0.0015	1.7 ± 0.5
	8.5	6.0 ± 0.1	0.012 ± 0.004	1.9 ± 0.6
	8.75	10.8 ± 0.3	0.021 ± 0.010	2.0 ± 0.9
	9.0	17.6 ± 0.3	0.038 ± 0.010	2.1 ± 0.6
	9.5	23.3 ± 0.3	0.040 ± 0.012	1.7 ± 0.5
[Hg(II)]$_S$[Zn(II)(OH$_2$/OH$^-$)]$_N$ (**GR**L2WL16CL30H)$_3^{n+}$	8.0	1.0 ± 0.1	0.0034 ± 0.0008	3.5 ± 1.1
	8.5	3.0 ± 0.1	0.011 ± 0.002	3.7 ± 0.7
	8.75	6.4 ± 0.2	0.022 ± 0.002	3.5 ± 0.5
	9.0	10.8 ± 0.4	0.038 ± 0.005	3.6 ± 0.6
	9.25	14.5 ± 0.4	0.059 ± 0.007	4.0 ± 0.6
	9.5	18.5 ± 0.6	0.064 ± 0.007	3.5 ± 0.5
[Hg(II)]$_S$[Zn(II)(OH$_2$/OH$^-$)]$_N$ (**GR**L16CL26TL30H)$_3^{n+}$	8.5	2.2 ± 0.3	0.0086 ± 0.0053	3.9 ± 2.9
	9.5	14.8 ± 1.4	0.056 ± 0.026	3.8 ± 2.1
[Hg(II)]$_S$[Zn(II)(OH$_2$/OH$^-$)]$_N$ (**GR**L16CL26DL30H)$_3^{n+}$	7.5	0.21 ± 0.04	NA[e]	NA[e]
	8.5	1.8 ± 0.4	0.0017 ± 0.0005	1.0 ± 0.5
	8.75	5.1 ± 0.3	0.0066 ± 0.0006	1.3 ± 0.2
	9.0	11.2 ± 0.8	0.0071 ± 0.0005	0.6 ± 0.1
	9.25	16.0 ± 0.9	0.028 ± 0.003	1.8 ± 0.3
	9.5	24.2 ± 2.5	0.024 ± 0.004	1.0 ± 0.2

a. Error bars result from fitting all individual rates measured (three per concentration of substrate, without averaging) to the Michaelis-Menten equation in Prism 5 (GraphPad Software)[26] or from Lineweaver-Burke analysis.

b. 10-20 µM active Zn(II)-bound complex.

c. pH 7.5-8.0 measured in 50 mM HEPES, 0.1 M Na$_2$SO$_4$; pH 8.5-9.5 measured in 50 mM CHES, 0.1 M Na$_2$SO$_4$.

d. Previously reported data included for comparison.[6]

e. Due to very low activity, the error was too high to obtain an accurate fitting for the individual k_{cat} and K_M values.

fold stronger than that for Co(II) binding to $(\textbf{TRI}L2WL23H)_3$. The extinction coefficient, also ~10-fold higher for $[Hg(II)]_S[Co(II)(OH_2/OH^-)_x]_N(\textbf{GR}L16CL26TL30H)_3{}^{n+}$, suggests a decrease in the coordination number.[33,34]

For Co(II) binding to $[Hg(II)]_S(\textbf{GR}L16CL26DL30H)_3{}^{n-}$, aliquots of $CoSO_4$ were added to a solution of 0.57 mM pep_3 in 50 mM HEPES buffer with 0.1 M Na_2SO_4 at pH 7.3 and the absorbance spectra measured from 400-750 nm. With increasing [Co(II)], the absorbance spectrum grows with a broad λ_{max} at 543 nm (Figure 4-13). The small peaks at higher energy (below 500 nm) are present before the addition of Co(II) and do not significantly change throughout the titration and so are not considered to be due to Co(II) binding. There is some non-specific binding contribution to the absorbance at 543 nm, which is subtracted out following a similar procedure as described above for $[Co(II)(OH_2/OH^-)_x]_N(\textbf{TRI}L2WL23H)_3{}^{n+}$ (ε for $[Co(II)(OH_2/OH^-)_x](\textbf{TRI}L2W)_3{}^{n+}$ at 543 nm is 4.55 M^{-1} cm^{-1}). The fitting of the binding curve gives a dissociation constant of 25 $\pm$ 4 μM and $\varepsilon_{543} = 101 \pm 3$ M^{-1} cm^{-1} (Table 4-3). The binding affinity is slightly stronger than that for $[Co(II)(OH_2/OH^-)_x]_N(\textbf{TRI}L2WL23H)_3{}^{n+}$ (35 $\pm$ 4 μM) and the extinction coefficient is about three-fold higher. The increase in extinction coefficient suggests a lower coordination number and falls into the range expected for a five-coordinate Co(II) protein complex.[33,34]

Characterization of Ester Hydrolysis.

a) Zn(II) site in $[Hg(II)]_S[Zn(II)(OH_2/OH^-)]_N(TRIL9CL19TL23H)_3{}^{n+}$. The complex $[Hg(II)]_S[Zn(II)(OH_2/OH^-)]_N(\textbf{TRI}L9CL19TL23H)_3{}^{n+}$ was measured for hydrolytic activity towards pNPA at pH 9.5. Some activity was observed and could be fit to the Michaelis-Menten equation for a catalytic efficiency of 8.2 $\pm$ 1.3 M^{-1} s^{-1}. However, very little saturation was actually observed, so while estimates of the K_M (~0.7 mM) and k_{cat} (~0.05 s^{-1}) can be obtained, these kinetic parameters have very high error bars. This is likely a result of poor folding of this construct, leading to hydrolytic activity probably representative of a mixture of bound Zn(II) and free His residues.

b) Zn(II) site in [Hg(II)]$_S$[Zn(II)(OH$_2$/OH⁻)]$_N$(GRL16CL26TL30H)$_3^{n+}$. The complex [Hg(II)]$_S$[Zn(II)(OH$_2$/OH⁻)]$_N$(**GR**L16CL26TL30H)$_3^{n+}$ exhibits saturation kinetics for pH-dependent *p*NPA hydrolysis (Table 4-4). The hydrolytic activity was

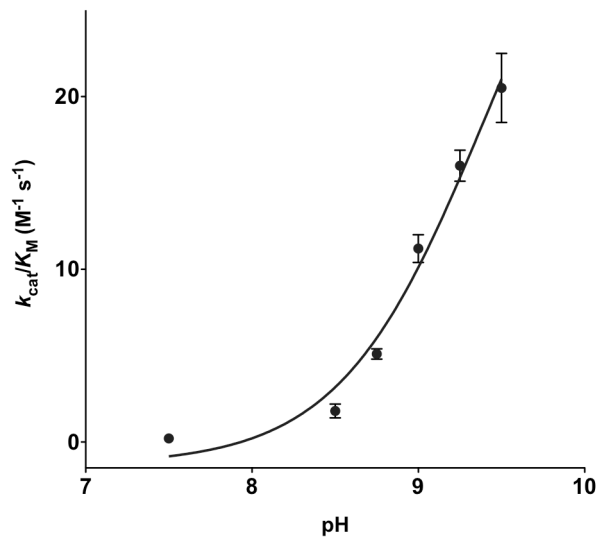**Figure 4-14. pH-dependency of k_{cat}/K_M for *p*NPA hydrolysis by [Hg(II)]$_S$[Zn(II)(OH$_2$/OH⁻)]$_N$(GRL16CL26DL30H)$_3^{n+}$. Error bars result from fitting all individual initial rates measured (three per concentration of substrate, without averaging) to the Michaelis-Menten equation in Prism 5 (GraphPad Software).[26] The fitting equation used for the pH dependence (eq 15) is described in the Results section.**
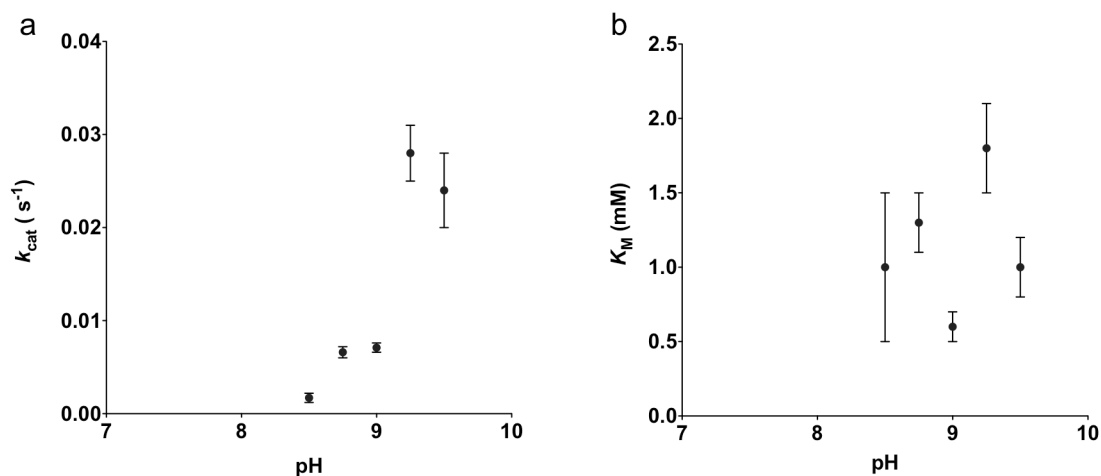

Figure 4-15. pH-dependency of a) k_{cat} and b) K_M parameters for *p*NPA hydrolysis by [Hg(II)]$_S$[Zn(II)(OH$_2$/OH⁻)]$_N$(GRL16CL26DL30H)$_3^{n+}$. Error bars result from fitting all individual initial rates measured (three per concentration of substrate, without averaging) to the Michaelis-Menten equation in Prism 5 (GraphPad Software).[26]

measured at two pH's, 8.5 and 9.5. As for all the peptides described in previous chapters, the K_M does not change with pH (~4 mM) and is very similar to the relatively high K_M observed for [Hg(II)]$_S$[Zn(II)(OH$_2$/OH$^-$)]$_N$(**GR**L2WL16CL30H)$_3^{n+}$ (Chapter 3). The k_{cat} is 0.0086 ± 0.0053 s^{-1} and 0.056 ± 0.026 s^{-1} at pH 8.5 and 9.5, respectively. The catalytic efficiency goes from 2.2 ± 0.3 M^{-1} s^{-1} at pH 8.5 to 14.8 ± 1.4 M^{-1} s^{-1} at pH 9.5, but remains lower than the corresponding value at pH 9.5 for [Hg(II)]$_S$[Zn(II)(OH$_2$/OH$^-$)]$_N$ (**GR**L2WL16CL30H)$_3^{n+}$ (18.5 ± 0.6 M^{-1} s^{-1}, Chapter 3).

Table 4-5. Kinetic pK_a, maximal efficiency, and maximal rate values for pNPA hydrolysis by Zn(II)-bound TRI and Grand peptides.

Peptide complex	pK_a[a]	$k_{cat}/K_{M(max)}$ [M^{-1} s^{-1}][b]	$k_{cat(max)}$ [s^{-1}][c]
[Zn(II)(OH$_2$/OH$^-$)]$_N$(**TRI**L2WL23H)$_3^{n+}$	9.2 ± 0.1	25 ± 2	~0.055
[Hg(II)]$_S$[Zn(II)(OH$_2$/OH$^-$)]$_N$(**TRI**L9CL23H)$_3^{n+}$	9.0 ± 0.1	31 ± 4	~0.053
[Zn(II)(OH$_2$/OH$^-$)]$_N$[Hg(II)]$_S$(**TRI**L9HL23C)$_3^{n+}$	9.2 ± 0.1	24 ± 3	~0.030
[Hg(II)]$_S$[Zn(II)(OH$_2$/OH$^-$)]$_N$(**TRI**L9CL19H)$_3^{n+}$	9.6 ± 0.1	27 ± 5	~0.076
[Hg(II)]$_S$[Zn(II)(OH$_2$/OH$^-$)]$_N$(**GR**L2WL16CL30H)$_3^{n+}$	9.2 ± 0.1	29 ± 3	~0.1
[Hg(II)]$_S$[Zn(II)(OH$_2$/OH$^-$)]$_N$(**GR**L16CL26DL30H)$_3^{n+}$	9.4 ± 0.2	39 ± 9	~0.039

a. Determined by fitting individual k_{cat}/K_M values versus pH.
b. Maximal catalytic efficiency from the fitting of k_{cat}/K_M values versus pH (assuming that 100% active enzyme complex is present).
c. Estimated maximal rate determined as described in the text.

c) Zn(II) site in [Hg(II)]$_S$[Zn(II)(OH$_2$/OH$^-$)]$_N$(GRL16CL26DL30H)$_3^{n+}$. The complex [Hg(II)]$_S$[Zn(II)(OH$_2$/OH$^-$)]$_N$(**GR**L16CL26DL30H)$_3^{n+}$ exhibits saturation kinetics for pH-dependent pNPA hydrolysis (Table 4-4). At pH 7.5, $k_{cat}/K_M = 0.21 ± 0.04$ M^{-1} s^{-1}, but the data could not be fitted accurately for the individual k_{cat} and K_M values. The kinetic parameters increase to 0.024 ± 0.004 s^{-1} for k_{cat} and 24.2 ± 2.5 M^{-1} s^{-1} for k_{cat}/K_M at pH 9.5. The K_M values remain essentially constant, at ~1 mM over the pH range from 8.0 to 9.5. As for the peptides in Chapter 2 and 3, these results indicate a chemical rate-limiting step. The pH-dependency profile can be fitted (k_{cat}/K_M vs pH) to eq 15, and a pK_a of 9.4 ± 0.2 is obtained (Figure 4-14, Table 4-5).

$$k_{obs} = \frac{\left(k_{max} * 10^{(pH-pK_a)}\right) + k_{min}}{1 + 10^{(pH-pK_a)}}$$

(15)

Further, the maximal k_{cat}/K_M, assuming 100% active Zn-hydroxide complex, is 39 ± 9 M^{-1} s^{-1}. A similar trend is found for k_{cat} vs pH, but given the larger errors in k_{cat} due to poor solubility of the substrate, the pK_a and especially the extrapolated maximal k_{cat} value from the fit are not reliable (Figure 4-15). Therefore, the maximal k_{cat} was estimated by using the maximal k_{cat}/K_M and the K_M. Based on this analysis, the maximal k_{cat} is ~0.039 s^{-1}.

d) Cd(II) site in [Cd(II)(OH$_2$/OH$^-$)$_x$]$_N$(TRIL23H)$_3$$^{n+}$. The complex [Cd(II)(OH$_2$/OH$^-$)$_x$]$_N$(**TRI**L23H)$_3$$^{n+}$ exhibits saturation kinetics for pNPA hydrolysis at pH 9.5, but little to no activity at pH 8.5 (Figure 4-16). The catalytic efficiency at pH 9.5 is 3.5 ± 0.2 M^{-1} s^{-1} and the rate is 0.009 ± 0.002 s^{-1}. The K_M is similar to that for the Zn(II)-bound peptide of the same sequence, 2.7 ± 0.7 mM. The data is consistent with a shift in the pK_a to a higher pH than for the Zn(II)-bound complex and is also consistent with the ^{113}Cd NMR pH titration described above, suggesting a pK_a of 9.5 or higher.

e) Co(II) site in [Co(II)(OH$_2$/OH$^-$)$_x$]$_N$(TRIL2WL23H)$_3$$^{n+}$. The complex [Co(II)(OH$_2$/OH$^-$)$_x$]$_N$(**TRI**L2WL23H)$_3$$^{n+}$ exhibits saturation kinetics for pNPA hydrolysis

Figure 4-16. p**NPA hydrolysis by [Cd(II)(OH$_2$/OH$^-$)$_x$]$_N$(TRIL23H)$_3$$^{n+}$ at pH 8.5 and 9.5 in 50 mM CHES buffer, 0.1 M Na$_2$SO$_4$. a) Plots of the initial rates at pH 9.5 vs [pNPA] and fitting to the Michaelis-Menten equation in Prism 5 (GraphPad Software).[26] b) Increase in absorbance at 348 nm (the isosbestic point between products p-nitrophenol and p-nitrophenolate, which are pH-dependent) as a function of time for both [Cd(II)(OH$_2$/OH$^-$)$_x$]$_N$(TRIL23H)$_3$$^{n+}$ and background containing (TRIL23H)$_3$ (described in Materials and Methods) to show the lack of activity by the Cd(II) complex at pH 8.5.**
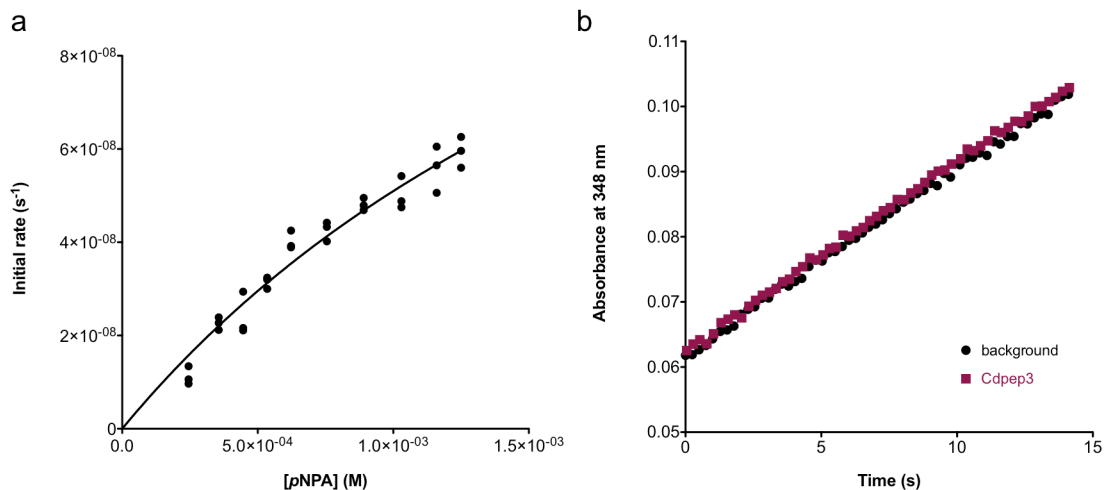
at pH 9.5 (Figure 4-17), although the coordination number of the catalytic species cannot be conclusively defined. The catalytic efficiency is 6.6 ± 0.6 M^{-1} s^{-1} (~30% of that of the original model $[Hg(II)]_S[Zn(II)(OH_2/OH^-)]_N(\textbf{TRI}L9CL23H)_3^{n+}$) and the rate is 0.026 ± 0.009 s^{-1} (compared to 0.04 s^{-1} for the original model). The K_M is noticeably increased (3.9 ± 1.6 mM) relative to the Zn(II)-bound L23H sites (~2 mM). This could be consistent with a higher coordination number around the Co(II) center, leaving less space near the metal center for substrate access.
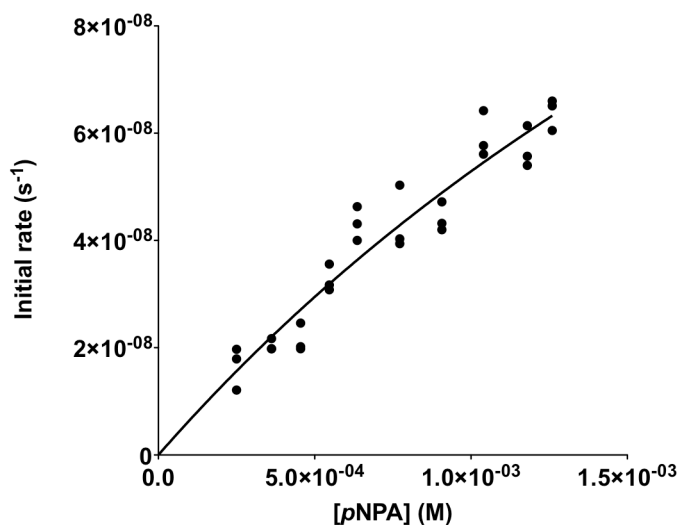

Figure 4-17. pNPA hydrolysis by $[Co(II)(OH_2/OH^-)_x]_N(\textbf{TRI}L2WL23H)_3^{n+}$ at 9.5 in 50 mM CHES buffer, 0.1 M Na_2SO_4. Plots of the initial rates at pH 9.5 vs [pNPA] and fitting to the Michaelis-Menten equation in Prism 5 (GraphPad Software).[26]

Discussion

The aim of the work presented in this chapter is to introduce second coordination sphere interactions around the active zinc center in a *de novo* designed 3SCC. In previous chapters, I showed how a minimal *de novo* designed zinc site in a 3SCC achieves a significant amount of hydrolytic activity, regardless of its location within the coiled coil. Although the catalytic efficiency achieved towards pNPA hydrolysis is faster than any synthetic model and most designed proteins, it remains ~100-fold less than that of the native enzyme, CAII.[6,7,28,42] More importantly, while Zn(II) binds strongly, the dissociation constant is still outside the range for native zinc proteins (nM to pM)[8,43–45]

and the pK_a at which the designed enzyme operates optimally is over two units higher than the native enzyme and outside of the physiological pH range.[46,47] As described above, it is generally accepted that these properties are tuned through secondary interactions around a metal site. Given that an excellent structural model has been obtained for the zinc center found in α-CA's, with a significant amount of catalytic activity and a fairly strong Zn(II)-binding affinity, it is now possible to examine whether such a minimal site may be built from the bottom up (in a scaffold very different from the native enzyme) to include secondary interactions for tuning these properties.

For my initial foray into designing secondary interactions around this *de novo* designed minimal zinc center, I chose to incorporate the residue that, when removed, has one of the largest effects on activity, binding affinity, and pK_a in CA, Thr199.[11,12] In CA, this residue forms a hydrogen bond to the coordinated water molecule (O-O distance = 2.7 Å, Figure 4-18). Using the crystal structure of $[Hg(II)]_S[Zn(II)(OH_2/OH^-)]_N$ (**CSL9PenL23H**)$_3{}^{n+}$ at pH 8.5, PyMOL was employed to model a Thr substitution which has the possibility of forming a hydrogen bond with the coordinated solvent (models were prepared using the mutagenesis option and PyMOL's rotamer library[48]). Since the water molecule is oriented towards the N-terminus (in $[Hg(II)]_S[Zn(II)(OH_2/OH^-)]_N$ (**CSL9PenL23H**)$_3{}^{n+}$), up into the hydrophobic core of the 3SCC, the Thr residue was substituted into the Leu layer directly above the His$_3$ layer. The modeled hydrogen-bonding distance is 2.5 Å (O-O distance) with the closest Zn-Thr distance at 3.4 Å (Zn-O distance, Figure 4-19). It is important to note that, due to the self-assembling nature of these 3SCCs, substitution of a single Thr in the sequence results in a three-fold substitution once the coiled coil is folded, so that there will be three Thr residues above the His$_3$ site. The resulting peptide, **TRI**L9CL19TL23H, did not fold well (Figure 4-1). Although the Hg(II)-bound version, through taking advantage of the structural site, exhibited a significant positive shift in the stability of the construct, it was still only ~60% folded overall (based on α-helical content). Further, examination of *p*NPA hydrolysis by $[Hg(II)]_S[Zn(II)(OH_2/OH^-)]_N$(**TRI**L9CL19TL23H)$_3{}^{n+}$ displayed an efficiency of only 8.2 ± 1.3 M^{-1} s^{-1} at pH 9.5 with a K_M of ~7 mM (saturation kinetics was essentially not observed since the maximum concentration of substrate that could be used was only 1.4 mM). This is likely due to relatively poor complex stability, as a result of
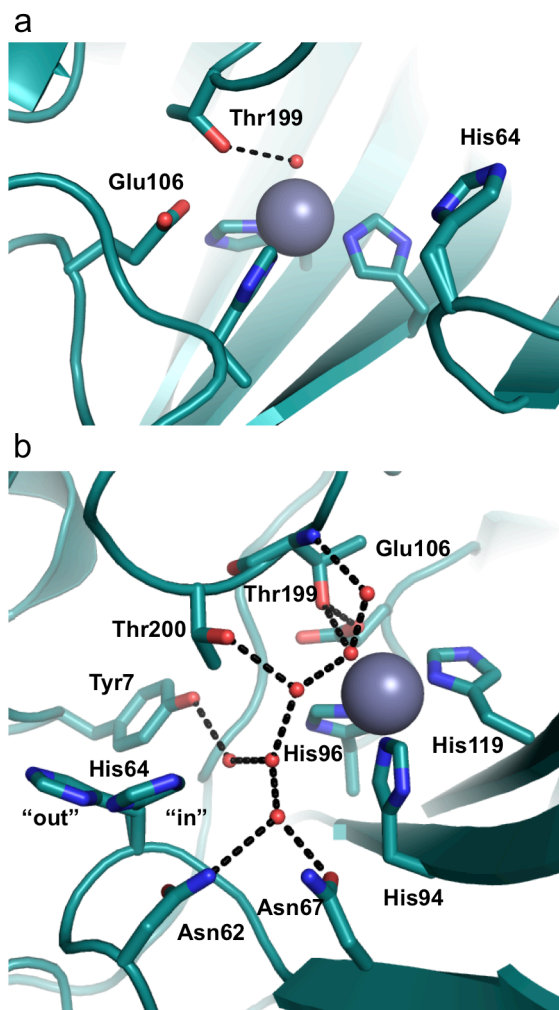
Figure 4-18. Ribbon diagrams of the active site and extended active site in human CAII (pdb 3KS3)[76]. a) Structure of the Zn(II)His$_3$O center in CA highlighting the hydrogen bond between Thr199 and Zn(II)-bound solvent. b) Structure of the extended active site of CA illustrating the hydrogen-bonding network.

incorporating a polar residue into the hydrophobic core of a sequence already containing two other mutations interrupting the Leu packing interactions.

The next step towards the design of secondary interactions was to utilize the corresponding more stable **Grand** sequence (Chapter 3) as a scaffold for incorporating potential hydrogen-bonding residues (**Grand** contains five total heptad repeats, whereas **TRI** has four). As for **TRI**L9CL23H, the Thr residue was placed into the Leu layer above the His$_3$ site to generate the sequence **GR**L16CL26TL30H. Fortunately, the **Grand** sequence is able to accommodate the polar substitution and folds well in both the absence and presence of Hg(II) (~90% α-helical content, Figure 4-2). Similarly to the **TRI**
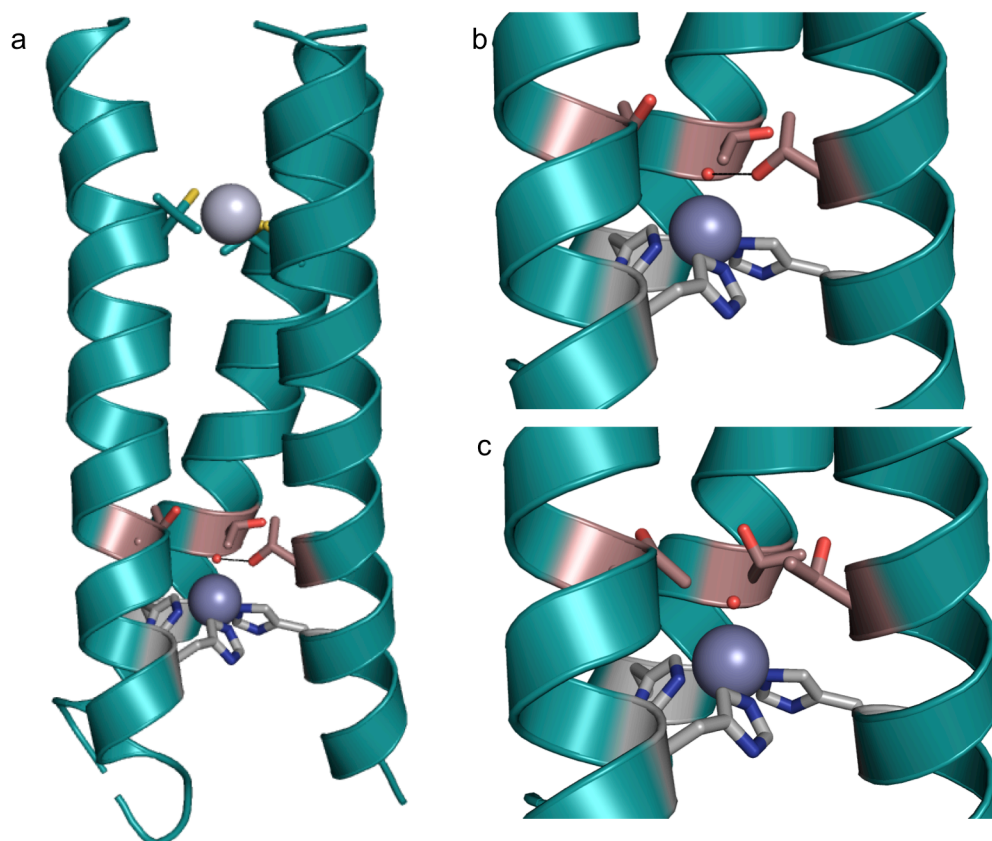
Figure 4-19. PyMOL model of $[Hg(II)]_S[Zn(II)(OH_2/OH^-)]_N$ $(TRIL9CL19TL23H)_3{}^{n+}$ based on the coordinates of the X-ray crystal structure of $[Hg(II)]_S[Zn(II)(OH_2/OH^-)]_N(CSL9PenL23H)_3{}^{n+}$ (pdb 3PBJ)[6]. a) Model of the entire 3SCC. c) Close-up of the Zn(II) site illustrating a potential hydrogen bond between a Thr residue in the 19th position and Zn(II)-bound solvent (O-O distance 2.5 Å. c) Close-up view of the Zn(II) site with alternate rotamers in which the hydroxyl groups orient towards the exterior of the 3SCC. Models were prepared in PyMOL using the mutagenesis option and PyMOL's rotamer library.[48]

peptides and **GR**L2WL16CL30H described in Chapters 2-3, the presence of the HgS$_3$ site in **GR**L16CL26TL30H provides increased thermodynamic stability to the folded complex (Figures 4-2-4-3). Having successfully obtained a stable design containing a potential hydrogen-bonding residue, both the hydrolytic activity towards *p*NPA and the Zn(II)-binding affinity were analyzed. At pH 7.5, the apparent dissociation constant for Zn(II) is ~6 nM, although the competition experiment did not work in both directions (the colorimetric chelator could not compete with the peptide) (Table 4-2). At pH 9.0, the competition could be completed in both directions, resulting in $K_d = 3.1 \pm 0.5$ nM, which is ~70-fold stronger than that for Zn(II) binding to $[Hg(II)]_S(TRIL9CL23H)_3{}^-$ ($K_d = 0.22$

± 0.06 μM) and ~35-fold stronger than that for $[Hg(II)]_S(\mathbf{GR}L2WL16CL30H)_3^-$ (K_d = 0.11 ± 0.05 μM). In CAII, the T199A mutation results in a ~15-75-fold decrease in Zn(II)-binding affinity (K_d = 60 pM) (depending on the reported dissociation constant for wild-type CAII used, 4 or 0.8 pM, Table 4-6).[8,9,49,50] The difference in binding affinities observed for the model system may suggest hydrogen bonding, but may also represent binding of the Thr hydroxyl group directly to Zn(II), perhaps displacing the water molecule (although the interior of the coiled coil can accommodate multiple water molecules bound to Zn(II) so it is possible no displacement would occur). The hydrolytic activity of $[Hg(II)]_S[Zn(II)(OH_2/OH^-)]_N(\mathbf{GR}L16CL26TL30H)_3^{n+}$ towards pNPA was evaluated at pH 8.5 and 9.5 and pH-dependent saturation kinetics was observed. The catalytic efficiency at pH 8.5 is 2.2 ± 0.3 M^{-1} s^{-1} and increases to 14.8 ± 1.4 M^{-1} s^{-1} at pH 9.5 (Table 4-4). The k_{cat} values are 0.0086 ± 0.0053 s^{-1} and 0.056 ± 0.026 s^{-1} at pH 8.5 and 9.5, respectively. The K_M, based on these two pH's appears to be pH-independent as it has been for all other peptides analyzes so far (~4 mM). While the k_{cat} at pH 9.5 is about the same as the maximal value estimated for $[Hg(II)]_S[Zn(II)(OH_2/OH^-)]_N$ $(\mathbf{TRI}L9CL23H)_3^{n+}$ (~0.053 s^{-1}) and slightly lower than that for $[Hg(II)]_S[Zn(II)(OH_2/OH^-)]_N(\mathbf{GR}L2WL16CL30H)_3^{n+}$ (~0.064 s^{-1}), the K_M is two-fold higher than for $[Hg(II)]_S[Zn(II)(OH_2/OH^-)]_N(\mathbf{TRI}L9CL23H)_3^{n+}$ and ~10% higher) than that for $[Hg(II)]_S[Zn(II)(OH_2/OH^-)]_N(\mathbf{GR}L2WL16CL30H)_3^{n+}$ (3.6 mM), suggesting that substrate access has been decreased. It is also apparent that simply incorporating this

Table 4-6. Properties of selected carbonic anhydrase variants.

Variant	Zinc K_d (pM)	pNPA k_{cat}/K_M [M^{-1} s^{-1}]	pK_a	CO_2 k_{cat}/K_M [μM^{-1} s^{-1}]
Wild type	4 ± 1[a] or 0.8 ± 0.1 [b]	2600 ± 50[c]	6.8 ± 0.1[d]	110 ± 10[c]
T199A	60 ± 10[e]	44 ± 2[c] or 15[f]	8.3 ± 0.1[c]	1.1 ± 0.05[c]
T199D[g]	4 ± 0.02			0.04
T199E[g]	0.02 ± 0.01			0.04

a. Taken from reference 8.
b. Taken from reference 9.
c. Taken from reference 11.
d. Taken from reference 46.
e. Taken from reference 77.
f. Taken from reference 12.
g. Taken from reference 51.
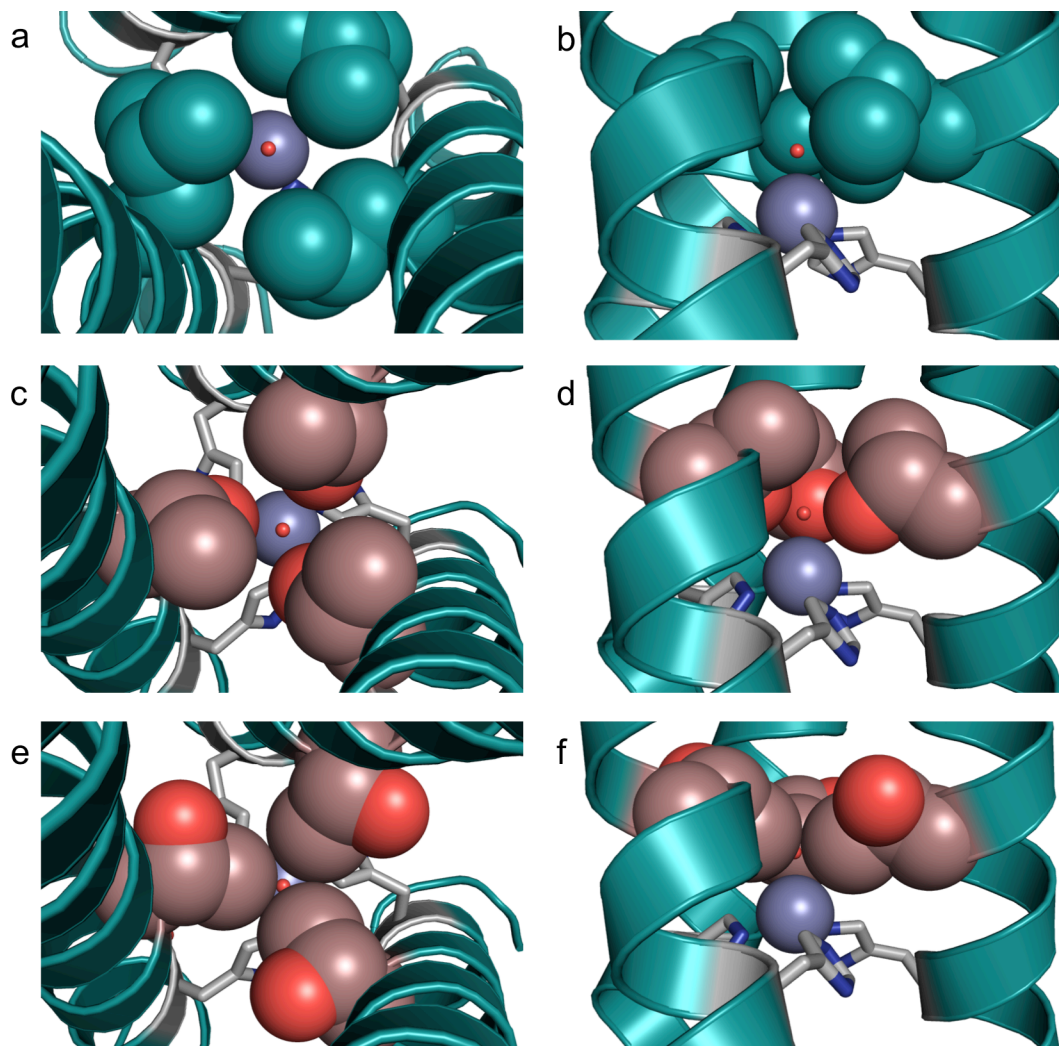
Figure 4-20. Comparison of the space filling structures around the Zn(II) site in the X-ray crystal structure of a) and b) $[Hg(II)]_S[Zn(II)(OH_2/OH^-)]_N$ $(CSL9PenL23H)_3{}^{n+}$ (pdb 3PBJ)[6] with PyMOL models of c), d), e), and f) $[Hg(II)]_S[Zn(II)(OH_2/OH^-)]_N(TRIL9CL19TL23H)_3{}^{n+}$ based on the coordinates of $[Hg(II)]_S[Zn(II)(OH_2/OH^-)]_N(CSL9PenL23H)_3{}^{n+}$. a) Top-down and b) side-on views of the Zn(II) site in $[Hg(II)]_S[Zn(II)(OH_2/OH^-)]_N(CSL9PenL23H)_3{}^{n+}$ with Leu 19 residues displayed as spheres. c) Top-down and d) side-on views of the Zn(II) site in the model $[Hg(II)]_S[Zn(II)(OH_2/OH^-)]_N(TRIL9CL19TL23H)_3{}^{n+}$ where Thr rotamers are oriented towards the interior of the 3SCC. e) Top-down and d) side-on views of the Zn(II) site in the model $[Hg(II)]_S[Zn(II)(OH_2/OH^-)]_N$ $(TRIL9CL19TL23H)_3{}^{n+}$ where Thr rotamers are oriented towards the exterior of the 3SCC and the methyl groups are packed in the interior. Models were prepared in PyMOL using the mutagenesis option and PyMOL's rotamer library.[48]

residue has not resulted in any positive change to the rate. In order to try to gain a better understanding of the potential interactions around the metal center, the model containing the Thr substitution described above was reevaluated to determine the packing interactions around the metal site (Figure 4-20). In fact, there are multiple rotamers of Thr which may be accommodated in the 3SCC, some for which the hydroxyl group is oriented towards the interior of the 3SCC (as it would need to be to form a hydrogen bond) and some in which the hydroxyl group is oriented towards the exterior. Since no further interactions to control the orientation of the Thr residues have been designed, it is possible that either or both situations may exist in the structure. From a chemical standpoint, it is likely that the hydroxyl groups will prefer to be oriented towards the hydrophilic interface of the 3SCC. While both mutants display an increase in steric bulk, the one in which all three Thr residues are oriented to the exterior and the methyl groups towards the interior clearly allows very little room for the coordinated water molecule and provides the best hydrophobic packing interactions for the structure (Figure 4-20). In light of these observations, it is not particularly surprising that substrate access is worse for this model than for $[Hg(II)]_S[Zn(II)(OH_2/OH^-)]_N(\textbf{TRI}L9CL23H)_3^{n+}$ or $[Hg(II)]_S[Zn(II)(OH_2/OH^-)]_N(\textbf{GR}L2WL16CL30H)_3^{n+}$.

In order to generate a sequence in which an oxygen atom is oriented into the interior of the 3SCC, it was reasoned that a residue containing two oxygen atoms was needed, so that one would always orient towards the interior for all potential rotamers. Two out of the 20 natural amino acids meet this condition, glutamate and aspartate. Based on models, Asp was chosen for this substitution since it has a shorter side chain and so is less likely to bind directly to Zn(II) (Figure 4-21). Depending on the rotamers, the potential hydrogen-bonding distances are 1.3 Å (probably too short) and 2.6 Å. The closest Zn(II)-Asp distances are 2.9 Å and 3.0 Å. The resulting peptide, **GR**L16CL26DL30H, folds well in both the presence and absence of Hg(II), although the percent α-helicity (~71-74%) is less than was observed for the Thr substitution in **GR**L16CL26TL30H (~90%) (Figure 4-2). This is reasonable given that the goal of the Asp substitution was to force polar interactions into the interior of the 3SCC, which was likely not achieved for **GR**L16CL26TL30H. As before, the presence of the Hg(II) site increased the thermodynamic stability of the complex towards denaturant (Figure 4-2).
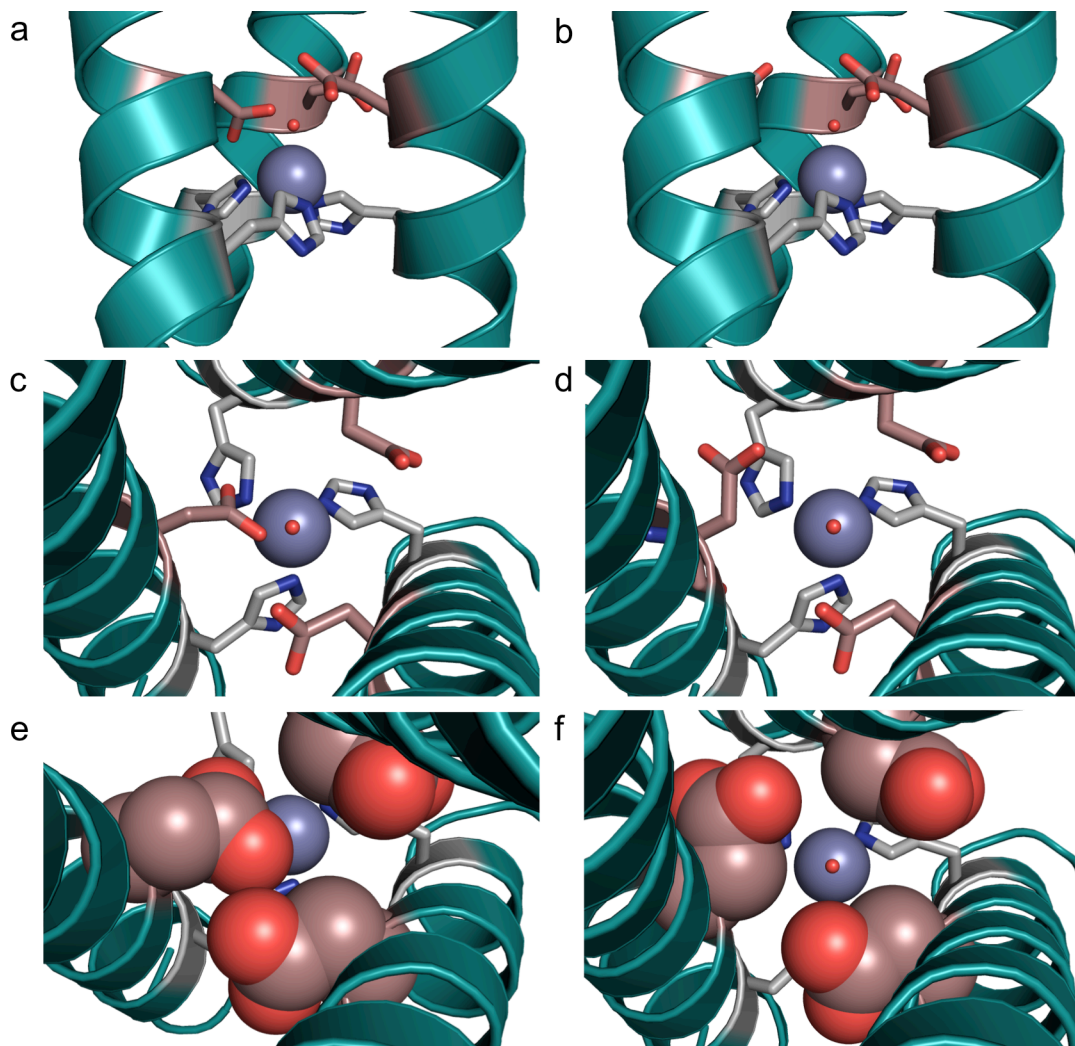
Figure 4-21. PyMOL model of $[Hg(II)]_S[Zn(II)(OH_2/OH^-)]_N$ **(TRIL9CL19DL23H)$_3^{n+}$ based on the coordinates of the X-ray crystal structure of $[Hg(II)]_S[Zn(II)(OH_2/OH^-)]_N$(CSL9PenL23H)$_3^{n+}$ (pdb 3PBJ)[6]. a) Side-on view with side chains shown as sticks, c) top-down view with side chains shown as sticks, and e) top-down view with Asp substitution shown as spheres for the model of one potential set of Asp rotamers. b) Side-on view with side chains shown as sticks, d) top-down view with side chains shown as sticks, and f) top-down view with Asp substitution shown as spheres for the model of another potential set of Asp rotamers. Models were prepared in PyMOL using the mutagenesis option and PyMOL's rotamer library.[48] Rotamers were chosen that displayed the least amount of potential clashing with surrounding residues.**

Evaluation of the Zn(II)-binding affinity produces similar results as for the Thr-containing peptide. The dissociation constant for Zn(II) binding to $[Hg(II)]_S$(**GR**L16CL26DL30H)$_3^{n-}$ at pH 7.5 is ~4 nM (Table 4-2). At pH 9.0, a

185

dissociation constant of 2.3 ± 1.4 nM is measured (high error, but not different than that for the Thr-containing peptide, 3.1 ± 0.5 nM). It is difficult to draw conclusions without a crystal structure, but the source of these high affinities (relative to those for sequences lacking Thr or Asp) may be due either to successful incorporation of hydrogen-bonding interactions or simply direct binding of another residue to Zn(II). In CA, T199 has been substituted for Asp and also Glu.[51] The Asp substitution results in no change to the Zn(II)-binding affinity and the crystal structure shows that each carboxylate oxygen is 2.5 Å away from Zn(II). The longer Glu residue, however, displaces Zn(II)-bound hydroxide in CA to bind to Zn(II) (Zn(II)-O separation is 2.2 Å), increasing the binding affinity by 200-fold (from 4 pM to 20 fM, Table 4-6). For the designed system, it is too difficult to draw conclusions based solely on the differences in binding affinities. While crystal structures or X-ray absorption spectroscopy (XAS) may ultimately be required, some information can be obtained by examining the UV-Vis spectra upon Co(II) substitution (to be described below) and will be obtained by applying EPR spectroscopy to Co(II)-substituted peptides (currently in progress with my collaborator, Dave Tierney at Miami University).

$[Hg(II)]_S[Zn(II)(OH_2/OH^-)]_N(\textbf{GR}L16CL26DL30H)_3^{n+}$ was also evaluated for its hydrolytic activity towards pNPA. As for the other sequences, pH-dependent saturation kinetics was observed over the range evaluated (7.5-9.5). The catalytic efficiency increases from 0.21 ± 0.04 M^{-1} s^{-1} at pH 7.5 to 24.2 ± 2.5 M^{-1} s^{-1} at pH 9.5 and the k_{cat} values from 0.0017 ± 0.0005 s^{-1} at pH 8.0 to 0.024 ± 0.004 s^{-1} at pH 9.5 (Figures 4-14-4-15, Table 4-4). The K_M values are generally pH-independent over the range and average ~1 mM. This indicates that substrate access is similar to that observed for the upside-down model $([Zn(II)(OH_2/OH^-)]_N[Hg(II)]_S(\textbf{TRI}L9HL23C)_3^{n+})$ described in Chapter 3 and is actually increased relative to both the original model and the other **Grand** peptides. The pH-dependent catalytic efficiencies are plotted vs pH and fitted for the pK_a (9.4 ± 0.2) and maximal k_{cat}/K_M (39 ± 9 M^{-1} s^{-1}) (Figure 4-14). Both of these values are a little higher than the corresponding values for the original model and the original **Grand** version (**GR**L2WL16CL30H), but not when the error bars are considered (Table 4-5). Therefore, the results from this model, in terms of kinetic parameters, demonstrate an improvement in substrate access with worsened rate, leading to an overall unchanged

catalytic efficiency. Again, in the absence of a crystal structure and, therefore, concrete knowledge of the coordination environment around Zn(II), it is hard to draw convincing conclusions. However, if the Asp residue does bind to displace the Zn(II)-bound hydroxide, the activity would likely have been completely removed (as it was for the CO_2 hydrase activity of T199D and T199E CA mutants, Table 4-6).[51] Since the rate was at least 50% of the original model and the same as $[Zn(II)(OH_2/OH^-)]_N[Hg(II)]_S$ (**TRI**L9HL23C)$_3{}^{n+}$, either a hydrogen-bond interaction was formed which affected the binding affinity but not the efficiency or pK_a, or Asp binds to Zn(II) in addition to the solvent molecule, altering the electronics around the site (although one might have expected this to modify the pK_a more drastically, it is difficult to determine all of the potential contributions without further study). The K_M is probably decreased because the likely combinations of rotamers, which orient the carboxylate group either towards the interface or towards the interior, lead to increased space around the Zn(II) site (note that it is probably unlikely, from a chemical standpoint, to have them all orienting towards the interior at the same time) (Figure 4-21).

While obtaining crystal structures of these models is the ideal, there are spectroscopic methods that may be used to gain more information about the catalytic metal-binding site in **GR**L16CL26TL30H and **GR**L16CL26DL30H. Metals such as Co(II) and Cd(II) have often been substituted for Zn(II) in many zinc proteins as spectroscopic probes.[34,52–54] Substitution with Cd(II) allows for the metal site to be probed using techniques such as [113]Cd NMR and [111m]Cd PAC spectroscopies, both of which are sensitive to the coordination environment around the Cd(II) ion. However, substitution with Cd(II) often results in little to no retention of catalytic activity (in CA, Cd(II) substitution results in a kinetic pK_a shift from 6.8 to 9.1 and with only about ~15% retention of CO_2 hydration activity and ~25% for esterase activity at high pH).[55,56] Substitution with high-spin Co(II) is a more common approach for zinc enzymes as significant activity is often retained and the site can be examined using UV-Vis and EPR spectroscopies.[33,34,54] Co(II) ions exhibit characteristic spectra sensitive to not only the number of atoms coordinated to Co(II), but also their identity (S, N, O). The drawbacks to using Co(II) to substitute Zn(II) are that it is redox-active and it cannot be guaranteed

that the coordination geometry of the substituted Co(II) center will be isomorphous with that of the Zn(II) center.[54,57]

The first metal substitution for the Zn(II) site in His-substituted **TRI** peptides to be discussed is Cd(II) because there is a large body of previous work in the group using ^{113}Cd NMR spectroscopy, allowing for the use of this technique to be fairly straightforward. The Cd(II)-substitution work into His$_3$ sites in the **TRI** peptides is a combination of my own work and that of a previous postdoctoral researcher in the group, Dr. Anna F. A. Peacock (who also examined Cd(II) binding using ^{111m}Cd PAC spectroscopy). Here, I will focus on my work involving the substitution of ^{113}Cd into **TRI**L23H (the peptide lacking the structural site) and the pH-dependence of the chemical shift(s), as well as esterase activity studies of $[Cd(II)(OH_2/OH^-)_x]_N(\textbf{TRI}L23H)_3{}^{n+}$. There are a few studies reporting the ^{113}Cd NMR spectra of varying ^{113}Cd-substituted CA isozymes[29–31], which have been previously summarized[36,53]. Generally, the chemical shifts are in the range of 146-262 ppm, depending on the isozyme and pH. Originally no chemical shift was observed at low pH ($< pK_a$) for ^{113}Cd-human CAI, although a chemical shift of 146 ppm was observed at pH 9.6.[29] This is close to the values predicted using computational methods (153-163 ppm).[58] The same work reported a chemical shift for ^{113}Cd-substituted bovine CAI at pH 8.0 of 214 ppm. It was found that the chemical shift was isozyme-dependent, so while no signal was observed for human CAI at pH 7.8, a shift of 226 ppm was observed for human CAII at pH 8.1.[52] Later, the low pH form of human CAI was reported to give rise to a chemical shift of ~223 ppm, which increased to 188 ppm in the presence of one equivalent of bicarbonate and up to 165 ppm in the presence of 120 equivalents of bicarbonate.[31] Smaller differences in chemical shifts were observed for human CAII at pH 8.1 from 232 ppm in the absence of any bicarbonate (CO$_2$-free solutions) to 216 ppm in the presence of 140 equivalents of bicarbonate. At high pH for bovine CA, the chemical shift goes from 262 ppm in the absence of CO$_2$ to 207 ppm in the presence of 100 equivalents of bicarbonate. Generally, the chemical shifts observed for CA shift continuously downfield with increasing pH, possibly due to the exchange of the solvent ligand between its aqua and hydroxide forms.[31] Unfortunately, no crystal structure of Cd(II)-substituted CA has been reported so the coordination environment cannot be definitively assigned. Small molecule model complex studies

have suggested that Cd(II) forms a five-coordinate aqua complex.[59,60] In the *de novo* designed 3SCC, insertion of [113]Cd gives rise to a single chemical shift at 146 ppm from pH 5.6 to 9.0 (Figure 4-6). This is similar to the computationally predicted chemical shifts[58] and that reported for human CAI at pH 9.6.[29] At pH 9.25 and 9.5, the shift splits into two signals, one still at ~148-149 ppm and the other at 175 ppm. Assuming that the Cd(II) center behaves similarly to Zn(II) and follows the same proposed catalytic mechanism, this may potentially represent deprotonation of a Cd(II)-bound solvent molecule. It should be noted that the pH-dependence observed for the CA enzymes is continuous and a single chemical shift is observed at each pH (no splitting into multiple peaks occurs).[31] This disparity between the design and CA may be due to differences in the exchange rates between different forms of the metal center. At pH 9.5, the intensities of the two species are roughly equal, suggesting that the pK_a is at least 9.5, or higher. The pH was then raised to 9.8 and a third signal downfield at 212 ppm is observed. Unfortunately, at high pH, it is possible for the salt bridge interactions between Lys and Glu residues of the 3SCC to be interrupted, consequently destabilizing the structure. Therefore, the origin of the chemical shift at 212 ppm cannot be confidently assigned and may be meaningless if the structure is not fully intact. Given that the chemical shift observed in the designed system is further upfield than most of the shifts reported for CA and matches the chemical shift which has been indicated to be due to the presence of bicarbonate in the coordination sphere, attempts at binding bicarbonate to $[^{113}Cd(II)(OH_2/OH^-)_x]_N(\mathbf{TRI}L23H)_3{}^{n+}$ were made (notably, all titrations were performed to exclude CO_2 and minimize air exposure as much as possible). Addition of up to five equivalents of CO_2 to a sample containing 14.4 mM $[Cd(II)(OH_2/OH^-)_x]_N(\mathbf{TRI}L23H)_3{}^{n+}$ did not produce any change to the chemical shift (Figure 4-7). For CA, a continuous change was observed, but the largest shifts were observed with the addition of a single equivalent of bicarbonate.[31] Further, based on CO_2 hydration studies to be discussed in Chapter 5, the concentrations of CO_2 present in solution are less than 2.5 mM and the K_M for $[Cd(II)(OH_2/OH^-)_x]_N(\mathbf{TRI}L23H)_3{}^{n+}$-catalyzed CO_2 hydration is high, ~9 mM, suggesting that CO_2 is unlikely to bind well to this complex. $[Cd(II)(OH_2/OH^-)_x]_N(\mathbf{TRI}L23H)_3{}^{n+}$ was also evaluated for its hydrolytic activity towards *p*NPA at pH 8.5 and 9.5 (Figure 4-16). While no activity was observed at pH 8.5, the efficiency at pH 9.5 of

3.5 ± 0.2 M^{-1} s^{-1} is ~15-20% of that observed for the Zn(II)-bound L23H sites in the presence and absence of the structural HgS_3 site. The pH trend is consistent with the ^{113}Cd NMR titration, suggesting a pK_a higher than that for Zn(II) (> 9.5 vs ~9.0). This is also consistent with the trend reported for CA, where the pK_a for Cd(II)-CA is shifted nearly two units higher (to 9.1) relative to that for Zn(II) (6.8), as measured by the esterase activity.[56] While it is possible to draw a number of parallels between the data for the designed protein and the Cd(II)-substituted native enzyme, CA, the lack of a crystal structure for either complex and the lack of any structurally characterized Cd(II)His$_3$O$_x$ site with accompanying ^{113}Cd NMR data precludes one from drawing a definitive conclusion of the coordination environment. Although there is a naturally occurring Cd(II)-CA with a reported crystal structure, it is from the β-family of CA enzymes and the coordination sphere contains two Cys and a His residue rather than three His residues, as for the α-CA's.[61] Based on these results, it can be concluded that Cd(II) in **TRI**L23H is certainly binding to all three His residues and at least one solvent molecule which is deprotonated at higher pH values. However, given the uncertainty in identifying the number of solvent molecules, Cd(II) may not be the best spectroscopic probe for examining the effects of incorporating hydrogen-bonding residues around the ZnHis$_3$ site.

Next, Co(II) was explored as a potential spectroscopic probe for the Zn(II) center in the *de novo* designed 3SCCs. First, Co(II) binding to the His$_3$ site in **TRI**L2WL23H was examined. The spectroscopic data obtained at pH 7.6 indicates stoichiometric Co(II) binding (after correction for non-specific binding using a control peptide lacking the binding site) with λ_{max} at 517 nm and a relatively low molar extinction coefficient (43 ± 1 M^{-1} s^{-1}) (Figure 4-8). Generally, the extinction coefficients for octahedral Co(II) complexes are not higher than 40 M^{-1} cm^{-1}.[33,34] Four- and five-coordinate complexes have absorptions about an order of magnitude higher than the range for octahedral complexes (5-40 M^{-1} cm^{-1}) but distorted symmetries complicate the distinction between the two. Given the low absorption resulting from Co(II) binding to **TRI**L2WL23H, it is likely to have adopted an octahedral geometry (probably CoN$_3$O$_3$). When Co(II) is substituted for tetrahedral Zn(II) in proteins, there are cases where it adopts the original tetrahedral geometry[62–64], but often it can also adopt five-coordinate[63,65,66] and sometimes six-coordinate geometries[66,67]. Model complex studies have suggested that the propensity of

Co(II) to adopt higher coordination numbers when substituted for Zn(II) may be underappreciated.[57] Co(II) substitution into CA has been reported to result in a tetrahedral geometry[62,66], although a five-coordinate geometry has been observed in the presence of sulfate (bound at pH 6.0)[62] and in the presence of citrate (pH 8.5, $CoHis_3(H_2O)_2$)[66]. An octahedral cobalt center was also reported in the presence of citrate at pH 6.0. That center was proposed to have oxidized to Co(III) on the basis of somewhat relaxed (~0.3 Å) bond distances and previous reports of Co(III)-CA in which octahedral geometry is observed.[68–70] However, in those cases oxidation of Co(II) required the use of excess H_2O_2 and the low pH at which the octahedral center is observed is not conducive towards oxidation (the rate of oxidation increases under alkaline conditions[34]). While oxidation of Co(II) in **TRI**L2WL23H must be considered, it seems unlikely to have occurred. The earlier Co(III)-CA complexes have molar absorptivities > 100 M^{-1} cm^{-1}, whereas octahedral Co(II) centers have much lower extinction coefficients (< 40 M^{-1} cm^{-1})[34] and more closely match the data for $[Co(II)(OH_2/OH^-)_x]_N(\mathbf{TRI}L2WL23H)_3{}^{n+}$. Further, Co(III) in CA renders the enzyme completely inactive whereas the $[Co(II)(OH_2/OH^-)_x]_N$ $(\mathbf{TRI}L2WL23H)_3{}^{n+}$ complex retains ~30% of the activity (see below) and Co(II) in CA retains most of the activity (for both pNPA hydrolysis and CO_2 hydration).[40,71–73] EPR studies (currently in progress with Dave Tierney) will be more conclusive since Co(III) will be diamagnetic and, therefore, would not give a signal, whereas the paramagnetic Co(II) center should give a signal. Assuming that Co(II) has not been oxidized upon insertion into **TRI**L2WL23H, its binding affinity obtained from fitting the absorbance data at 517 nm (described in the Materials and Methods section) at pH 7.6 ($K_d = 35 \pm 4$ μM) is ~60-fold weaker than that for Zn(II) at pH 7.5 ($K_d = 0.6 \pm 0.1$ μM). This is consistent with the general observation that Co(II) substitution into zinc enzymes, including CAII, usually results in lower binding affinities.[34,44]

One of the original goals of incorporating Co(II) into **TRI**L2WL23H was to determine whether a spectroscopic pK_a analogous to the kinetic pK_a observed for Zn(II) may be measured. Although, based on UV-Vis spectroscopy, Co(II) substitution into **TRI**L2WL23H is clearly not isomorphous with Zn(II), it was still considered worthwhile to examine the pH-dependence of $[Co(II)(OH_2/OH^-)_x]_N(\mathbf{TRI}L2WL23H)_3{}^{n+}$. The pH titration of $[Co(II)(OH_2/OH^-)_x]_N(\mathbf{TRI}L2WL23H)_3{}^{n+}$ indicates that Co(II) binding is

evident beginning at pH 5.5, with a spectrum identical to that described above for pH 7.6, and with only a slight broadening of the peak at 517 nm up to pH 9.75 (Figure 4-10). As the pH is increased further, the spectral features begin to include additional peaks at ~580 nm and ~630 nm. These peaks continue to grow up until pH 10.65, after which Co(II) likely begins to fall out of the unfolding peptide. The extinction coefficients for the new peaks are 30 M^{-1} cm^{-1} or less. The final spectrum most closely resembles that reported for Co(II) in basic solution ($[Co(OH)_4]^{2-}$ or $[Co(OH)_3(H_2O)]^-$), although with much lower extinction coefficients.[74] Given the data, one conclusion that may be definitively drawn is that there is clearly a pH-dependence for the Co(II) center, and it suggests a relatively high pK_a for the Co(II) center (> 9.5).

Another route towards examining the Co(II) center in proteins is to study the binding of anions, given the spectroscopic sensitivity of this metal ion. The binding of a large variety of anions to Co(II)-substituted CAs has been reported.[36,75] Chloride was chosen for titration with $[Co(II)(OH_2/OH^-)_x]_N(\textbf{TRI}L2WL23H)_3^{n+}$. Although relatively high concentrations of chloride are required to convert the Co(II) spectrum, there is clear evidence for chloride binding along with a decrease in the number of ligands bound to the metal ion (the extinction coefficient at λ_{max}, 590 nm, increases to ~200 M^{-1} cm^{-1}) (Figure 4-11). The chloride-bound spectrum for CA is reported to have peaks at 495 nm ($\varepsilon = 160$ M^{-1} cm^{-1}), 552 nm ($\varepsilon = 220$ M^{-1} cm^{-1}), 592 nm ($\varepsilon = 270$ M^{-1} cm^{-1}), and 719 nm ($\varepsilon = 4$ M^{-1} cm^{-1}).[75] The relative molar absorptivities at 495 nm, 552 nm, and 592 nm are similar to those observed for $[Co(II)(Cl^-)(OH_2/OH^-)_x]_N(\textbf{TRI}L2WL23H)_3^{n+}$ at 555 nm, 609 nm, and 590 nm (Figure 4-11). Fitting a plot of the absorbance at 590 nm vs chloride concentration gives an estimate of the binding affinity of chloride for the Co(II) center in the designed protein ($K_d = 0.145 \pm 0.004$ M). The weakness of the chloride affinity is reasonable given the high inhibition constant for another anion, acetate (Chapters 2-3). It is also in the same range as the K_I for CAII at pH 7.55 (0.19 M)[39–41] and is stronger than the K_d for chloride binding to Co(II) in a zinc finger mutant peptide with a Co(II)Cys$_2$His coordination sphere ($K_d = 0.8$ M).[38]

$[Co(II)(OH_2/OH^-)_x]_N(\textbf{TRI}L2WL23H)_3^{n+}$ effectively catalyzes pNPA hydrolysis, like all of the Zn(II)-bound **TRI** peptides examined so far but with only ~30% of the catalytic efficiency at pH 9.5 ($k_{cat}/K_M = 6.6 \pm 0.6$ M^{-1} s^{-1}) and ~50% of the rate (0.026 ±

0.009 s^{-1}) (Figure 4-17). The K_M is increased nearly two-fold to 3.9 ± 1.6 mM from ~2 mM for Zn(II) in the same peptide. This is reasonable if Co(II) has a higher coordination number than Zn(II) (which is tetrahedral) since there will be more bound water molecules in the hydrophobic cavity around the active site precluding easy substrate success.

Although there are still a number of questions regarding Co(II) binding to **TRI**L2WL23H, the UV-Vis spectra can be used to determine whether there are changes in the coordination environments of the active sites of **GR**L16CL26TL30H and **GR**L16CL26DL30H. UV-Vis spectroscopy should help to determine whether the Thr residue in **GR**L16CL26TL30H or Asp residue in **GR**L16CL26DL30H may be binding to the Co(II) center. Examination of the UV-Vis spectra for the titration of Co(II) into [Hg(II)]$_S$(**GR**L16CL26TL30H)$_3{}^{n-}$ at pH 7.6 reveals significant differences relative to the [Co(II)(OH$_2$/OH$^-$)$_x$]$_N$(**TRI**L2WL23H)$_3{}^{n+}$ spectra. The λ_{max} is shifted to 557 nm and there is a shoulder around 522 nm (Figure 4-12). Importantly, the extinction coefficient increases nearly seven-fold (to 296 ± 4 M^{-1} cm^{-1}), suggesting a decrease in the coordination number around Co(II) to four or five. Differentiating between four- and five-coordinate Co(II) centers (tetrahedral vs square pyramidal or trigonal bipyramidal) is difficult on the basis of UV-Vis spectroscopy. Further examination using EPR and NMR is likely needed, however, it can be proposed that the Thr substitution alters the first coordination sphere of the metal center. One possible reason is that the packing of the methyl groups (Figure 4-20, as discussed in reference to the hydrolytic activity of [Hg(II)]$_S$[Zn(II)(OH$_2$/OH$^-$)]$_N$(**GR**L16CL26TL30H)$_3{}^{n+}$) leaves less room for multiple solvent molecules to be bound to Co(II). The other possibility is that direct coordination of Thr displaces multiple water molecules. The binding affinity of Co(II) to this site is ~10-fold stronger than that for **TRI**L2WL23H (K_d = 3.2 vs 32 μM), which may suggest binding of another protein ligand.

The binding of Co(II) to the other substituted peptide for potential hydrogen bond formation, **GR**L16CL26DL30H (pH 7.3), shares more similarities with **TRI**L2WL23H than with **GR**L16CL26TL30H. The binding affinities are close, K_d = 25 ± 4 μM for the Asp-substituted peptide and 35 ± 4 μM for **TRI**L2WL23H. The Co(II)-binding spectrum is similar in shape to that for [Co(II)(OH$_2$/OH$^-$)$_x$]$_N$(**TRI**L2WL23H)$_3{}^{n+}$ and has not split into multiple peaks (as for [Hg(II)]$_S$[Co(II)(OH$_2$/OH$^-$)$_x$]$_N$(**GR**L16CL26TL30H)$_3{}^{n+}$),

193

although the λ_{max} is red-shifted from 517 nm to 543 nm. The extinction coefficient (101 ± 3 M^{-1} cm^{-1}) has more than doubled relative to that for **TRI**L2WL23H, again suggesting a decrease in coordination number, to four or five. However, a decrease all the way to four-coordinate is considered unlikely to have occurred because it is expected to be coupled with a splitting of the absorption band into multiple peaks.[34] As for **GR**L16CL26TL30H, further examination of Co(II) binding using other techniques will be required, however it can be concluded that the Asp substitution induces a change to the coordination sphere around the metal center. Further characterization of these systems along with full structural characterization of the Zn(II) center in these peptides (X-ray crystallography and XAS) should clarify the structure-function relationship of these *de novo* designed metallopeptides and allow for further design improvements.

Conclusion

Herein I have presented the first steps towards building up complexity in a minimal *de novo* designed zinc active site. Using the hydrogen-bonding interaction between T199 in CA and the Zn(II)-bound solvent molecule as inspiration, Thr and Asp residues were introduced above the Zn(II)-bound solvent molecule in the hydrophobic interior of the designed 3SCC. While the original sequence length (30 residues, **TRI**) was not sufficient to accommodate the polar substitutions, **Grand** (37 residues) folded well in the presence of Thr or Asp. In both cases, the binding affinities increased ~70-100-fold relative to those for Zn(II) in the L23H sites and ~35-fold relative to the Zn(II)-binding site in **GR**L2WL16CL30H, consistent with either direct binding of additional amino acid side chain(s) to the metal center or incorporation of a hydrogen-bonding interaction. Examination of *p*NPA hydrolysis for each design demonstrated opposite effects for the Thr and Asp substitutions. The presence of Thr increases the K_M ~two-fold relative to **TRI**L9CL23H and ~10% relative to **GR**L2WL16CL30H, while having little effect on the rate, and is consistent with packing of the methyl groups in the interior rather than orientation of a hydroxyl group towards Zn(II)-OH⁻. On the other hand, the presence of Asp results in a decrease in the K_M (by ~50%) and in the k_{cat} (~50%) resulting in overall unchanged catalytic efficiency. Co(II) substitution into each of these sites, when compared to UV-Vis spectral data for $[Co(II)(OH_2/OH^-)_x]_N(\textbf{TRI}L2WL23H)_3{}^{n+}$, suggests

a decrease in the coordination number from six to four or five. While the metal center geometry in $[Co(II)(OH_2/OH^-)_x]_N(\mathbf{TRI}L2WL23H)_3{}^{n+}$ does not match the geometry for the Zn(II) center (probably octahedral vs tetrahedral), differences in the Co(II)-binding spectra for the Thr- and Asp-substituted peptides suggests notable changes to the coordination environment, although, whether or not hydrogen bonds are formed or additional amino acid ligands bind to the metal center cannot yet be confirmed. Both Cd(II)- and Co(II)-binding studies are very useful in the analysis of these designed systems and, with further structural and spectroscopic characterization to confirm coordination environments in both the designs described here and related designed systems, may be used to resolve similar metal-binding sites in native proteins. Overall, this work suggests that using a three-fold symmetric coiled coil peptide towards the design of secondary interactions is not ideal since substitution of a single residue in the sequence results in a three-fold substitution in the coiled coil. It is likely that if a single Thr or Asp residue could be introduced near the active site, different results would be obtained. This is especially probable in the case of substitution with anionic Asp residues, which may repulse each other and adversely affect the structure when present three-fold in the 3SCC. Future work will involve the development of methods to build asymmetric systems where single substitutions can be inserted to build hydrogen-bonding networks.

References

(1)   Domsic, J. F.; Williams, W.; Fisher, S. Z.; Tu, C.; Agbandje-McKenna, M.; Silverman, D. N.; McKenna, R. *Biochemistry* **2010**, *49*, 6394–6399.
(2)   Pannetier, F.; Ohanessian, G.; Frison, G. *Dalton Trans.* **2011**, *40*, 2696–2968.
(3)   Vita, C.; Roumestand, C.; Toma, F.; Ménez, A. *Proc. Natl. Acad. Sci. U.S.A.* **1995**, *92*, 6404–6408.
(4)   Marino, S. F.; Regan, L. *Chem. Biol.* **1999**, *6*, 649–655.
(5)   Dwyer, M. A.; Looger, L. L.; Hellinga, H. W. *Proc. Natl. Acad. Sci. U.S.A.* **2003**, *100*, 11255–11260.
(6)   Zastrow, M. L.; Peacock, A. F. A.; Stuckey, J. A.; Pecoraro, V. L. *Nat. Chem.* **2012**, *4*, 118–123.
(7)   Zastrow, M. L.; Pecoraro, V. L. *J. Am. Chem. Soc.* **2013**, *135*, 5895–5903.
(8)   Kiefer, L. L.; Krebs, J. F.; Paterno, S. A.; Fierke, C. A. *Biochemistry* **1993**, *32*, 9896–9900.
(9)   Hunt, J. A.; Fierke, C. A. *J. Biol. Chem.* **1997**, *272*, 20364–20372.
(10)   Song, H.; Wilson, D. L.; Farquhar, E. R.; Lewis, E. A.; Emerson, J. P. *Inorg. Chem.* **2012**, *51*, 11098–11105.
(11)   Krebs, J. F.; Ippolito, J. A.; Christianson, D. W.; Fierke, C. A. *J. Biol. Chem.* **1993**, *268*, 27458–27466.
(12)   Liang, Z.; Xue, Y.; Behravan, G.; Jonsson, B. H.; Lindskog, S. *Eur. J. Biochem.* **1993**, *211*, 821–827.
(13)   Chan, W. C.; White, P. D. *Fmoc Solid Phase Peptide Synthesis: A Practical Approach*; Chan, W. C.; White, P. D., Eds.; Oxford University Press: New York, 2000; Vol. 222.
(14)   Farrer, B. T.; Harris, N. P.; Balchus, K. E.; Pecoraro, V. L. *Biochemistry* **2001**, *40*, 14696–14705.
(15)   Habeeb, A. F. *Meth. Enzymol.* **1972**, *25*, 457–464.
(16)   Riddles, P.; Blakeley, R.; Zerner, B. *Meth. Enzymol.* **1983**, *91*, 49–60.
(17)   Mantle, M.; Stewart, G.; Zayas, G.; King, M. *Biochem. J.* **1990**, *266*, 597–604.
(18)   Dieckmann, G. R.; McRorie, D. K.; Lear, J. D.; Sharp, K. A.; DeGrado, W. F.; Pecoraro, V. L. *J. Mol. Biol.* **1998**, *280*, 897–912.
(19)   Rush, R. M.; Yoe, J. H. *Anal. Chem.* **1954**, *26*, 1345–1347.
(20)   Sadek, F. S.; Schmid, R. W.; Reilley, C. N. *Talanta* **1959**, *2*, 38–51.
(21)   Talmard, C.; Bouzan, A.; Faller, P. *Biochemistry* **2007**, *46*, 13658–13666.
(22)   Shaw, C. F.; Laib, J. E.; Savas, M. M.; Petering, D. H. *Inorg. Chem.* **1990**, *29*, 403–408.
(23)   Mekmouche, Y.; Coppel, Y.; Hochgräfe, K.; Guilloreau, L.; Talmard, C.; Mazarguil, H.; Faller, P. *ChemBioChem* **2005**, *6*, 1663–1671.
(24)   Laib, J.; Shaw, C. F.; Petering, D. H.; Eidsness, M. K.; Elder, R. C.; Garvey, J. S. *Biochemistry* **1985**, *24*, 1977–1986.
(25)   Säbel, C. E.; Neureuther, J. M.; Siemann, S. *Anal. Biochem.* **2010**, *397*, 218–226.
(26)   GraphPad Prism version 5.00 for Mac, GraphPad Software, San Diego California USA, www.graphpad.com.
(27)   Cobas, C.; Cruces, J.; Sardina, F. J. MestRec-C **2000**.
(28)   Verpoorte, J. A.; Mehta, S.; Edsall, J. T. *J. Biol. Chem.* **1967**, *242*, 4221–4229.

(29) Armitage, I. M.; Pajer, R. T.; Schoot Uiterkamp, A. J. M.; Chlebowski, J. F.; Coleman, J. E. *J. Am. Chem. Soc.* **1976**, *98*, 5710–5712.

(30) Sudmeier, J. L.; Bell, S. J. *J. Am. Chem. Soc.* **1977**, *99*, 4499–4500.

(31) Jonsson, N. B.; Tibell, L. A.; Evelhoch, J. L.; Bell, S. J.; Sudmeier, J. L. *Proc. Natl. Acad. Sci. U.S.A.* **1980**, *77*, 3269–3272.

(32) Coleman, J. E.; Coleman, R. V *J. Biol. Chem.* **1972**, *247*, 4718–4728.

(33) Bertini, I.; Luchinat, C. *Adv. Inorg. Biochem.* **1984**, *6*, 71–111.

(34) Maret, W.; Vallee, B. L. *Meth. Enzymol.* **1993**, *226*, 52–71.

(35) Lindskog, S. *J. Biol. Chem.* **1963**, *238*, 945–951.

(36) Bertini, I.; Luchinat, C.; Scozzafava, A. *Struct. Bond* **1982**, *48*, 45–92.

(37) Lindskog, S. *Biochemistry* **1966**, *5*, 2641–2646.

(38) Merkle, D. L.; Schmidt, M. H.; Berg, J. M. *J. Am. Chem. Soc.* **1991**, *113*, 5450–5451.

(39) Pocker, Y.; Storm, D. R. *Biochemistry* **1968**, *7*, 1202–1214.

(40) Thorslund, A.; Lindskog, S. *Eur. J. Biochem.* **1967**, *3*, 117–123.

(41) Ward, R. L.; Cull, M. D. *Arch. Biochem. Biophys.* **1972**, *150*, 436–439.

(42) Innocenti, A.; Scozzafava, A.; Parkkila, S.; Puccetti, L.; De Simone, G.; Supuran, C. T. *Bioorg. Med. Chem. Lett.* **2008**, *18*, 2267–2271.

(43) Hitomi, Y.; Outten, C. E.; O'Halloran, T. V *J. Am. Chem. Soc.* **2001**, *123*, 8614–8615.

(44) McCall, K. A.; Fierke, C. A. *Biochemistry* **2004**, *43*, 3979–3986.

(45) Maret, W. *J. Nutr.* **2003**, *133*, 1460s–1462s.

(46) Fierke, C. A.; Calderone, T. L.; Krebs, J. F. *Biochemistry* **1991**, *30*, 11054–11063.

(47) Christianson, D. W.; Fierke, C. A. *Acc. Chem. Res.* **1996**, *29*, 331–339.

(48) The PyMOL Molecular Graphics System, Version 1.5.0.4 Schrödinger, LLC.

(49) Hunt, J. A.; Ahmed, M.; Fierke, C. A. *Biochemistry* **1999**, *38*, 9054–9062.

(50) Fierke, C. A.; Thompson, R. B. *Biometals* **2001**, *14*, 205–222.

(51) Ippolito, J. A.; Baird, T. T.; McGee, S. A.; Christianson, D. W.; Fierke, C. A. *Proc. Natl. Acad. Sci. U.S.A.* **1995**, *92*, 5017–5021.

(52) Armitage, I. M.; Schoot Uiterkamp, A. J. .; Chlebowski, J. F.; Coleman, J. E. *J. Magn. Reson.* **1978**, *29*, 375–392.

(53) Armitage, I. M.; Reilly, B. In *Cadmium: From Toxicity to Essentiality*; Sigel, A.; Sigel, H.; Sigel, R. K., Eds.; Springer Netherlands: Dordrecht, 2013; Vol. 11, pp. 117–144.

(54) Bennett, B. In *Metals in Biology*; Hanson, G.; Berliner, L., Eds.; Springer New York: New York, NY, 2010; Vol. 29, pp. 345–370.

(55) Tibell, L.; Lindskog, S. *Biochim. Biophys. Acta* **1984**, *788*, 110–116.

(56) Bauer, R.; Limkilde, P.; Johansen, J. T. *Biochemistry* **1976**, *15*, 334–342.

(57) Kremer-Aach, A.; Kläui, W.; Bell, R.; Strerath, A.; Wunderlich, H.; Mootz, D. *Inorg. Chem.* **1997**, *36*, 1552–1563.

(58) Hemmingsen, L.; Olsen, L.; Antony, J.; Sauer, S. P. A. *J. Biol. Inorg. Chem.* **2004**, *9*, 591–599.

(59) Kimblin, C.; Parkin, G. *Inorg. Chem.* **1996**, *35*, 6912–6913.

(60) Parkin, G. *Chem. Commun. (Cambridge, U. K.)* **2000**, 1971–1985.

(61) Xu, Y.; Feng, L.; Jeffrey, P. D.; Shi, Y.; Morel, F. M. M. *Nature* **2008**, *452*, 56–61.

(62) Håkansson, K.; Wehnert, A.; Liljas, A. *Acta Crystallogr. D Biol. Crystallogr.* **1994**, *50*, 93–100.

(63) Crawford, P. A.; Yang, K.; Sharma, N.; Bennett, B.; Crowder, M. W. *Biochemistry* **2005**, *44*, 5168–5176.

(64) Werth, M. T.; Tang, S.-F.; Formicka, G.; Zeppezauer, M.; Johnson, M. K. *Inorg. Chem.* **1995**, *34*, 218–228.

(65) Garrity, J. D.; Bennett, B.; Crowder, M. W. *Biochemistry* **2005**, *44*, 1078–1087.

(66) Avvaru, B. S.; Arenas, D. J.; Tu, C.; Tanner, D. B.; McKenna, R.; Silverman, D. N. *Arch. Biochem. Biophys.* **2010**, *502*, 53–59.

(67) Kleifeld, O.; Rulísek, L.; Bogin, O.; Frenkel, A.; Havlas, Z.; Burstein, Y.; Sagi, I. *Biochemistry* **2004**, *43*, 7151–7161.

(68) Shinar, H.; Navon, G. *Biochim. Biophys. Acta* **1974**, *334*, 471–475.

(69) Shinar, H.; Navon, G. *Eur. J. Biochem.* **1979**, *93*, 313–322.

(70) Navon, G.; Shinar, H. *Inorg. Chim. Acta* **1980**, *46*, 51–55.

(71) Lindskog, S.; Nyman, P. O. *Biochim. Biophys. Acta* **1964**, *85*, 462–474.

(72) Coleman, J. E. *Nature* **1967**, *214*, 193–194.

(73) Kogut, K. A.; Rowlett, R. S. *J. Biol. Chem.* **1987**, *262*, 16417–16424.

(74) Cotton, F. A.; Goodgame, D. M. L.; Goodgame, M. *J. Am. Chem. Soc.* **1961**, *83*, 4690–4699.

(75) Bertini, I.; Canti, G.; Luchinat, C.; Scozzafava, A. *J. Am. Chem. Soc.* **1978**, *100*, 4873–4877.

(76) Avvaru, B. S.; Kim, C. U.; Sippel, K. H.; Gruner, S. M.; Agbandje-McKenna, M.; Silverman, D. N.; McKenna, R. *Biochemistry* **2010**, *49*, 249–251.

(77) Kiefer, L. L.; Paterno, S. A.; Fierke, C. A. *J. Am. Chem. Soc.* **1995**, *117*, 6831–6837.

Chapter V. Functionalities of a *de novo* designed metalloprotein

Introduction

Although there are now several examples of *de novo* designed metalloenzymes, many have not been evaluated for activity towards a native enzyme substrate.[1–5] While numerous small molecule enzyme model complexes are evaluated for their reactivity towards both non-native and native substrates, these studies are not done under "protein-like" conditions. In reference to carbonic anhydrase (CA), in particular, there are several examples of model complexes which may catalyze the native CO_2 hydration reaction; however, none of these do so in completely aqueous solution or with the real amino acid ligands.[6–13] As a result, parallels between protein matrix effects on the catalytic metal site and the reactivity may not be drawn. On the other hand, the often large and complex (multi-domain in many cases) structures of native metalloenzymes can make it difficult to uncover direct connections between discrete structural features and the enzymatic reaction. Therefore, gearing the *de novo* design of metalloenzymes towards building catalysts for evolved substrates of native metalloenzymes can potentially illuminate structure-function relationships to a level at which could then be applied to the preparation of highly efficient catalysts for a variety of applications.

CA catalyzes the reversible hydration of CO_2 with an efficiency close to the diffusion limit and catalytic turnover of ~1 million s^{-1} (Chapter 1). CA catalyzes numerous reactions in addition to its native reaction, including the hydrolysis of esters such as *p*-nitrophenyl acetate (*p*NPA). The hydrolysis of *p*NPA is thought to have a similar reaction mechanism to that for CO_2 hydration, where a Zn(II)-hydroxide nucleophile promotes hydration of the carbonyl group of CO_2 or *p*NPA, along with stabilization of an oxyanionic intermediate (Figure 5-1).[14,15] However, the steric and electronic natures of these two substrates do differ significantly, including the respective intermediates and transition states that lead to and from them. In CAII, this gives rise to a
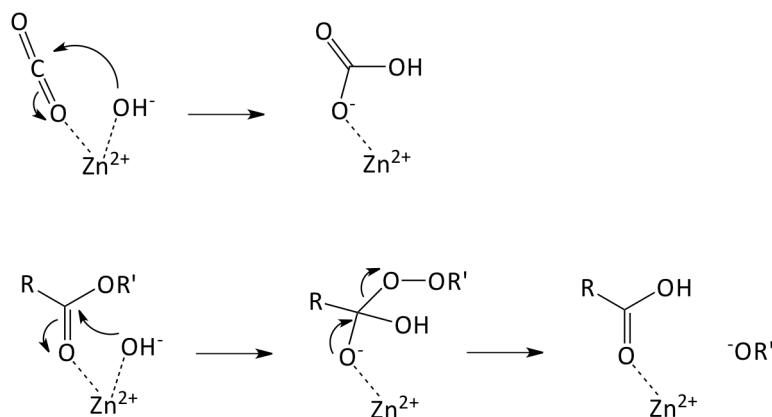
Figure 5-1. Mechanistic similarity between CO_2 hydration (top) and ester hydrolysis (bottom). Both reactions proceed by hydroxide nucleophilic attack and an oxyanionic product or intermediate.

~10^5-fold difference in the catalytic efficiencies towards hydrolysis of these substrates (CO_2 is the more efficiently catalyzed substrate of CA, Table 5-1). Further, hydrolysis of an activated substrate, such as *p*NPA (which has a leaving group with a pK_a of ~7), is not as challenging as hydrolysis of a non-activated substrate because of the inherently high rates for base-catalyzed hydrolysis, which, in this case, is not limited by leaving group departure but by the rate of hydroxide attack.[15] Given these considerations, it is worthwhile to test whether this *de novo* designed metalloenzyme system can efficiently catalyze the physiological reaction that CA evolved to catalyze at diffusion-limited rates. Achieving such a feat in a *de novo* designed system will attest to the level of understanding of how structure is related to function in native metalloenzymes.

Table 5-1. Kinetic parameters for CO_2 hydration and *p*NPA hydrolysis by carbonic anhydrase II.

Reaction	k_{cat}/K_M [$M^{-1} s^{-1}$]	k_{cat} [s^{-1}]	K_M (mM)
*p*NPA hydrolysis	2.60 (±0.05) x $10^{3(a)}$	$79^{(b)}$	30.53 ± $2.10^{(b)}$
CO_2 hydration[a]	1.10 (±0.10) x 10^8	9.8 (±1.0) x10^5	8.2

a. Taken from reference 24.
b. Taken from reference 32.

The sequences for the peptides in this chapter (Table 5-2) vary the position of the Zn(II) site and also examine its placement into a more stable sequence (Chapter 3). The original model sequence, **TRI**L9CL23H, is examined in detail and as a function of pH. The corresponding sequence lacking the structurally stabilizing HgS_3 site is evaluated at a

Table 5-2. TRI and Grand peptide family sequences used in these studies.

Peptide	a b c d e f g				
TRIL2W	Ac-G WKALEEK	LKALEEK	LKALEEK	LKALEEK	G-NH$_2$
TRIL2WL23H	Ac-G WKALEEK	LKALEEK	LKALEEK	HKALEEK	G-NH$_2$
TRIL9CL23H	Ac-G LKALEEK	CKALEEK	LKALEEK	HKALEEK	G-NH$_2$
TRIL9HL23C	Ac-G LKALEEK	HKALEEK	LKALEEK	CKALEEK	G-NH$_2$
TRIL9CL19H	Ac-G LKALEEK	CKALEEK	LKAHEEK	LKALEEK	G-NH$_2$
GRL2WL16CL30H	Ac-G WKALEEK	LKALEEK	CKALEEK	LKALEEK HKALEEK	G-NH$_2$

N- and C-termini are capped by Ac and NH$_2$ groups (acetylated and amidated), respectively.

single pH, where high activity is observed for the original model. In Chapter 3, I discussed the effects of varying the position of the active site along the sequence and inserting it into the more stable **Grand** sequence, especially with respect to substrate access. One goal of testing for CO$_2$ hydration using these *de novo* designed metallopeptides is to evaluate how reactivity and, in particular, substrate access, may vary due to the different steric natures of the two substrates. The work presented in this chapter will complement earlier detailed analyses of *p*NPA hydrolysis by these peptides (Chapters 2-3), with the goal of facilitating a deeper understanding of how their structures can influence metal center reactivity.

Materials and Methods

The nomenclature used to describe the metal complexes prepared in these studies is as described in Chapter 2.

Peptide Synthesis and Purification. Peptides were synthesized on an Applied Biosystems 433A peptide synthesizer using standard protocols[16] and purified as described previously[17] (by reverse-phase HPLC on a C18 column at a flow rate of 10 mL/min using a linear gradient varying from 0.1% TFA in water to 0.1% TFA in 9:1 CH$_3$CN:H$_2$O over 25-35 minutes). Pure peptides were characterized by electrospray mass spectrometry. Peptide stock solutions were prepared in doubly distilled water that had been purged with argon to minimize oxidation of thiol-containing peptides. The concentrations for **TRI** peptides containing Cys sites were determined by calculating the thiol concentration using a published assay with 5,5'-dithiobis-(2-nitrobenzoic acid) (Ellman's reagent).[18,19]

The concentrations for **Grand** peptides (one heptad repeat longer) containing Cys sites were similarly determined using a published assay with 4,4'-dipyridyl disulphide[20] or were based on the tryptophan absorbance at 280 nm using ε = 5500 M^{-1} cm^{-1}. Concentrations of **TRI**L2WL23H solutions were based on the tryptophan absorbance at 280 nm using ε = 5500 M^{-1} cm^{-1}. Concentrations of **TRI**L23H solutions were based on amino acid analysis performed by the Protein Structure Facility at the University of Michigan.

CO$_2$ Hydration Activity Assays. Initial rates of CO_2 hydration were measured at 25.0 °C in an OLIS RSM Stopped Flow Spectrophotometer. Since CO_2 does not have spectral properties which may monitored, the changing pH-indicator method is used.[21] The buffer/indicator pair used depends on the pH at which the activity was evaluated. For pH 8.0-9.0, TAPS/m-cresol purple (λ_{max} = 578 nm) was used and for pH 9.25-9.5, CHES/thymol blue (λ_{max} = 590 nm) was used. The ionic strength of the buffer was maintained at 0.1 M with Na_2SO_4. Saturated solutions of CO_2 were prepared by bubbling the gas (Matheson Tri-Gas, Inc., Research Grade) through deionized, distilled water. Dilutions were made using gas-tight syringes and a final check of the CO_2 concentration was possible during the experiment.[21] CO_2 concentrations ranged from ~2-19 mM. The buffer concentration was maintained at 50 mM in the reaction cell. All rates measured on the stopped flow spectrophotometer were initiated by rapid 1:1 mixing of the substrate with a buffer/indicator solution containing the desired catalyst (water for the spontaneous reaction and 10 or 20 μM $ZnSO_4$ + excess peptide [20-50 μM, depending on the Zn(II)-binding affinity] for the catalyzed reaction) and monitored over a very short time interval in order to record only the initial linear portion of the reaction. At least four replicates were performed for each substrate concentration. Where possible, two separate catalyst solutions were prepared and separately tested over the range of substrate concentrations to confirm reproducibility.

CO$_2$ hydration is accompanied by a release of protons, which, using this method, can be monitored by observing the change in absorbance of the indicator anion (assuming its response is rapid relative to CO_2 hydration). Because the buffer will take up protons in addition to the indicator, a buffer factor must be determined in order to calculate accurate

rates for CO_2 hydration. The buffer factor (Q) is obtained from the full reaction traces of each set of data by following Khalifah's method.[21] At each concentration of CO_2, three full reaction traces for both background and catalyst are recorded to yield the total value for the absorbance change that occurs. The concentration of CO_2 vs ΔA for each reaction trace is plotted and the trend should be linear. The slope of the line is the experimental buffer factor, which may be applied to any initial rate to yield the rate of CO_2 turnover. The buffer factor may also be calculated (eq 1), given knowledge of the buffer and indicator pK_a values and the difference between extinction coefficients for the acidic and basic forms of the indicator ($\Delta\varepsilon$ was determined experimentally by preparing calibration curves for both the acidic and basic forms and is 38000 M^{-1} cm^{-1} for thymol blue and 30000 M^{-1} cm^{-1} for m-cresol purple). The pK_a values for the buffers and indicators used are found in the literature, but some variability was uncovered (for example, three pK_a values for CHES are found: 9.2, 9.3, and 9.5, two of which are from different Sigma Aldrich sources, and for thymol blue: 8.9, 8.96, and 9.2). Plugging different variations of these numbers into eq 1 yields buffer factors ranging from 0.053 to 0.082, indicating that, while the calculated value is useful for comparison, the best route is to determine these values experimentally. The pK_a for TAPS is 8.4 and for m-cresol purple is 8.3.

$$Q = \left(\frac{[B]}{L\Delta\varepsilon[In]}\right)\left(\frac{K_B}{K_{In}}\right)\left(\frac{K_{In} + [H^+]}{K_B + [H^+]}\right)^2$$

(1)

After analysis of the full reaction traces and determination of the buffer factor (see Figure 5-2 for a representative plot and full reaction trace at pH 9.5), the initial rates from the first 5-10% of the reaction, v, were plotted as a function of [S] and fitted in Prism 5 (GraphPad Software)[22] to the Michaelis-Menten equation (Figure 5-3 shows representative plots of the partial reaction trace collected and the data chosen for the initial rate determination at pH 9.5). The concentration of catalyst (10-20 µM) was used to calculate the final kinetic parameters, k_{cat} and k_{cat}/K_M. All reported rates account for the uncatalyzed background reaction. Rates due to excess (not Zn(II)-bound) peptide, $[Hg(II)_S](\textbf{TRI}L9CL23H)_3{}^-$, were negligible compared to the background.
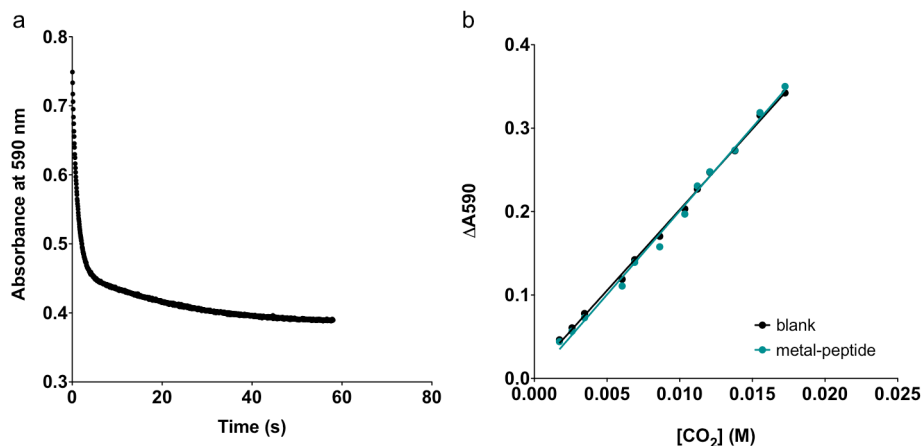
Figure 5-2. Representative data for the determination of the experimental buffer factor, Q. a) Full reaction trace recorded for $[Zn(II)(OH_2/OH^-)]_N$ $(TRIL2WL23H)_3{}^{n+}$ at pH 9.5 in 50 mM CHES, 0.1 M Na_2SO_4. The decrease in absorbance is measured at 590 nm, the λ_{max} for thymol blue. **b)** The average of three full reaction trace determinations for the blanks and metal-peptide solutions are taken and plotted vs estimated $[CO_2]$. The slope of the line is the experimental Q (for this plot, at pH 9.5, it is 0.0563 for the blanks and 0.0539 for metal-peptide; the average of the two is applied towards converting raw initial rates into those representing CO_2 turnover). Errors are less than 5%. Q is also used to determine the actual concentration of CO_2, by multiplying it by the absorbance changes from each full reaction trace.
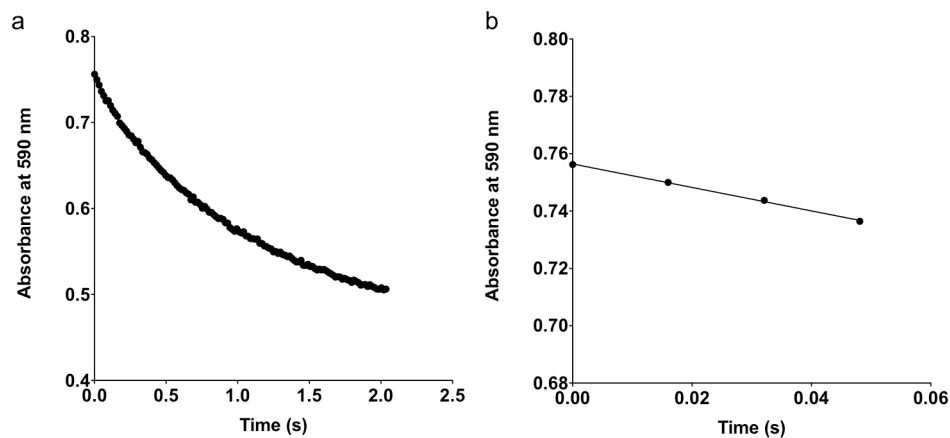

Figure 5-3. Representative data for initial rate determination in CO_2 hydration experiments. a) Partial reaction trace recorded for $[Zn(II)(OH_2/OH^-)]_N$ $(TRIL2WL23H)_3{}^{n+}$ at pH 9.5 in 50 mM CHES, 0.1 M Na_2SO_4. The decrease in absorbance is measured at 590 nm, the λ_{max} for thymol blue. **b)** The initial portion of the reaction is linearly fitted to give an initial rate for CO_2 hydration. Initial rates are determined within the first 5-10% of the reaction.

204

Table 5-3. pH-dependent kinetic parameters for CO_2 hydration by Zn(II)- and Cd(II)-bound TRI and Grand peptides.[a]

Peptide complex[b]	pH[c]	k_{cat}/K_M [M^{-1} s^{-1}] x 10^4	k_{cat} [s^{-1}]	K_M [mM]
[Hg(II)]$_S$[Zn(II)(OH$_2$/OH$^-$)]$_N$(**TRI**L9CL23H)$_3{}^{n+}$	8.0	1.4 ± 0.6	~370	~25
	8.5	4.5 ± 0.9	1410 ± 610	~31
	9.0	5.7 ± 1.5	1350 ± 620	~24
	9.25	12.6 ± 3.6	1410 ± 370	11.4 ± 5.9
	9.5	18.2 ± 3.7	1710 ± 340	9.4 ± 3.4
[Zn(II)(OH$_2$/OH$^-$)]$_N$(**TRI**L2WL23H)$_3{}^{n+}$	9.5	~10.6	~930	~8.8
[Zn(II)(OH$_2$/OH$^-$)]$_N$[Hg(II)]$_S$(**TRI**L9HL23C)$_3{}^{n+}$	9.5	5.2 ± 0.7	640 ± 100	12.4 ± 3.6
[Hg(II)]$_S$[Zn(II)(OH$_2$/OH$^-$)]$_N$(**TRI**L9CL19H)$_3{}^{n+}$	9.5	6.4 ± 1.6	750 ± 180	11.7 ± 5.5
[Hg(II)]$_S$[Zn(II)(OH$_2$/OH$^-$)]$_N$(**GR**L2WL16CL30H)$_3{}^{n+}$	9.5	7.4 ± 3.4	730 ± 290	~9.8
[Cd(II)(OH$_2$/OH$^-$)$_x$]$_N$(**TRI**L23H)$_3{}^{n+}$	9.5	10.1 ± 3.3	920 ± 240	~9.1

a. Error bars result from fitting separate individual rates (each averaged rate from determinations on separate days, where available, for each concentration of substrate, averaged rates from a single day come from 3-7 measurements) to the Michaelis-Menten equation in Prism 5 (GraphPad Software)[22].
b. 10-20 μM active Zn(II)- or Cd(II)-bound complex.
c. pH 8.0-9.0 measured in 50 mM TAPS, 0.1 M Na$_2$SO$_4$; pH 9.25-9.5 measured in 50 mM CHES, 0.1 M Na$_2$SO$_4$.

Results

Characterization of CO_2 hydration.

a) **Zn(II) site in [Hg(II)]$_S$[Zn(II)(OH$_2$/OH$^-$)]$_N$(TRIL9CL23H)$_3{}^{n+}$.**
[Hg(II)]$_S$[Zn(II)(OH$_2$/OH$^-$)]$_N$(**TRI**L9CL23H)$_3{}^{n+}$ exhibits saturation kinetics for CO_2 hydration in buffered aqueous solution, with k_{cat} = 1710 ± 340 s^{-1} and k_{cat}/K_M = 1.82 (±0.37) x 10^5 M^{-1} s^{-1} at pH 9.5 (25 °C, 10 μM catalyst, Table 5-3 and Figure 5-4). All three Michaelis-Menten parameters, k_{cat}, k_{cat}/K_M, and K_M, are dependent on pH (Figures 5-5-5-7). Both rate and efficiency generally increase with increasing pH, while the K_M decreases. The increase in rate and efficiency is consistent with deprotonation of a Zn(II)-
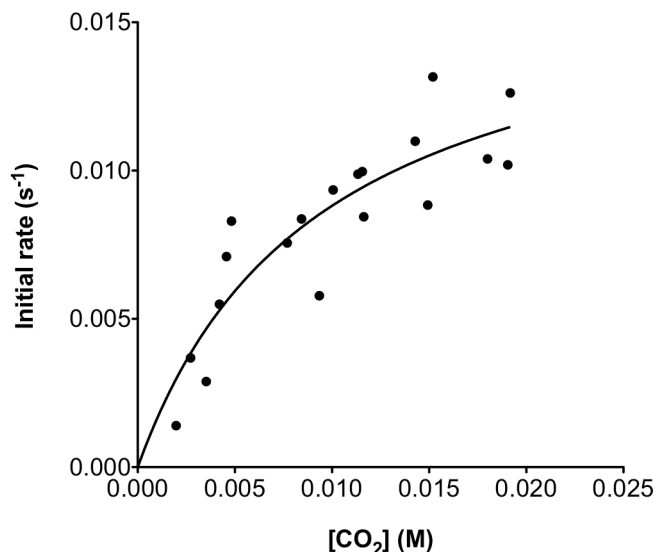
Figure 5-4. CO_2 hydration by 10 μM $[Hg(II)]_S[Zn(II)(OH_2/OH^-)]_N$ (TRIL9CL23H)$_3{}^{n+}$ at pH 9.5 in 50 mM CHES buffer, 0.1 M Na_2SO_4. Plot of the initial rates at pH 9.5 vs $[CO_2]$ and fitting to the Michaelis-Menten equation in Prism 5 (GraphPad Software).[22]

aqua ligand to produce the active Zn(II)-hydroxide species. The pH-dependency profile can be fitted (k_{cat}/K_M vs pH) to eq 2, and a pK_a of 10.3 ± 1.4 is obtained (Figure 5-6).

$$k_{obs} = \frac{\left(k_{max} * 10^{(pH-pK_a)}\right) + k_{min}}{1 + 10^{(pH-pK_a)}}$$

(2)

The maximal k_{cat}/K_M obtained from this fit is ~1.2 x 10^6 M^{-1} s^{-1}. As described in Chapter 2, for pNPA hydrolysis by $[Hg(II)]_S[Zn(II)(OH_2/OH^-)]_N$(**TRI**L9CL23H)$_3{}^{n+}$, this pH-dependency profile may also be fit for the midpoint (in this case, pK_a = 9.2 ± 0.1). For pNPA hydrolysis, the values obtained from the two fitting methods agree with one another. I observe here that the pK_a values obtained by these two methods are within experimental error, but only due to the large error bars associated with the determinations. The discrepancy results from a poorly defined pH profile, suggesting that data at additional pH values may be needed to establish this curve better (in the 9.0-9.5 range and above 9.5, if possible). If the pK_a value in eq 2 is constrained to 9.2 and the efficiency at pH 9.0 removed from the fitting, a maximal k_{cat}/K_M of ~2.6 x 10^5 M^{-1} s^{-1} is obtained (Figure 5-6b, inset). Using K_M = 9.4 mM, the maximal k_{cat} would be ~2400 s^{-1}.
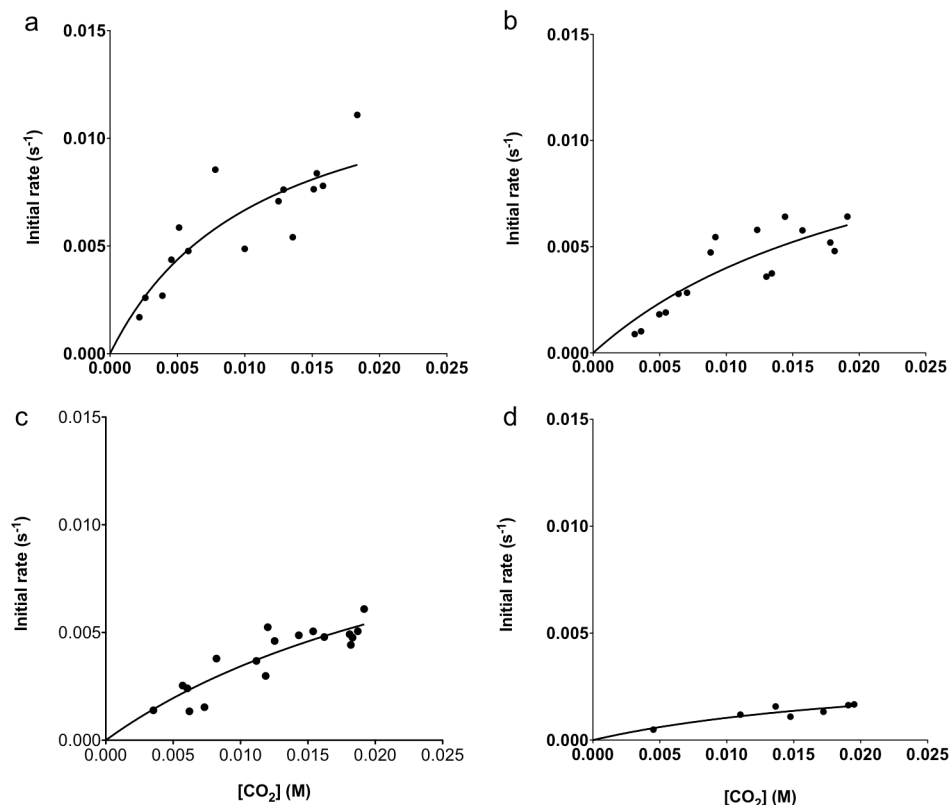
Figure 5-5. CO_2 hydration by 10 μM $[Hg(II)]_S[Zn(II)(OH_2/OH^-)]_N$ $(TRIL9CL23H)_3{}^{n+}$ at a) pH 9.25 in 50 mM CHES buffer, 0.1 M Na_2SO_4, b) pH 9.0 in 50 mM TAPS buffer, 0.1 Na_2SO_4, c) pH 8.5 in 50 mM TAPS buffer, 0.1 Na_2SO_4, d) pH 8.0 in 50 mM TAPS buffer, 0.1 Na_2SO_4. Plots of the initial rates at each pH vs [CO_2] are fitted to the the Michaelis-Menten equation in Prism 5 (GraphPad Software).[22]

Individual k_{cat} and K_M values have high error bars, particularly at low pH where the K_M is well outside of the range of substrate concentrations used in the experiment. The general trends are that the k_{cat} increases with increasing pH (consistent with *p*NPA hydrolysis data and the deprotonation of Zn-OH$_2$ to form an active Zn-OH$^-$ nucleophile, as with CAII) and that the K_M increases with decreasing pH, suggesting that substrate access worsens with decreasing pH. However, the k_{cat}/K_M should be very well defined under these conditions.

b) Zn(II) site in $[Zn(II)(OH_2/OH^-)]_N(TRIL2WL23H)_3{}^{n+}$.
$[Zn(II)(OH_2/OH^-)]_N(TRIL2WL23H)_3{}^{n+}$ exhibits saturation kinetics for CO_2 hydration in buffered aqueous solution, with $k_{cat} \sim 930$ s^{-1} and $k_{cat}/K_M \sim 1.1 \times 10^5$ M^{-1} s^{-1} at pH 9.5 (25 °C, 10 μM catalyst, Table 5-3 and Figure 5-8). The K_M, ~8.8 mM, is about the same as
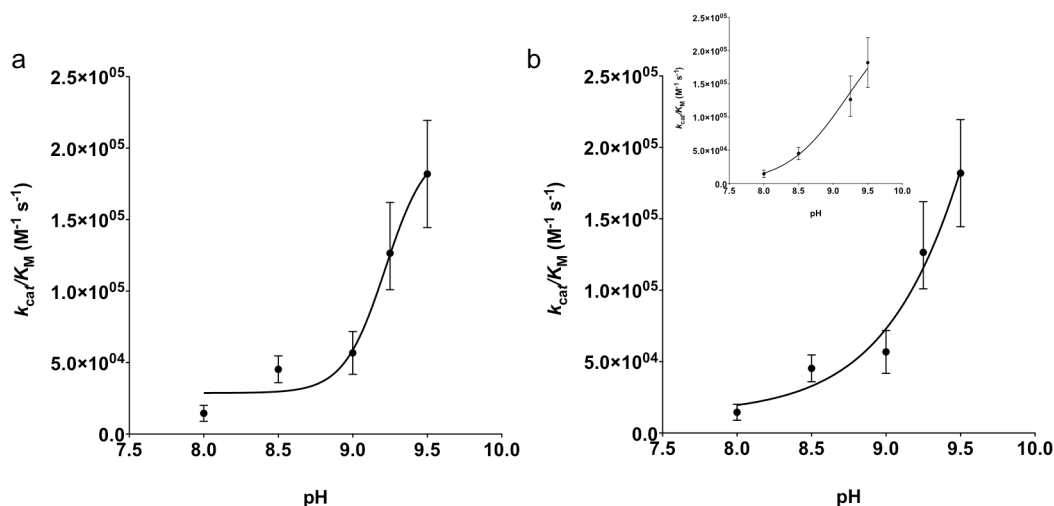
Figure 5-6. pH-dependency of CO_2 hydration by 10 μM $[Hg(II)]_S[Zn(II)(OH_2/OH^-)]_N(TRIL9CL23H)_3{}^{n+}$. Plots of a) k_{cat}/K_M vs pH fitted for the midpoint ($pK_a = 9.2 \pm 0.1$) and b) k_{cat}/K_M vs pH fitted to eq 2 ($pK_a = 10.3 \pm 1.4$ and maximal k_{cat}/K_M ~1.2 x 10^6 M^{-1} s^{-1}). Results shown are in 50 mM TAPS (pH 8.0-9.0) or 50 mM CHES (pH 9.25-9.5), both 0.1 M Na_2SO_4. The pK_a presumably represents the deprotonation of $Zn-OH_2$ to form the active $Zn-OH^-$ nucleophile, as with CAII. However, the discrepancy between the two fits suggests more data is needed, particularly above pH 9.5 and between 9.0-9.5 to better define the curve for fitting to eq 2. For example, when the pH 9.0 point is removed from the eq 2 fit, the pK_a is significantly lowered to ~9.6. When the pH 9.0 point is removed and the pK_a constrained to 9.2 in eq 2 (inset to b)), the maximal efficiency can be determined (2.6 x 10^5 M^{-1} s^{-1}).
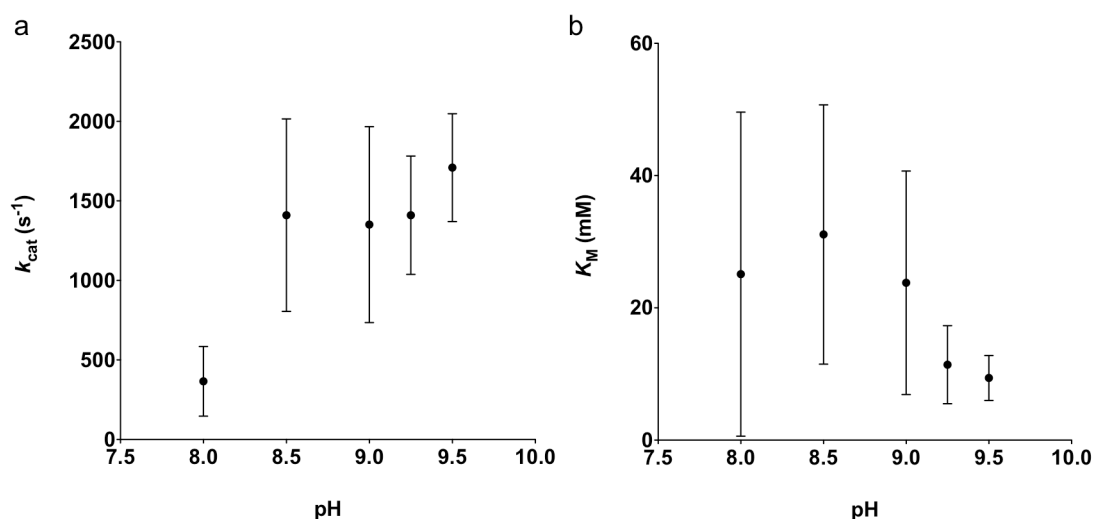

Figure 5-7. pH-dependency of a) k_{cat} and b) K_M parameters for CO_2 hydration by 10 μM $[Hg(II)]_S[Zn(II)(OH_2/OH^-)]_N(TRIL9CL23H)_3{}^{n+}$. Results shown are in 50 mM TAPS (pH 8.0-9.0) or 50 mM CHES (pH 9.25-9.5), both 0.1 M Na_2SO_4.

that for $[Hg(II)]_S[Zn(II)(OH_2/OH^-)]_N(\textbf{TRI}L9CL23H)_3{}^{n+}$ (~9.4 mM). The rate is just over 50% of that for the original model, suggesting a loss in activity in the absence of the structurally stabilizing site (no loss was observed for pNPA hydrolysis). Correspondingly, the efficiency is close to 60% poorer than that for the original model with the HgS_3 site.
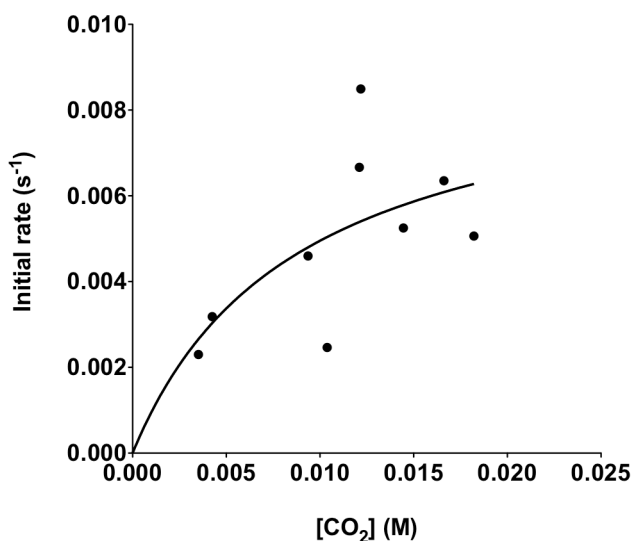

Figure 5-8. CO_2 hydration by 10 μM $[Zn(II)(OH_2/OH^-)]_N(\textbf{TRI}L2WL23H)_3{}^{n+}$ at pH 9.5 in 50 mM CHES buffer, 0.1 M Na_2SO_4. Plot of the initial rates at pH 9.5 vs $[CO_2]$ and fitting to the Michaelis-Menten equation in Prism 5 (GraphPad Software).[22]

c)   Zn(II)   site   in $[Zn(II)(OH_2/OH^-)]_N[Hg(II)]_S(\textbf{TRI}L9HL23C)_3{}^{n+}$.
$[Zn(II)(OH_2/OH^-)]_N[Hg(II)]_S(\textbf{TRI}L9HL23C)_3{}^{n+}$ exhibits saturation kinetics for CO_2 hydration in buffered aqueous solution, with $k_{cat} = 640 \pm 100$ s^{-1} and $k_{cat}/K_M = 0.52$ (± 0.07) x 10^5 M^{-1} s^{-1} at pH 9.5 (25 °C, 20 μM catalyst, Table 5-3 and Figure 5-9). The K_M (12.4 $\pm$ 3.6 mM) is slightly above, but essentially in the same range, as those for the L23H sites considering the error. The rate is decreased further from that for $[Zn(II)(OH_2/OH^-)]_N(\textbf{TRI}L2WL23H)_3{}^{n+}$, the complex lacking the structurally stabilizing site ($k_{cat} = 930 \pm 480$ s^{-1}), although the error bars on these individual kinetic parameters are high. The catalytic efficiency is ~50% less than that for $[Zn(II)(OH_2/OH^-)]_N(\textbf{TRI}L2WL23H)_3{}^{n+}$.

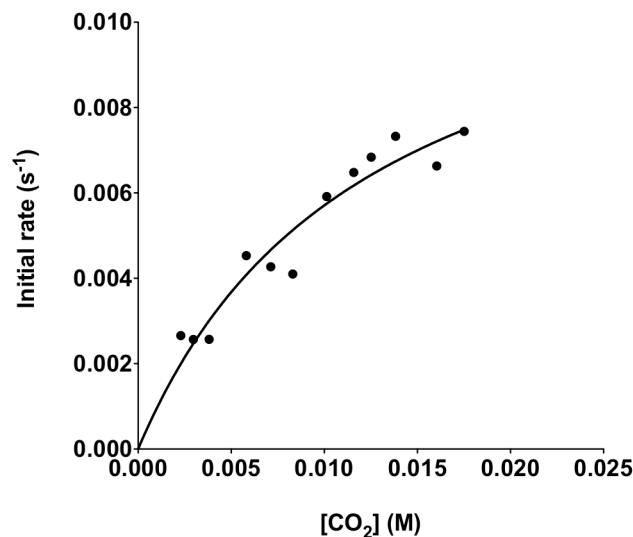**Figure 5-9. CO_2 hydration by 20 μM $[Zn(II)(OH_2/OH^-)]_N[Hg(II)]_S$ $(TRIL9HL23C)_3{}^{n+}$ at pH 9.5 in 50 mM CHES buffer, 0.1 M Na_2SO_4. Plot of the initial rates at pH 9.5 vs $[CO_2]$ and fitting to the Michaelis-Menten equation in Prism 5 (GraphPad Software).[22]**

    d) Zn(II) site in $[Hg(II)]_S[Zn(II)(OH_2/OH^-)]_N(TRIL9CL19H)_3{}^{n+}$. $[Hg(II)]_S[Zn(II)(OH_2/OH^-)]_N(\mathbf{TRI}L9CL19H)_3{}^{n+}$ exhibits saturation kinetics for CO_2 hydration in buffered aqueous solution, with k_{cat} = 750 ± 180 s^{-1} and k_{cat}/K_M = 0.64 (±0.16) x 10^5 M^{-1} s^{-1} at pH 9.5 (25 °C, 20 μM catalyst, Table 5-3 and Figure 5-10). The K_M, 11.7 ± 5.5 mM, is the same (within error) as that for $[Zn(II)(OH_2/OH^-)]_N[Hg(II)]_S(\mathbf{TRI}L9HL23C)_3{}^{n+}$, demonstrating that CO_2 access is not as sensitive to changes around the Zn(II) site as observed for *p*NPA. The rate is also similar to that for $[Zn(II)(OH_2/OH^-)]_N[Hg(II)]_S(\mathbf{TRI}L9HL23C)_3{}^{n+}$ (k_{cat} = 640 ± 100 s^{-1}), noting that the error bars on these individual kinetic parameters are high. The catalytic efficiency is also similar to that for $[Zn(II)(OH_2/OH^-)]_N[Hg(II)]_S(\mathbf{TRI}L9HL23C)_3{}^{n+}$.

    e) Zn(II) site in $[Hg(II)]_S[Zn(II)(OH_2/OH^-)]_N(GRL2WL16CL30H)_3{}^{n+}$. $[Hg(II)]_S[Zn(II)(OH_2/OH^-)]_N(\mathbf{GR}L2WL16CL30H)_3{}^{n+}$ exhibits saturation kinetics for CO_2 hydration in buffered aqueous solution, with k_{cat} = 730 ± 290 s^{-1} and k_{cat}/K_M = 0.74 (±0.34) x 10^5 M^{-1} s^{-1} at pH 9.5 (25 °C, 20 μM catalyst, Table 5-3 and Figure 5-11). The K_M, ~9.8 mM, is about the same as those for all of the above peptide complexes. The rate is closest to that for $[Hg(II)]_S[Zn(II)(OH_2/OH^-)]_N(\mathbf{TRI}L9CL19H)_3{}^{n+}$ (750 ± 180 s^{-1}),
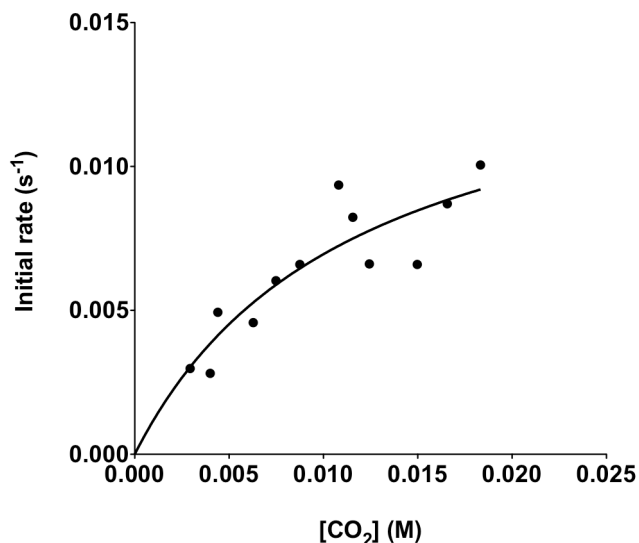
Figure 5-10. CO_2 hydration by 20 μM $[Hg(II)]_S[Zn(II)(OH_2/OH^-)]_N$ $(TRIL9CL19H)_3{}^{n+}$ at pH 9.5 in 50 mM CHES buffer, 0.1 M Na_2SO_4. Plot of the initial rates at pH 9.5 vs $[CO_2]$ and fitting to the Michaelis-Menten equation in Prism 5 (GraphPad Software).[22]
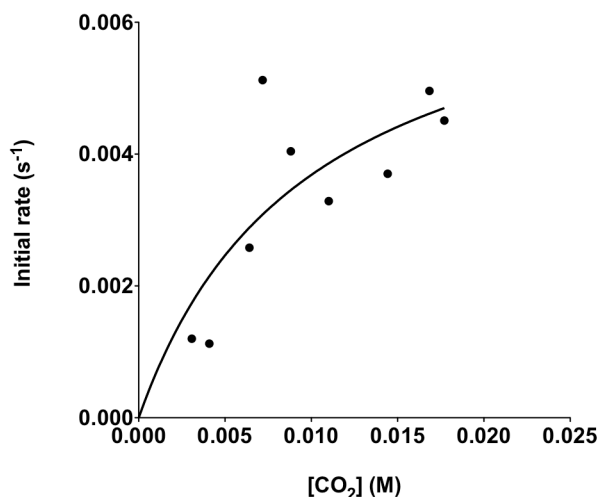
Figure 5-11. CO_2 hydration by 20 μM $[Hg(II)]_S[Zn(II)(OH_2/OH^-)]_N$ $(GRL2WL16CL30H)_3{}^{n+}$ at pH 9.5 in 50 mM CHES buffer, 0.1 M Na_2SO_4. Plot of the initial rates at pH 9.5 vs $[CO_2]$ and fitting to the Michaelis-Menten equation in Prism 5 (GraphPad Software).[22]

noting that the error bars on these individual kinetic parameters are high. The catalytic efficiency is also similar to those for $[Zn(II)(OH_2/OH^-)]_N[Hg(II)]_S(TRIL9HL23C)_3{}^{n+}$ and $[Hg(II)]_S[Zn(II)(OH_2/OH^-)]_N(TRIL9CL19H)_3{}^{n+}$.

211

f) Cd(II) site in $[Cd(II)(OH_2/OH^-)_x]_N(TRIL23H)_3^{n+}$. $[Cd(II)(OH_2/OH^-)_x]_N$ $(TRIL23H)_3^{n+}$ exhibits saturation kinetics for CO_2 hydration in buffered aqueous solution, with $k_{cat} = 920 \pm 240$ s^{-1} and $k_{cat}/K_M = 1.0$ (± 0.3) x 10^5 M^{-1} s^{-1} at pH 9.5 (25 °C, 20 μM catalyst, Table 5-3 and Figure 5-12). The K_M, ~9.1 mM, is consistent with the K_M's measured for each of the Zn(II)-bound complexes described above. The rate and catalytic efficiency values are closest to those for $[Zn(II)(OH_2/OH^-)]_N(TRIL2WL23H)_3^{n+}$ (930 ± 480 s^{-1} and 1.1 (± 0.9) x 10^5 M^{-1} s^{-1}, respectively).
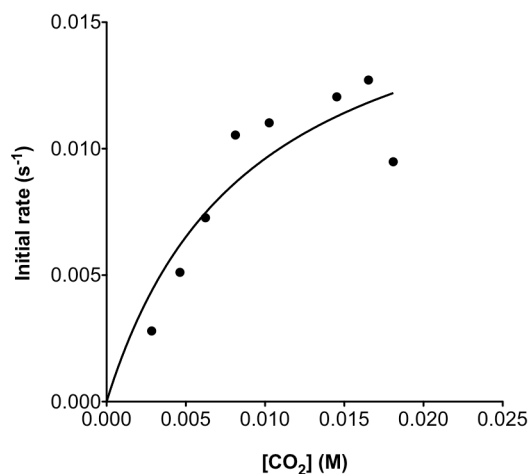
Figure 5-12. CO_2 hydration by 20 μM $[Cd(II)(OH_2/OH^-)_x]_N(TRIL23H)_3^{n+}$ at pH 9.5 in 50 mM CHES buffer, 0.1 M Na_2SO_4. Plot of the initial rates at pH 9.5 vs $[CO_2]$ and fitting to the Michaelis-Menten equation in Prism 5 (GraphPad Software).[22]

Discussion

The aim of the work presented in this chapter is to determine whether a family of *de novo* designed Zn(II) metalloenzymes can catalyze the hydration of CO_2, the evolved substrate of the highly efficient zinc metalloenzyme, carbonic anhydrase (CA). In previous chapters, I have described the reactivity of several metal-peptide complexes with a variety of designed sequences towards the activated ester substrate, *p*NPA. While the hydrolysis of *p*NPA is thought to have a similar reaction mechanism to that for CO_2 hydration, the sterics and electronics do differ between these molecules so *p*NPA hydrolysis does not strictly represent the evolved reaction of the target enzyme.[14,15] In order to evaluate the catalytic power of the *de novo* designed Zn(II) metalloenzymes

towards a physically relevant reaction, the reactivity of the active site in several different sequences is examined.

First, the original designed metal-peptide complex, $[Hg(II)]_S[Zn(II)(OH_2/OH^-)]_N(\textbf{TRI}L9CL23H)_3{}^{n+}$, was tested for its ability to hydrate CO_2 over the pH range 8.0-9.5. As for pNPA hydrolysis, the highest efficiency is observed at the highest pH (9.5), consistent with a Zn(II)-hydroxide active species. At pH 9.5, the efficiency reaches 1.82 ($\pm$0.37) x 10^5 M^{-1} s^{-1}, the rate 1710 $\pm$ 340 s^{-1}, and the Michealis constant (K_M) is 9.4 mM (Figure 5-4). As for CAII, the relative efficiency for CO_2 hydration is much faster than that for pNPA hydrolysis (it is ~10^5-fold faster for CAII and close to 10^4-fold faster [using a maximal k_{cat}/K_M of 2.6 x 10^5 M^{-1} s^{-1}] for the designed system). The maximal efficiencies are used, in part, because the pK_a for CAII is lower (6.8)[23] than that for the designed system (9.2). As discussed in Chapter 4, the higher pK_a for the designed system is likely due to a lack of secondary interactions, which are known to be important for tuning the pK_a in the native system. While the Michaelis-Menten constant is similar to that for CAII (8.2 mM, Table 5-1), the efficiency is several hundred-fold slower (~400-500-fold, depending on the efficiency of CAII used to make the comparison, given that the reported values include 1.10 ($\pm$0.10) x 10^8 M^{-1} $s^{-1(24)}$ and 9.2 x 10^7 M^{-1} $s^{-1(25)}$). The rate is, similarly, several hundred-fold slower. The similarity between the K_M values, representative of substrate access, is not surprising because CO_2 does not specifically bind to the active site of CA and likely also does not bind in the designed complex. The kinetic parameters for $[Hg(II)]_S[Zn(II)(OH_2/OH^-)]_N(\textbf{TRI}L9CL23H)_3{}^{n+}$-catalyzed CO_2 hydration all appear to be pH-dependent. The catalytic efficiencies increase with increasing pH from 1.4 ($\pm$0.6) x 10^4 M^{-1} s^{-1} at pH 8.0 to 1.82 ($\pm$0.37) x 10^5 M^{-1} s^{-1} at pH 9.5. Plotting these efficiencies as a function of pH yields a curve that may be fitted for the pK_a (Figure 5-6). Based on the midpoint fitting (pK_a = 9.2 $\pm$ 0.1), the kinetic pK_a is about the same as that for pNPA hydrolysis catalyzed by this metal-peptide complex (9.0 $\pm$ 0.1). The maximal catalytic efficiency (2.6 x 10^5 M^{-1} s^{-1}) is estimated using eq 2 and constraining the pK_a to 9.2. The K_M values appear to decrease with increasing pH (note that the error bars are very high). The k_{cat} also appears to be pH-dependent and may increase with increasing pH (Figure 5-7), but, as a consequence of the high K_M values, the error bars are too high for complete

confidence in this trend. Further, for CAII, the catalytic efficiency and rates both increase with increasing pH and have a pK_a of 6.8. It is generally accepted that the K_M for CAII is pH-independent (pH 5.8-8.8)[21], however there was a conflicting earlier report in which the K_M decreased with increasing pH (from 18 mM to 9.3 mM in the pH range of 6.3-7.55).[26] The disagreement between these results is proposed to be due to higher errors in the earlier measurements and may also result from the narrower pH range measured. In order to minimize the errors in the designed system, these experiments should probably be carried out with higher catalyst concentrations (although this will require significantly more peptide).
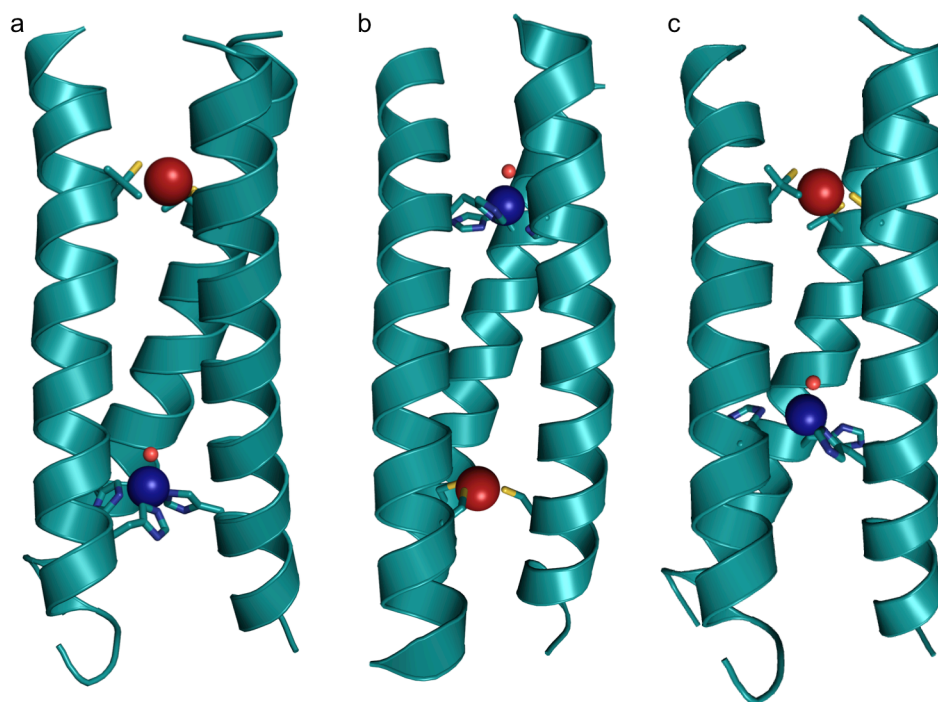
Figure 5-13. Comparison of the X-ray crystal structure of a) [Hg(II)]$_S$[Zn(II)(OH$_2$/OH$^-$)]$_N$(CSL9PenL23H)$_3{}^{n+}$ (3PBJ)[33] with PyMOL models of b) [Zn(II)(OH$_2$/OH$^-$)]$_N$[Hg(II)]$_S$(TRIL9HL23C)$_3{}^{n+}$ based on the coordinates of 2JGO[34] and c) [Hg(II)]$_S$[Zn(II)(OH$_2$/OH$^-$)]$_N$(TRIL9CL19H)$_3{}^{n+}$ based on the coordinates of 3PBJ. Models were prepared in PyMOL using the mutagenesis option and PyMOL's rotamer library.[35] Figure adapted from ref 36.

Given that the highest activity is observed at pH 9.5, yielding smaller errors than the rates at lower pH values, as well as higher efficiencies, each of the other varied metal-peptide complexes were measured for hydration of CO_2 at pH 9.5. First, the complex [Zn(II)(OH$_2$/OH$^-$)]$_N$(**TRIL2WL23H**)$_3{}^{n+}$ (which lacks the structurally stabilizing site) was

tested. The catalytic efficiency ($\sim 1.1 \times 10^5$ M^{-1} s^{-1}) and rate (~ 930 s^{-1}) may both be ~ 40-50% slower than those for the original model complex, which included the stabilizing site. However, the error associated with these determinations is large (> 50%) and could mean that this model is just as active as the original. The K_M is about the same (Table 5-3). This is interesting as it suggests that while the stabilizing site is not very important for pNPA hydrolysis (the rates are similar both with and without it), it could be beneficial with respect to CO_2 hydration activity. This stabilizing site is probably especially important at high pH, where increased fraying of the coiled coil structure is expected. Apparently, this enhanced stability at high pH may be especially important for CO_2 hydration activity. Examining the pH-dependence of hydration activity by this complex may provide further insight. If the same rates are observed, at lower pH values, as those for the original model, it would suggest that increased fraying of the structure at high pH really is detrimental to the activity. Further, the high errors associated with kinetic parameters at pH 9.5 may be a direct result of having a less stable protein.

Next, a variant in which the active Zn(II) site and the structurally stabilizing site are switched relative to the C- and N-termini, respectively, is examined (Figure 5-13). As explained in Chapter 3, this sequence is hypothesized to result in a 3SCC in which the Zn(II) site is near the N-terminus, with the solvent molecule oriented towards the solvent (to provide increased substrate access). pNPA hydrolysis activity and inhibition by acetate support this model because the K_M is about two-fold lower than that for the original model (improved access) and the K_I is close to 40% lower. However, CO_2 is a much smaller substrate than pNPA, so a less pronounced difference in the K_M value is expected. Indeed, the K_M for CO_2 hydration by $[\text{Zn(II)(OH}_2/\text{OH}^-)]_N[\text{Hg(II)}]_S(\textbf{TRI}L9HL23C)_3{}^{n+}$ at pH 9.5 is 12.4 ± 3.6 mM, essentially within error of that for $[\text{Hg(II)}]_S[\text{Zn(II)(OH}_2/\text{OH}^-)]_N(\textbf{TRI}L9CL23H)_3{}^{n+}$ (9.4 ± 3.4 mM) (Table 5-3). As was observed for pNPA hydrolysis at pH 9.5, the catalytic rate of $[\text{Zn(II)(OH}_2/\text{OH}^-)]_N[\text{Hg(II)}]_S(\textbf{TRI}L9HL23C)_3{}^{n+}$ is much slower than that for the original model (640 ± 100 s^{-1} vs 1710 ± 340 s^{-1}). In the case of pNPA hydrolysis, the lower K_M balances out the detrimental effect of the lower rate, resulting in a similar catalytic efficiency. The catalytic efficiency for CO_2 hydration by

$[Zn(II)(OH_2/OH^-)]_N[Hg(II)]_S(\textbf{TRI}L9HL23C)_3{}^{n+}$ is also much slower than that for the original model (0.52 (± 0.07) x 10^5 M^{-1} s^{-1} vs 1.82 (± 0.37) x 10^5 M^{-1} s^{-1}).

The next sequence variation to be studied is **TRI**L9CL19H. In this complex, the active metal site is moved from an **a** to a **d** position in the heptad and also further into the interior of the coiled coil, presumably with the solvent molecule oriented towards the N-terminus and, therefore, well into the hydrophobic interior (Figure 5-13). For Cys-substituted **TRI** variants, thiolate conformations differ between the two sites as do the pK_a values for Cd(II) binding.[27,28] When this variant was evaluated for pNPA hydrolysis, a slightly higher K_M was observed. The kinetic pK_a was also increased to 9.6 ± 0.1, so the rate and efficiency observed at pH 9.5 was much less than that for the original model at pH 9.5. A similar pattern for the rate and efficiency is observed for CO_2 hydration in which both parameters are less than those for $[Hg(II)]_S[Zn(II)(OH_2/OH^-)]_N(\textbf{TRI}L9CL19H)_3{}^{n+}$ (Table 5-3). No noticeable difference in the K_M is observed which is, again, not surprising because the steric natures of CO_2 and pNPA are different. An examination of the pH-dependency of CO_2 hydration by this model would likely provide further useful insight.

The next variant examined was the corresponding **Grand** sequence, **GR**L2WL16CL30H. The extra heptad in **Grand**, relative to **TRI**, contributes ~9 kcal mol^{-1} more stability to the complex.[29,30] Understanding how the Zn(II) site in this complex may react towards CO_2 is very important because the ultimate goal will be to generate a sequence with a hydrogen-bonding network (Chapter 4) that can accommodate the necessary residues for fine-tuning the structure and function of this designed enzyme. When $[Hg(II)]_S[Zn(II)(OH_2/OH^-)]_N(\textbf{GR}L2WL16CL30H)_3{}^{n+}$ was evaluated for its reactivity towards CO_2, it was found that, as for the other sequence variations described, the rate (730 ± 290 s^{-1}) and catalytic efficiency (0.74 (± 0.34) x 10^5 M^{-1} s^{-1}) were both significantly less than those for the original model, $[Hg(II)]_S[Zn(II)(OH_2/OH^-)]_N(\textbf{TRI}L9CL23H)_3{}^{n+}$ (pH 9.5, Table 5-3). The K_M value (~9.8 mM) is, again, consistent with those obtained for all of the other peptides and that for CAII (8.2 mM).[24] This differs from the results obtained by measuring pNPA hydrolysis, where the K_M value was nearly double that for the original model. Additionally, the catalytic efficiency towards pNPA hydrolysis was similar for the two, since the rate went

up for $[Hg(II)]_S[Zn(II)(OH_2/OH^-)]_N(\textbf{GR}L2WL16CL30H)_3{}^{n+}$ relative to $[Hg(II)]_S[Zn(II)(OH_2/OH^-)]_N(\textbf{TRI}L9CL23H)_3{}^{n+}$ at pH 9.5. Despite this loss in CO_2 hydration activity for the **Grand** complex relative to the original model, its efficiency is more than sufficient for further development towards the inclusion of hydrogen-bonding networks. Further, this result argues against a conclusion reported by Der *et al.*[3] That paper, which reported the MID1-Zn design (an interface $ZnHis_3O$ site which catalyzes the hydrolysis of *p*NPA with an efficiency ~20-fold faster than $[Hg(II)]_S[Zn(II)(OH_2/OH^-)]_N(\textbf{TRI}L9CL23H)_3{}^{n+}$), and was described in Chapter 2, suggested that hydrolysis of *p*NPA by $[Hg(II)]_S[Zn(II)(OH_2/OH^-)]_N(\textbf{TRI}L9CL23H)_3{}^{n+}$ was likely to occur via dissociation of a peptide subunit. However, this result, in which a peptide with much higher folding energies retains significant hydrolytic efficiency, argues against such a mechanism.

In Chapter 4, I also described the use of spectroscopic probe metals in these designs (Cd(II) and Co(II)). Here, I have examined $[Cd(II)(OH_2/OH^-)_x]_N(\textbf{TRI}L23H)_3{}^{n+}$ for its reactivity towards CO_2 at pH 9.5. The K_M is similar to those for all of the Zn(II) complexes, but the rate and efficiency (920 ± 240 s^{-1} and 1.0 (± 0.3) x 10^5 M^{-1} s^{-1}, respectively) are essentially the same as those for $[Zn(II)(OH_2/OH^-)]_N(\textbf{TRI}L2WL23H)_3{}^{n+}$, the original model lacking the structural HgS_3 site (Table 5-3). This differs greatly from the result obtained through examining *p*NPA hydrolysis (the efficiency for the Cd(II) complex was only 3.5 ± 0.2 M^{-1} s^{-1} relative to 23.3 ± 0.3 M^{-1} s^{-1} for the Zn(II)-bound complex at pH 9.5), which was proposed to be due to a variation in the kinetic pK_a. Here, it appears as if CO_2 hydration does not discriminate between these two different metal centers in the designed metalloenzymes. In addition to repeating each of this kinetic determinations for CO_2 hydration at this pH, and perhaps others, it may be useful to examine the reactivity of the Co(II) complex towards CO_2 hydration, which, while also slower than the Zn(II) complex for *p*NPA hydrolysis ($k_{cat}/K_M = 6.6 \pm 0.6$ M^{-1} s^{-1}), is faster than $[Cd(II)(OH_2/OH^-)_x]_N(\textbf{TRI}L23H)_3{}^{n+}$.

Overall, each of these complexes can effectively catalyze the hydration of CO_2, demonstrating success in preparing *de novo* designed metalloenzymes that can catalyze native enzyme reactions. Although there are many examples of Zn(II) complexes that can catalyze CO_2 hydration[6–13], the macrocyclic amine, [12]aneN$_4$, and Brown's phosphine

217

complex (described in Chapter 2 with respect to pNPA hydrolysis) are among the fastest models.[10,12] The fastest N_3-type model, therefore, is tris(4,5-di-n-propyl-2-imidazolyl)phosphine, with a reported second-order rate constant of 2480 M^{-1} s^{-1}.[10] CAII can catalyze this reaction with a maximum turnover of ~1 million s^{-1} and a catalytic efficiency that is essentially diffusion-limited (~10^8 M^{-1} s^{-1}).[24,25] This is ~30000-fold faster than [12]aneN$_4$ and 37000-fold faster than the more structurally faithful tris(4,5-di-n-propyl-2-imidazolyl)phosphine complex.[10,12] Through these CO_2 hydration studies, I have found that the original *de novo* designed Zn(II)-peptide, [Hg(II)]$_S$[Zn(II)(OH$_2$/OH$^-$)]$_N$(**TRI**L9CL23H)$_3$$^{n+}$, attains a maximal k_{cat}/K_M of 2.6 x 10^5 M^{-1} s^{-1}. This catalytic efficiency is over 100-fold faster than any previously reported model complex or *de novo* designed metalloenzyme (while MID1-Zn efficiently hydrolyzes pNPA[3], its activity towards CO_2 is unknown, although it would prove useful towards evaluating the effects of significantly increased space and solvent exposure around this interface site relative to the more buried site present in these **TRI** peptides) and within ~400-500-fold of CAII.

Conclusion

Herein I have described the evaluation of several *de novo* designed Zn(II) enzymes (all of which are extremely efficient catalysts for hydrolyzing the activated substrate, pNPA) for their hydration efficiency towards the physiological substrate of CA, CO_2. Despite the ability of the native enzyme to catalyze many reactions, a strong assessment of the designed system is whether it can catalyze the hydration of this evolved substrate. It is found that each of these designed complexes can effectively catalyze this reaction, all with efficiencies exceeding the highest reported second-order rate constants for related model complexes. The highest efficiency is observed for the original model complex, [Hg(II)]$_S$[Zn(II)(OH$_2$/OH$^-$)]$_N$(**TRI**L9CL23H)$_3$$^{n+}$, which contains a structurally stabilizing site in the 9th position and the active ZnHis$_3$O site in the 23rd position. Variation of this complex (through removal of the stabilizing site and shifting the location of the site along the sequence, as well as placing both sites into a longer sequence of higher stability) demonstrates that, while up to 3.5-fold of the efficiency can

be lost at pH 9.5, activity is still sufficient enough to remain over 20-fold higher than any reported model complex. Clearly, the efficiency is several hundred-fold short of the fastest native CA isozyme (although it does fall at least an order of magnitude closer to the range of many of the less efficient, yet still native, CA isozymes[31]), suggesting that secondary interactions are needed for fine-tuning and improving the designed Zn(II) site's properties. Although the original coiled coil model complex appears to be the most highly active, it is important to note that (relative to small molecule model complexes), the metallated **Grand** and site variation sequences remain significantly efficient towards CO_2 hydration. This is an essential piece of information since, as described in Chapter 4, the incorporation of hydrogen-bonding residues requires the more stable **Grand** sequence and the design of larger hydrogen-bonding networks may require a variation in the relative location of the site. These results are inspiring as they indicate the possibility of preparing truly effective protein-based catalysts for a variety of applications and specifically, for CO_2 reactivity, towards the development of systems for CO_2 sequestration, which is of great environmental importance.

References

(1)   Kaplan, J.; DeGrado, W. F. *Proc. Natl. Acad. Sci. U.S.A.* **2004**, *101*, 11566–11570.

(2)   Faiella, M.; Andreozzi, C.; de Rosales, R. T. M.; Pavone, V.; Maglio, O.; Nastri, F.; DeGrado, W. F.; Lombardi, A. *Nat. Chem. Biol.* **2009**, *5*, 882–884.

(3)   Der, B. S.; Edwards, D. R.; Kuhlman, B. *Biochemistry* **2012**, *51*, 3933–3940.

(4)   Khare, S. D.; Kipnis, Y.; Greisen, P. J.; Takeuchi, R.; Ashani, Y.; Goldsmith, M.; Song, Y.; Gallaher, J. L.; Silman, I.; Leader, H.; Sussman, J. L.; Stoddard, B. L.; Tawfik, D. S.; Baker, D. *Nat. Chem. Biol.* **2012**, *8*, 294–300.

(5)   Tegoni, M.; Yu, F.; Bersellini, M.; Penner-Hahn, J. E.; Pecoraro, V. L. *Proc. Natl. Acad. Sci. U.S.A.* **2012**, *109*, 21234–21239.

(6)   Woolley, P. *Nature* **1975**, *258*, 677–682.

(7)   Huguet, J.; Brown, R. S. *J. Am. Chem. Soc.* **1980**, *102*, 7571–7572.

(8)   Brown, R. S.; Curtis, N. J.; Huguet, J. *J. Am. Chem. Soc.* **1981**, *103*, 6953–6959.

(9)   Brown, R. S.; Salmon, D.; Curtis, N. J.; Kusuma, S. *J. Am. Chem. Soc.* **1982**, *104*, 3188–3194.

(10)   Slebocka-Tilk, H.; Cocho, J. L.; Frackman, Z.; Brown, R. S. *J. Am. Chem. Soc.* **1984**, *106*, 2421–2431.

(11)   Zhang, X.; van Eldik, R.; Koike, T.; Kimura, E. *Inorg. Chem.* **1993**, *32*, 5749–5755.

(12)   Zhang, X.; van Eldik, R. *Inorg. Chem.* **1995**, *34*, 5606–5614.

(13)   Nakata, K.; Shimomura, N.; Shiina, N.; Izumi, M.; Ichikawa, K.; Shiro, M. *J. Inorg. Biochem.* **2002**, *89*, 255–266.

(14)   Verpoorte, J. A.; Mehta, S.; Edsall, J. T. *J. Biol. Chem.* **1967**, *242*, 4221–4229.

(15)   Gould, S. M.; Tawfik, D. S. *Biochemistry* **2005**, *44*, 5444–5452.

(16)   Chan, W. C.; White, P. D. *Fmoc Solid Phase Peptide Synthesis: A Practical Approach*; Chan, W. C.; White, P. D., Eds.; Oxford University Press: New York, 2000; Vol. 222.

(17)   Farrer, B. T.; Harris, N. P.; Balchus, K. E.; Pecoraro, V. L. *Biochemistry* **2001**, *40*, 14696–14705.

(18)   Habeeb, A. F. *Meth. Enzymol.* **1972**, *25*, 457–464.

(19)   Riddles, P.; Blakeley, R.; Zerner, B. *Meth. Enzymol.* **1983**, *91*, 49–60.

(20)   Mantle, M.; Stewart, G.; Zayas, G.; King, M. *Biochem. J.* **1990**, *266*, 597–604.

(21)   Khalifah, R. G. *J. Biol. Chem.* **1971**, *246*, 2561–2573.

(22)   GraphPad Prism version 5.00 for Mac, GraphPad Software, San Diego California USA, www.graphpad.com.

(23)   Fierke, C. A.; Calderone, T. L.; Krebs, J. F. *Biochemistry* **1991**, *30*, 11054–11063.

(24)   Krebs, J. F.; Ippolito, J. A.; Christianson, D. W.; Fierke, C. A. *J. Biol. Chem.* **1993**, *268*, 27458–27466.

(25)   Jackman, J. E.; Merz, K. M.; Fierke, C. A. *Biochemistry* **1996**, *35*, 16421–16428.

(26)   Gibbons, B. H.; Edsall, J. T. *J. Biol. Chem.* **1964**, *239*, 2539–2544.

(27)   Matzapetakis, M.; Farrer, B. T.; Weng, T.-C.; Hemmingsen, L.; Penner-Hahn, J. E.; Pecoraro, V. L. *J. Am. Chem. Soc.* **2002**, *124*, 8042–8054.

(28)   Chakraborty, S.; Touw, D. S.; Peacock, A. F. A.; Stuckey, J.; Pecoraro, V. L. *J. Am. Chem. Soc.* **2010**, *132*, 13240–13250.

(29)   Ghosh, D.; Lee, K.-H.; Demeler, B.; Pecoraro, V. L. *Biochemistry* **2005**, *44*, 10732–10740.

(30)   Su, J. Y.; Hodges, R. S.; Kay, C. M. *Biochemistry* **1994**, *33*, 15501–15510.

(31)   Supuran, C. T. *Curr. Pharm. Des.* **2008**, *14*, 603–14.

(32)   Innocenti, A.; Scozzafava, A.; Parkkila, S.; Puccetti, L.; De Simone, G.; Supuran, C. T. *Bioorg. Med. Chem. Lett.* **2008**, *18*, 2267–2271.

(33)   Zastrow, M. L.; Peacock, A. F. A.; Stuckey, J. A.; Pecoraro, V. L. *Nat. Chem.* **2012**, *4*, 118–123.

(34)   Touw, D. S.; Nordman, C. E.; Stuckey, J. A.; Pecoraro, V. L. *Proc. Natl. Acad. Sci. U.S.A.* **2007**, *104*, 11969–11974.

(35)   The PyMOL Molecular Graphics System, Version 1.5.0.4 Schrödinger, LLC.

(36)   Zastrow, M. L.; Pecoraro, V. L. *J. Am. Chem. Soc.* **2013**, *135*, 5895–5903.

Chapter VI. Conclusions

De novo protein design represents an effective approach for reproducing metal sites in minimal structures.[1–3] Beginning with a minimal *de novo* designed protein, one can determine and sequentially incorporate first, only those features absolutely required for formation of a metal-binding site, and then, features towards building increasing complexity for fine-tuning the properties of the original site. Truly building a metalloenzyme *de novo* is the ultimate test to scientists' knowledge about structure-function relationships. Meeting such a challenge should place one in a position to then design a metalloenzyme for reactivity towards any substrate, native or not, for a variety of potential applications. Towards the development of this fundamental knowledge, my research has focused on the preparation of *de novo* designed two-site metallopeptides, in which one metal site provides structural stability to the complex and the other is a hydrolytically active ZnN_3O site for mimicking the zinc metalloenzyme, carbonic anhydrase (CA).

I have reported the first dual-site combined structural and functional metalloprotein for Zn(II)-dependent hydrolysis (Chapter 2). Prior to initial publication of this work (2012)[4], there were no other examples of *de novo* designed hydrolytic metalloenzymes[5,6] and there are still no other examples of *de novo* designed metalloproteins containing two different metals in two different coordination environments with distinct functions.[7] The design of this dual-site hydrolytic metalloenzyme employs the sequence **TRI**L9CL23H with substitutions in the 9th (Cys for a stabilizing HgS_3 site) and 23rd (His for the ZnN_3O catalytic site) positions. Chemical denaturation studies display significantly enhanced thermodynamic stability of the α-helical coiled coil in the presence of the HgS_3 site, confirming its role as a structurally stabilizing site. This Hg(II)-enhanced stability was exploited to obtain X-ray quality crystals of the **TRI** analog metal-peptide complex, $[Hg(II)]_S[Zn(II)(OH_2/OH^-)]_N(\textbf{CS}L9PenL23H)_3{}^{n+}$ (at pH 8.5 and 7.5), in which Hg(II) is

bound in the S_3 site and Zn(II) is bound as tetrahedral $ZnHis_3O$. Each structure contains two independent trimers within the asymmetric unit and, while the $ZnHis_3X$ sites are all similar, the HgS_3 site varies between most of them. At pH 8.5, trigonal HgS_3 in one trimer mimics the structural site of the metalloregulatory protein MerR[8] and provides the first structural evidence of a Hg(II)-thiolate site in any of these designed metalloproteins.[9,10] The T-shaped HgS_3 site in the other trimer provides structural evidence for another proposed Hg(II)-thiolate species in the **TRI** family of peptides, and fits the model for the pH-dependence of Hg(II) binding to thiolate sites (at low pH, one of the Cys residues remains protonated and unbound, while the other two are bound as thiolates).[9] At pH 7.5, the HgS_3 sites in both trimers have T-shaped geometries with additional excess Hg(II) at the hydrophilic exterior of the coiled coil. The excess Hg(II) is present in two conformations, one of which is bound to the sulfur-containing residue (which also exists in two conformations, with one oriented to the interior of the trimer and one to the exterior) and the other to an exterior carboxylate residue. This structural finding is exciting as it is consistent with the multisite exchange scheme proposed for Cd(II) where free Cd(II) interacts with surface Glu residues prior to insertion into the coiled coil.[11] Therefore, not only have I prepared a structurally stabilizing metal site exploiting previous work on the **TRI** peptides, but I have been able to provide the first structural evidence for both the pH-dependent Hg(II)-binding model[9] and the multisite metal exchange scheme[11].

The $ZnHis_3O$ site from the structure at pH 8.5 may be overlayed with the active site structure of CAII to demonstrate the achievement of a *de novo* designed Zn(II) site nearly identical to that of the native enzyme, despite drastic differences in the surrounding protein fold and the lack of any designed secondary interactions. In solution, the designed metal complex, $[Hg(II)]_S[Zn(II)(OH_2/OH^-)]_N(\textbf{TRI}L9CL23H)_3{}^{n+}$, binds Zn(II) with a low μM K_d at pH 7.5 and 9.0 (similar to related designed Zn(II) sites[12–17]) and exhibits pH-dependent saturation kinetics for the hydrolysis of *p*NPA with a maximal catalytic efficiency of 31 ± 4 M^{-1} s^{-1}, assuming 100% active Zn(II)-hydroxide species. The K_M, ~2 mM, is pH-independent and the k_{cat} and k_{cat}/K_M both increase with increasing pH, suggesting a chemical rate-limiting step. The efficiencies are pH-dependent ($pK_a = 9.0 \pm 0.1$), presumably due to deprotonation of Zn(II)-aqua to form the active species,

Zn(II)-OH$^-$, as for CAII (pK_a = 6.8).[18] No synthetic Zn(II)N$_x$ model complex[19–24] can compete with this designed enzyme for hydrolysis of *p*NPA. As compared to the native enzyme, CAII, the design is only ~100-fold less efficient towards *p*NPA hydrolysis. Although one example of a *de novo* designed interface ZnHis$_3$ site (MID1-Zn) can catalyze *p*NPA hydrolysis with a maximal efficiency ~20-fold faster than [Hg(II)]$_S$[Zn(II)(OH$_2$/OH$^-$)]$_N$(**TRI**L9CL23H)$_3{}^{n+(5)}$, its reactivity towards CO$_2$ hydration (the physiological reaction for CA) has not yet been tested. However, [Hg(II)]$_S$[Zn(II)(OH$_2$/OH$^-$)]$_N$(**TRI**L9CL23H)$_3{}^{n+}$ can catalyze CO$_2$ hydration with a maximal catalytic efficiency of ~2.6 x 10^5 M^{-1} s^{-1} and maximal rate of ~2400 s^{-1} (Chapter 5). These kinetic parameters represent a complex that is certainly faster than any previous synthetic small molecule model complex. More significantly, the maximal catalytic efficiency falls within/close (~1.2-fold less relative to CAIII and ~40-fold less relative to CAXIII) to the range of efficiencies achieved by nature with the different CA isozymes (3.0 x 10^5-1.5 x 10^8 M^{-1} s^{-1}).[25] Further, the design remains only ~400-500-fold less efficient than CAII (the fastest of the CA isozymes, therefore representing the most rigorous criterion). *These results make this the first hydrolytic metalloenzyme designed from scratch that is competitive with one of the most efficient known natural metalloenzymes.* This work clearly demonstrates that it is possible to remove the active site from a native enzyme, embed it into an entirely different and minimized fold while retaining the "protein-like" environment and still achieve significant catalytic activity similar to highly evolved native metalloenzymes.

Similar kinetic parameters for the corresponding metal complex lacking the structural HgS$_3$ site are observed and confirm that the thermodynamic stability conferred by HgS$_3$ to the protein is not detrimental to the catalytic ZnN$_3$O site. Often, there is a trade-off between thermodynamic stability of a protein structure and its enzymatic activity that must be met. In the case of this *de novo* designed system, no loss in catalytic efficiency, rate, or change in K_M (substrate access) or K_I (acetate inhibition of *p*NPA hydrolysis) are observed for the complex lacking the HgS$_3$ site, [Zn(II)(OH$_2$/OH$^-$)]$_N$(**TRI**L2WL23H)$_3{}^{n+}$. This is especially important for developing multi-metal site proteins where one may want to incorporate multiple sites for a variety of functions without detrimentally affecting the folding or function of the protein.

Incorporation of secondary interactions involving polar residues for hydrogen bonding may be offset by the presence of a structural site. This work clearly demonstrates the utility of *de novo* designed α-helical coiled coils towards the development of multi-metal site enzymes.

As discussed throughout, secondary interactions, including hydrogen-bonding networks, are crucial towards achieving maximal activity and optimal properties in native metalloenzymes. The design of a hydrogen-bonding network into the model complex may be dependent on the metal site location in the three-stranded coiled coil (3SCC) and other considerations, such as solvent and substrate access and metal-binding affinities. Kinetic analyses on two more **TRI** peptides, both of which retained the structurally stabilizing site (not necessarily in the same position), but altered the position of the ZnN_3 site demonstrate that catalytic efficiency can be retained while controlling individual kinetic parameters and metal site properties. **TRI**L9HL23C flips the positions of the structural site and the catalytic site and **TRI**L9CL19H retains the position of the HgS_3 site, but moves the catalytic ZnN_3O site one Leu layer closer to the N-terminus, further into the hydrophobic core of the coiled coil, and from an **a** position to a **d** position. The most notable change in the case of **TRI**L9HL23C, as predicted, is a lower K_M for *p*NPA hydrolysis (relative to L23H) and lower K_I for acetate inhibition, both of which confirm increased substrate, solvent, and inhibitor access to the Zn(II)-OH⁻ species. This may be important for the development of *de novo* systems with substrate selectivity based on the steric nature of the substrate. Although the kinetic pK_a is retained for $[Zn(II)(OH_2/OH^-)]_N[Hg(II)]_S(\textbf{TRI}L9HL23C)_3^{n+}$, that for $[Hg(II)]_S[Zn(II)(OH_2/OH^-)]_N(\textbf{TRI}L9CL19H)_3^{n+}$ is increased to 9.6 ± 0.1, due either to the location of the metal site further within the coiled coil or because it is a **d** site and the His ligands may be oriented differently. The Zn(II)-binding affinities to each of these sites remain similar to those reported for related designed Zn(II)-binding systems in minimal structures, and suggest a limit to the binding affinity that may be achieved using three protein ligands and no stabilizing secondary interactions.[12–15] Overall, the position of the Zn(II) active site along the 3SCC affects the binding affinities, rates, substrate, solvent, and inhibitor access, and kinetic pK_a's but does not collectively change the overall

catalytic efficiency, further supporting that a minimal first coordination sphere Zn(II) site in a helical structure is "enough" to attain a significant amount of hydrolytic activity.

Having built a foundation for the design of effective mononuclear Zn(II) active sites in this series of 3SCCs, polar residues (Thr, Asp) were inserted with the goal of developing hydrogen-bonding interactions. Establishing that the **TRI** sequence cannot accommodate an additional polar substitution into its core and remain well folded prompted me to move forward using the more stable **Grand** sequences, **GR**L16CL26TL30H and **GR**L16CL26DL30H. Both exhibit significant pNPA hydrolysis activity, with similar kinetic parameters to the **TRI** peptides and $[Hg(II)]_S[Zn(II)(OH_2/OH^-)]_N(\mathbf{GR}L2WL16CL30H)_3{}^{n+}$. The primary kinetic difference between the Thr-substituted peptide and that containing Asp was in the K_M value (much lower for the Asp-containing peptide, probably because the packing of anionic residues in the site may push the fold apart somewhat). More notably, the binding affinities for Zn(II) to the metal sites in both of these polar residue-containing complexes increased ~70-fold relative to the L23H sites in **TRI** at pH 9.0. Possibly, Thr or Asp binds to the Zn(II) center (without displacing solvent since the activity is maintained) or, alternatively, hydrogen bonding is occurring as both of these events are known to result in increased affinities.[26–28] Spectral data for Co(II) binding to **TRI**L2WL23H at pH 7.6 supports an octahedral Co(II) site, while the data for Co(II) binding to $[Hg(II)]_S(\mathbf{GR}L16CL26TL30H)_3{}^{n-}$ and $[Hg(II)]_S(\mathbf{GR}L16CL26DL30H)_3{}^{n-}$ indicates decreased coordination numbers (four or five). However, further characterization is required for complete understanding. The symmetry of the designs I have described throughout this dissertation yield three-fold polar substitutions above the His$_3$ site, which may lead to mixed coordination spheres and complicate spectral analysis. A definitive conclusion from this work on incorporating polar residues is that asymmetric designs will be required for building hydrogen-bonding networks.

Overall, my doctoral work has built a strong foundation for the *de novo* design of minimal hydrolytic Zn(II) active sites within α-helical coiled coil structures, in the presence and absence of separate stabilizing metal sites. One of the initial questions asked, about whether the primary coordination sphere of a native metalloenzyme active site may be removed from its protein matrix and embedded into a very different and

minimized fold and retain both structure and function, has been clearly answered. The primary coordination sphere structure of such a ZnN_3O site from CAII inserted into a 3SCC is a near-perfect match. More importantly, the minimal center retains significant hydrolytic activity towards both an activated substrate and the physiological substrate. This designed Zn(II) enzyme is the fastest *de novo* designed metalloenzyme for a native reaction. This work inspires confidence in the potential for preparing effective protein-based catalysts for a variety of applications. More specifically, for reactivity towards CO_2, one may imagine the development of systems for CO_2 sequestration, which is of great environmental importance.

The future directions for this project are numerous given the success of building a highly active *de novo* metalloenzyme. Of course, the development of a hydrogen-bonding channel within the coiled coil is considered the ultimate goal. Design of such a channel, like that found in CA, has not been achieved in any system. Further characterization of the sites developed in Chapter 4, which contain polar residues near the active metal centers, will determine the next steps for optimizing this system. It is almost certain that development of a hydrogen-bonding network for stabilization of the metal site and optimization of its reactivity will require an asymmetric structure, in which insertion of a single residue does not result in a three-fold presence of that residue within the self-assembling coiled coil. There are already other members of the Pecoraro group working on creating asymmetric sites in designed α-helical structures (coiled coils and also three-helix bundles consisting of a single peptide chain).

This designed hydrolytic Zn(II) center should also be tested for its reactivity towards substrates of other Zn(II) enzymes, such phosphate esters and other more sterically-hindered esters, thioesters, and peptides, in order to establish the range of its catalytic power. It may also be tested for its ability to promote activation of substrates such as alcohols, as in the mechanism for alcohol dehydrogenase (Chapter 1). While some of these reactions center around mononuclear Zn(II) centers, usually requiring assistance with activation of the Zn(II)-bound nucleophile via a nearby basic residue, many center around dinuclear Zn(II) centers. As described in Chapter 1, there are currently no examples of catalytic designed systems where either a nearby basic residue is used to promote reactivity of the Zn(II) center or which apply a dinuclear Zn(II) center.

The work being pursued in the Pecoraro group towards the development of an asymmetric center may be used towards approaching the first point for a mononuclear center (where asymmetric sites may be required to implement a single basic residue near the metal site). Design of a dinuclear center is also realistic in this system, using the **Grand** sequence, by substituting adjacent Leu layers with residues for binding Zn(II). All of these systems may be used towards the development of a better understanding of the structure-function relationship in hydrolytic Zn(II) enzymes.

While the patterns for Zn(II) binding in the first coordination sphere are very well understood, the surrounding interactions (whether dependent on a particular fold or not) are much more poorly understood. Given the extreme importance of Zn(II) enzymes to all forms of life, achieving such a goal is critical for supporting a wide range of biotechnological and pharmaceutical applications. More broadly, the insight gained from designing Zn(II) metalloproteins may be applied to the understanding of metalloenzymes relying on a variety of other metals and the development of applications based on any metal center.

References

(1)   Lu, Y.; Yeung, N.; Sieracki, N.; Marshall, N. M. *Nature* **2009**, *460*, 855–862.

(2)   Nanda, V.; Koder, R. L. *Nat. Chem.* **2010**, *2*, 15–24.

(3)   Zastrow, M. L.; Pecoraro, V. L. *Coord. Chem. Rev.* **2013**, *257*, 2565–2588.

(4)   Zastrow, M. L.; Peacock, A. F. A.; Stuckey, J. A.; Pecoraro, V. L. *Nat. Chem.* **2012**, *4*, 118–123.

(5)   Der, B. S.; Edwards, D. R.; Kuhlman, B. *Biochemistry* **2012**, *51*, 3933–3940.

(6)   Khare, S. D.; Kipnis, Y.; Greisen, P. J.; Takeuchi, R.; Ashani, Y.; Goldsmith, M.; Song, Y.; Gallaher, J. L.; Silman, I.; Leader, H.; Sussman, J. L.; Stoddard, B. L.; Tawfik, D. S.; Baker, D. *Nat. Chem. Biol.* **2012**, *8*, 294–300.

(7)   Tanaka, T.; Mizuno, T.; Fukui, S.; Hiroaki, H.; Oku, J.-I.; Kanaori, K.; Tajima, K.; Shirakawa, M. *J. Am. Chem. Soc.* **2004**, *126*, 14023–14028.

(8)   Wright, J. G.; Tsang, H. T.; Penner-Hahn, J. E.; O'Halloran, T. V. *J. Am. Chem. Soc.* **1990**, *112*, 2434–2435.

(9)   Iranzo, O.; Thulstrup, P. W.; Ryu, S.-B.; Hemmingsen, L.; Pecoraro, V. L. *Chem.-- Eur. J.* **2007**, *13*, 9178–9190.

(10)   Pecoraro, V. L.; Peacock, A. F. A.; Iranzo, O.; Luczkowski, M. *ACS Symp. Ser.* **2009**, *1012*, 183–197.

(11)   Chakraborty, S.; Iranzo, O.; Zuiderweg, E. R. P.; Pecoraro, V. L. *J. Am. Chem. Soc.* **2012**, *134*, 6191–6203.

(12)   Pessi, A.; Bianchi, E.; Crameri, A.; Venturini, S.; Tramontano, A.; Sollazzo, M. *Nature* **1993**, *362*, 367–369.

(13)   Müller, H. N.; Skerra, A. *Biochemistry* **1994**, *33*, 14126–14135.

(14)   Vita, C.; Roumestand, C.; Toma, F.; Ménez, A. *Proc. Natl. Acad. Sci. U.S.A.* **1995**, *92*, 6404–6408.

(15)   Kiyokawa, T.; Kanaori, K.; Tajima, K.; Koike, M.; Mizuno, T.; Oku, J.-I.; Tanaka, T. *J. Pept. Res.* **2004**, *63*, 347–353.

(16)   Suzuki, K.; Hiroaki, H.; Kohda, D.; Nakamura, H.; Tanaka, T. *J. Am. Chem. Soc.* **1998**, *120*, 13008–13015.

(17)   Patel, K.; Srivastava, K. R.; Durani, S. *Bioorg. Med. Chem.* **2010**, *18*, 8270–8276.

(18)   Fierke, C. A.; Calderone, T. L.; Krebs, J. F. *Biochemistry* **1991**, *30*, 11054–11063.

(19)   Kimura, E.; Shiota, T.; Koike, T.; Shiro, M.; Kodama, M. *J. Am. Chem. Soc.* **1990**, *112*, 5805–5811.

(20)   Pérez Olmo, C.; Böhmerle, K.; Vahrenkamp, H. *Inorg. Chim. Acta* **2007**, *360*, 1510–1516.

(21)   Koerner, T. B.; Brown, R. S. *Can. J. Chem.* **2002**, *80*, 183–191.

(22)   Bazzicalupi, C.; Bencini, A.; Bianchi, A.; Fusi, V.; Giorgi, C.; Paoletti, P.; Valtancoli, B.; Zanchi, D. *Inorg. Chem.* **1997**, *36*, 2784–2790.

(23)   Sprigings, T. G.; Hall, C. D. *J. Chem. Soc. Perkin Trans. II* **2001**, 2063–2067.

(24)   Jairam, R.; Potvin, P. G.; Balsky, S. *J. Chem. Soc. Perkin Trans. II* **1999**, 363–368.

(25)   Supuran, C. T. *Curr. Pharm. Des.* **2008**, *14*, 603–14.

(26)   Christianson, D. W.; Fierke, C. A. *Acc. Chem. Res.* **1996**, *29*, 331–339.

(27)   Kiefer, L. L.; Paterno, S. A.; Fierke, C. A. *J. Am. Chem. Soc.* **1995**, *117*, 6831–6837.

(28)   Ippolito, J. A.; Baird, T. T.; McGee, S. A.; Christianson, D. W.; Fierke, C. A.
       Proc. Natl. Acad. Sci. U.S.A. **1995**, *92*, 5017–5021.